universität wien

MASTERARBEIT / MASTER'S THESIS

Titel der Masterarbeit / Title of the Master's Thesis

„Visible light photocatalytic hydrocarboxylation of electron deficient olefins“

verfasst von / submitted by

Thomas Bauhoff, BSc

angestrebter akademischer Grad / in partial fulfilment of the requirements for the degree of

Master of Science (MSc)

Wien, 2023 / Vienna 2023

Studienkennzahl lt. Studienblatt / degree programme code as it appears on the student record sheet:	UA 066 862
Studienrichtung lt. Studienblatt / degree programme as it appears on the student record sheet:	Masterstudium Chemie
Betreut von / Supervisor:	Univ.-Prof. Davide Bonifazi, PhD

Danksagung

Allen voran möchte ich mich bei Univ.-Prof. Dr. **Katharina Schröder** bedanken, die mir überhaupt erst die Möglichkeit gab meine Masterarbeit in ihrer Forschungsgruppe durchführen zu dürfen und mir die Gelegenheit gab das mir damals gänzlich neue und interessante Feld der Photokatalyse betreten zu dürfen.

Ebenfalls danken möchte ich allen Kollegen der Forschungsgruppe, welche für ein entspanntes Arbeitsklima gesorgt haben und mir immer bei Fragen geholfen haben. Dabei möchte ich mich besonders bei meinen beiden Betreuern **Ádám Márk Pálvölgyi** und **Fabian Scharinger** bedanken, die mir nicht nur jederzeit bei Unklarheiten oder Problemen zur Hilfe gekommen sind, sondern mir auch viel Motivation während der Arbeit mitgegeben haben. Ein weiterer Dank gebührt **Olga Lanaridi**, die mir bei der sprachlichen Verfeinerung dieser Arbeit zur Hand gegangen ist.

Zusätzlich möchte ich mich bei meinen Freunden **Andreas Riegler**, **Claudia Rabijasz**, **Florian Smalcerz**, **Marlis Haslinger** & **Michael Beckmann** bedanken, die mir nicht nur während der Masterarbeit, sondern während des gesamten Studiums immer zur Seite gestanden sind und mir auch in meinen Tiefphasen immer Kraft und Unterstützung gegeben haben.

Ein besonderer Dank gebührt meinen Eltern, die mein gesamtes Leben über immer eine große emotionale und finanzielle Stütze für mich waren und mir ermöglicht haben, meinen Traum, in Wien studieren zu dürfen, ausleben zu dürfen. Euch schulde ich meinen größten Dank, denn ohne euch wäre ich nicht hier und hätte niemals all die großartigen Ereignisse der letzten Jahre erlebt und niemals die Menschen, die ich heute meine engsten Freunde nenne, kennengelernt.

Abstract

In the context of this master thesis, a new method for the photocatalytic hydrocarboxylation of electron-deficient olefins is presented, which can be performed using formic acid as a cost-effective and easily accessible C1 source.

To meet the demands of sustainable chemistry, a synthetic procedure was developed that is characterized by its ease of handling and feasibility under mild reaction conditions. The method herein presented allows the synthesis of carboxylic acids from electron-deficient olefins without the requirement for inert atmosphere and can be conducted at room temperature with visible light as the energy source.

These mild reaction conditions not only offer economic and ecological advantages but also enable the utilization of a wide range of diverse substrate classes. Therefore, successful hydrocarboxylations of acrylates, anilides, and sulfonamides were demonstrated using this method.

Furthermore, a mechanism for the developed reaction system is proposed, which is supported by conducted mechanistic investigations, including quantum yield determination, isotopic labeling studies, and control experiments.

Kurzfassung

Im Rahmen dieser Masterarbeit wird eine neue Methode zur photokatalysierten Hydrocarboxylierung elektronendefizitärer Olefine vorgestellt, welche unter direktem Einsatz von Ameisensäure als kostengünstige und einfach einsetzbare C_1 Quelle durchgeführt werden kann.

Um den heutigen Ansprüchen nachhaltiger Chemie gerecht zu werden, wurde dabei eine Synthese entwickelt, welche sich durch ihre leichte Handhabbarkeit und Durchführbarkeit unter milden Reaktionsbedingungen auszeichnet. So erlaubt die hier vorgestellte Methode eine Synthese von Carbonsäuren ausgehend von Olefinen, welche vollständig auf den Einsatz von Schutzgasatmosphäre verzichtet und unter Raumtemperatur bei Einsatz von Licht im visuellen Bereich angewendet werden kann.

Diese schonenden Reaktionsbedingungen besitzen nicht nur ökonomische und ökologische Vorteile, sondern ermöglichen ebenfalls den Einsatz einer Vielzahl diverser Substratklassen. So konnten erfolgreiche Hydrocarboxylierungen von Acrylaten, Aniliden und Sulfonamiden demonstriert werden.

Zusätzlich konnte ein Mechanismus für das entwickelte Reaktionssystem vorgeschlagen werden, welcher durch durchgeführte mechanistische Untersuchungen wie Quantenausbeutenbestimmung, Isotopenmarkierungs- sowie Kontrollstudien gestützt wird.

List of abbreviations

4CzIPN	2,4,5,6-Tetra(carbazol-9-yl)benzene-1,3-dicarbonitrile
4DPAIPN	2,4,5,6-Tetrakis(diphenylamino)isophthalonitrile
A	Acceptor
Ac	Acetyl
ACN	Acetonitrile
APT	Attached proton test
Ar	Argon
Ar-	Aryl
BET	Back electron transfer
^{t}Bu	*tert*-Butyl
COSY	(Homonuclear) correlation spectroscopy
CT	Charge transfer
CuOTf	Copper triflate
Cy	Cyclohexyl
D	Donor
DABCO	1,4-Diazabicyclo[2.2.2]octane
DBU	1,8-Diazabicyclo(5.4.0)undec-7-ene
DCA	9,10-Dicyanoanthracene
DCM	Dichloromethane
DHP	Dihydropyridine
DMA	Dimethylacetamide
DMF	Dimethylformamide
DMSO	Dimethyl sulfoxide
EDA	Electron donor acceptor

EnT	Energy transfer
ET	Electron transfer
EtOAc	Ethyl acetate
EWG	Electron withdrawing group
EY	Eosin Y
fac	facial
FG	Functional group
(g)	Gaseous
[H]	Reduction
HAT	Hydrogen atom transfer
HMBC	Heteronuclear multiple bond correlation spectroscopy
HSQC	Heteronuclear single quantum coherence spectroscopy
Ir-1	(*see* [Ir(dtbbpy)(ppy)$_2$])
[Ir(ppy)$_3$]	Tris[2-phenylpyridine]iridium
[Ir(dtbbpy)(ppy)$_2$]	[4,4′-*Bis*(1,1-dimethylethyl)-2,2′-bipyridin-*N*1,*N*1′]*bis*[2-(2-pyridinyl-*N*)phenyl-C]iridium(III)
ISC	Intersystem crossing
(l)	Liquid
LED	Light emitting diode
LG	Leaving group
NMR	Nuclear magnetic resonance spectroscopy
[O]	Oxidation
PC	Photocatalyst
PE	Light petrol
^{i}Pr	*iso*-Propyl

rt	Room temperature
$[Ru(bpy)_3]$	Tris(bipyridine)ruthenium
Sac	Sacrificial agent
SCE	Saturated calomel electrode
SET	Single electron transfer
Sub	Substrate
TCBQ	Tetrachloro-1,4-benzoquinone
TCE	Trichloroethylene
TEMPO	(2,2,6,6-Tetramethylpiperidin-1-yl)oxyl
THF	Tetrahydrofurane
TLC	Thin layer chromatography
TMP	2,2,6,6-tetramethylpiperidine
TMS	Tetramethylsilane
TMS-	Trimethylsilyl
TPT	Triphenylpyrylium
UV	Ultraviolet light
Vis	Visible light

TABLE OF CONTENT

1. Introduction

Carboxylic acids play a crucial role in our daily life and are used in various fields. For instance, esters of *ortho*-phthalic acid are used as plasticizers in the polymer industry, while other simple carboxylic acids have a significant role in the food industry.[1] They are often used as flavor or fragrance substances, such as ascorbic acid or citric acid, or they can be important preservatives, such as propionic acid and its salts.

Additionally, they hold a fundamental role in numerous pharmaceutical formulations, often serving as anti-inflammatory agents or cholesterol-lowering drugs. Atorvastatin, a representative of the latter category, is one of the most profitable prescription drugs thus far reported.[1,2]

Due to the diverse and extensive use of this compound class, various industrial processes have been developed to produce it on large scale in order to meet the existing demand.

While there are also important industrial syntheses starting from other precursor molecules, such as the Monsanto process (and its derived Cativa process) for acetic acid synthesis from methanol, in many large-scale processes, olefin building blocks are preferred as substrate sources. This is mainly due to their favorable and abundant availability from the petrol industry.[3,4]

The most significant industrial process dates back to Otto Roelen's discovery in 1938, known as the hydroformylation reaction which remains one of the most widely used methods for the synthesis of linear carboxylic acid products through oxidation of the corresponding aldehydes (Scheme 1).

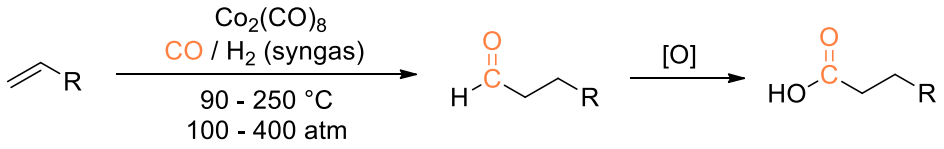

Scheme 1: Otto Roelen's general hydroformylation (& oxidation) strategy.

Although this process is well-researched and controllable, it has the disadvantage of requiring at least two synthetic steps to convert an olefin to a carboxylic acid. An alternative method that circumvents the multi-step synthetic approach was published by Walter Reppe at BASF published that reported the direct hydrocarboxylation of olefins to linear carboxylic acids. This process remains one of the main production methods for various carboxylic acids, such as the synthesis of propionic acid, alongside the hydroformylation-oxidation method.[3–6]

All the processes have the use of carbon monoxide as the carbonylation or carboxylation source in common. This molecule, generally known for its extremely high toxicity, poses significant logistical challenges in terms of handling and storage. In an era where sustainable chemistry is gaining an increasing influence on science and industry, other potential C1 sources, i.e., molecules carrying functional groups attached to only one carbon atom, such as CO_2 or formates, have attracted growing interest in recent decades.[4,7]

The latter C1 source, besides significantly lower toxicity, also has another decisive advantage over carbon monoxide: Its availability in both liquid and solid state (in the form of salts) allows easier laboratory handling and industrial-scale application/processing. Modern methods, such as microreactor synthesis, combinatorial synthesis, and high-throughput synthesis, are much better suited for handling liquid/solid systems compared to gaseous ones, making HCOOH and its derivatives very attractive surrogates for CO.[8]

The first direct transition metal-catalyzed hydrocarboxylation of olefins using formic acid as the C1 source dates back to Simonato *et al*. in 2001. Under strong acidic conditions, formic acid is dehydrated, generating CO *in situ*, which is then converted by the iridium catalyst at temperatures above 150 °C (Scheme 2).[8–10]

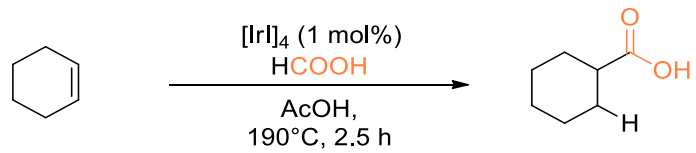

Scheme 2: First discovered transition metal-catalyzed hydrocarboxylation reaction with HCOOH.[8]

Similar reactions are also possible with other transition metal complexes, as demonstrated by the continued work of Simonato *et al*.[11] using rhodium-based and the work of Shi *et al*.[12] using palladium-based catalysts.

Despite these impressive advancements, these methods also bear significant disadvantages compared to the direct use of CO gas. Successful transformations, often leading to just moderate yields, mostly require harsh conditions, such as very high temperatures and the need for a highly acidic environment, leading not only to high energy consumption and poorer atom economy, compared to the original processes with carbon monoxide, but also severely limiting the range of substrates that can withstand these conditions.[8]

Although recent research, such as the work of Beller and co-workers,[13] aims to address and mitigate these issues, the reaction conditions remain one of the biggest challenges for the hydrocarboxylation of olefins using formic acid as a C1 source.

Due to the thermodynamically favored and difficult-to-control side reaction in which formic acid decomposes to CO_2 and hydrogen gas instead of CO and water, acidic environment and elevated temperature are often necessary to favor the latter reaction pathway[13] (Scheme 3).

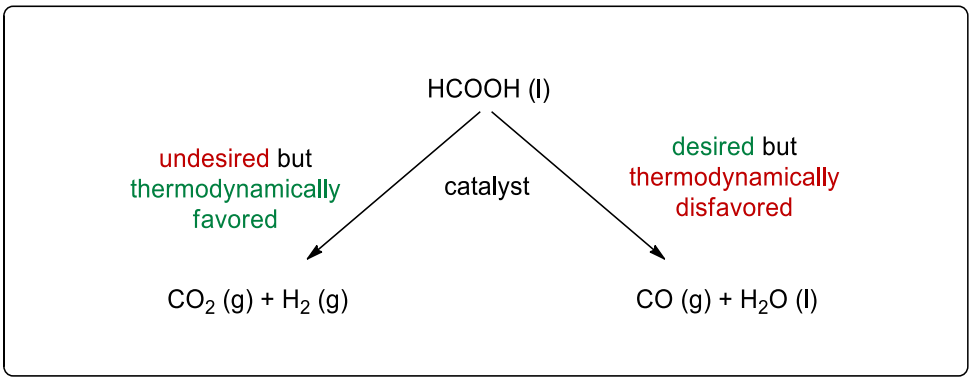

Scheme 3: Decomposition products of HCOOH hydrogen source in decarboxylation reaction.[13]

Combined with the rapidly growing popularity of the research field of photochemistry, in recent decades, these circumstances have led to an increasing focus on alternative synthesis methods based on photocatalysis instead of traditional transition metal catalysis, with the aim of developing reaction setups that can be performed under milder conditions.

2. Photochemical Transformations

The field of photochemistry is a research branch that dates back to over a century, and it was originally based on sunlight as the sole light source. At that time, only a few known light-induced chemical transformations existed, most of which were accidentally discovered. As a result, photochemistry was long perceived as a niche area in organic synthesis. However, this perception fundamentally changed in the second half of the last century with the development of a wide range of affordable light sources, ranging from household lamps to LEDs. The availability of various light sources, controllable in terms of intensity, wavelength range, and other parameters, enabled photochemical research to be conducted not only more effectively but also reproducibly.[14,15]

As early as 1912, Ciamician, one of the pioneers of photochemistry, already envisioned that photochemistry would become the environmentally friendlier alternative to classical thermochemistry in the future. Although this prediction has not yet been fully realized, photochemistry is regarded today as a promising "greener" alternative, particularly in times when sustainability is increasingly valued.[16–18]

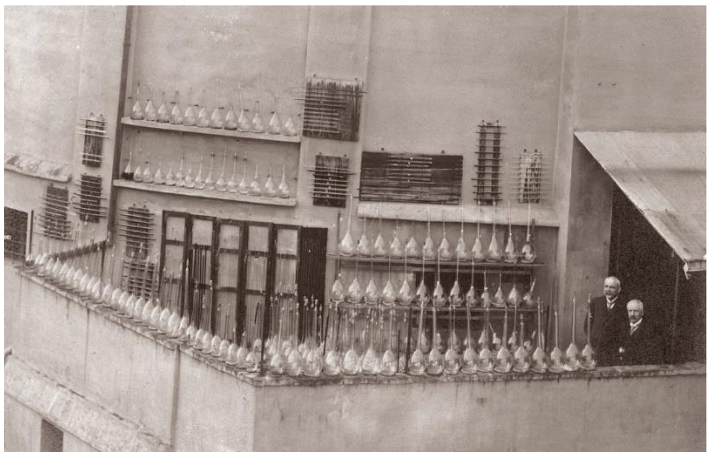

Figure 1: Ciamician and Silber conducting photochemical experiments under sunlight at the University of Bologna (ca. 1912).[17]

This is not only because alternative, often milder energy input methods can be used instead of classical heat-transfer methods, but also because photochemical transformations often exhibit better atom economy than their thermal counterparts. The reasons for this can vary: Firstly, substrates can get directly and selectively excited and transformed, thus eliminating the need for additional aiding reagents and, therefore, minimizing the formation of byproducts. Secondly, photosensitizers or photocatalysts can often be employed, which are only required in minimal quantities. Also, often environmentally benign solvents, such as water and some ionic liquids, can be applied, which are generally preferable, especially for industrial-scale synthesis.[17,18]

Another essential reason for the growing interest in photochemistry in recent decades is its complementarity and orthogonality to classical thermochemistry. Photochemistry allows for transformations that would be virtually inconceivable in thermochemistry, as it can produce thermodynamically disfavored products, such as small-ring systems (Scheme 4).[17,18]

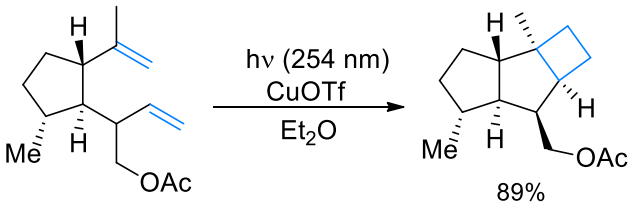

Scheme 4: Example of a [2+2] photocyclization, which would be impossible under standard thermodynamical conditions without any usage of light.[18]

Additionally, thermally hard-to-achieve decomposition reactions, isomerization (Scheme 5), additions, eliminations, hydrogen-atom transfer reactions, and single-electron transfer reactions can be synthetically exploited.[17,18]

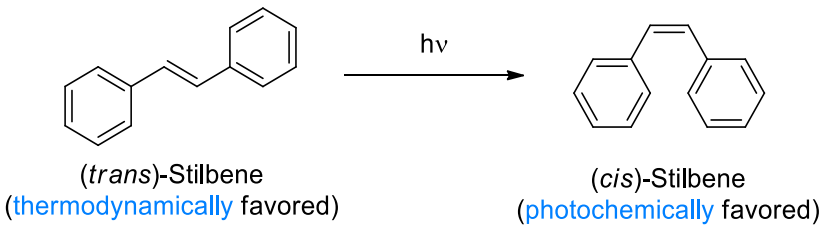

Scheme 5: Example of a photoinduced *trans-cis* isomerization.[19]

2.1 Essential (Photo-)physicochemical Factors

In designing a successful photochemical/catalytic reaction setup, knowledge of several important photo-physicochemical and electrochemical properties is essential. The reactivity of photochemical systems can be explained using the Jablonski scheme (Figure 2). Prior to irradiation (hν) with a light source, the substrate or catalyst is in its ground state s_0 and gets excited to the singlet excited state s_1 through photon absorption. From this state, the molecule has three possible pathways to release its excess energy.

- The first possibility, which occurs in most cases, would be the release of excess energy through internal conversion, which represents a non-radiative pathway.
- An alternative way to release energy would be in form of light emission, a radiative transition pathway, commonly known as fluorescence.
- The last possibility is the transition from the singlet state s_1 to the spin forbidden triplet excited state t_1, known as intersystem crossing (ISC). This is particularly desirable for photoredox catalysts, as the reverse transition and relaxation to the ground state are also spin forbidden, allowing for a longer living excited state.

Similarly, to the excited singlet state, in the triplet state, the molecule then can release energy either radiatively, also referred to as phosphorescence, or non-radiatively through internal conversion. In the latter possibility, which initiates a photochemical reaction, excess energy is dissipated through a chemical reaction. Essentially, this process can be classified in energy transfer (EnT) and electron transfer (ET).[20]

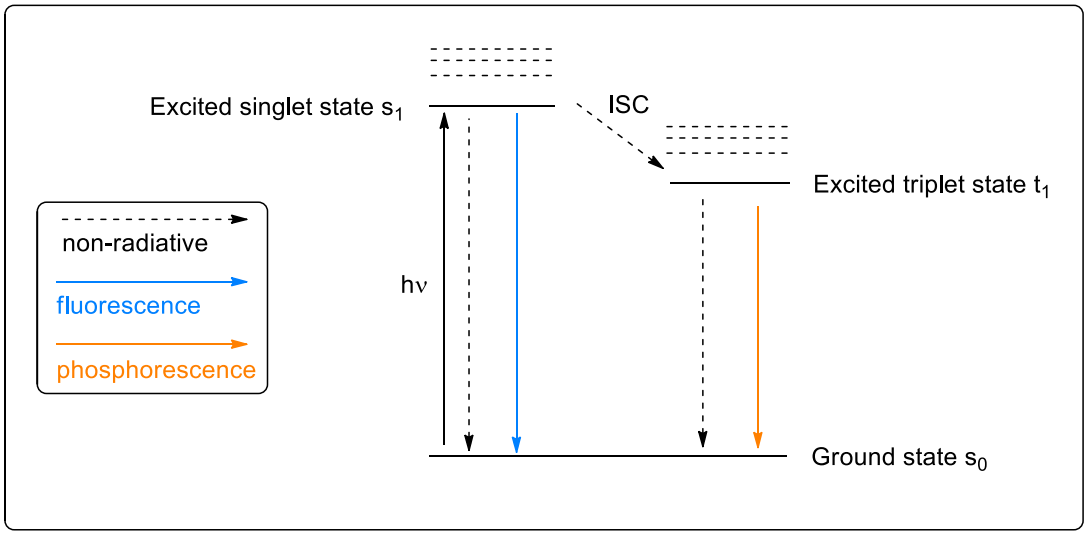

Figure 2: Simplified Jablonski scheme.[20]

These processes are crucial for the design of the reaction setup, ranging from the choice of the light source to the selection of substrates, reagents, solvents, and, if considered, the catalyst design. These choices depend on the specific photophysical and electrochemical properties of the involved components.[20]

2.1.1 The Light Source

For successful excitation of the target molecule or catalyst, there needs to be some degree of overlap between the absorption band of the molecule of interest and the emission source. Ideally, the absorption band of the corresponding molecule should be red-shifted to minimize the energy required for excitation. This helps avoid excitation of other reactants in the system and minimizes competing photochemical reactivity.[20]

Light-emitting diodes (LEDs) have proven to be extremely useful for this purpose, as they provide high intensity and cover a very narrow emission wavelength range, thereby allowing for maximum selectivity in excitation (Figure 3).[20]

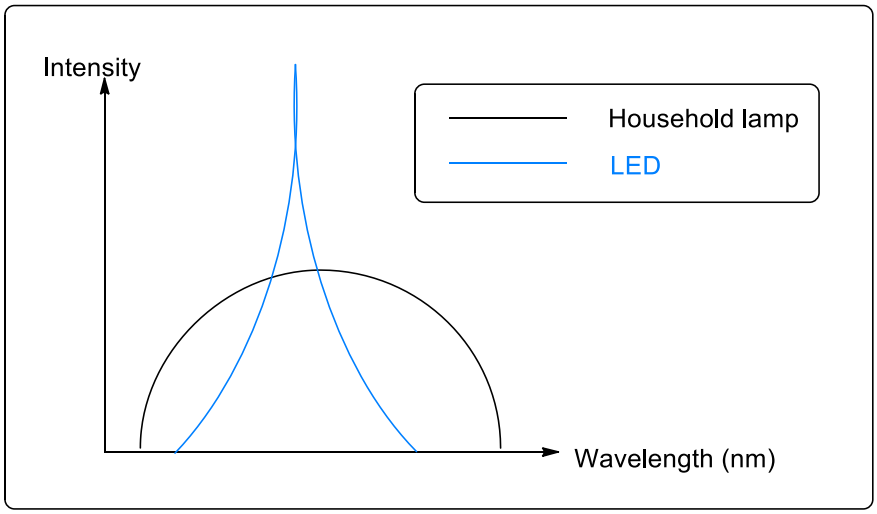

Figure 3: (Simplified) scheme comparing a LED with a household lamp.[20]

2.1.2 Quantum Yield and Lifetime of the Excited State

For a bimolecular photochemical reaction to occur, the excited molecule must remain in its excited state long enough to undergo a reaction before competing non-radiative pathways come into play. For singlet excited states s_1, a general rule of thumb is that the fluorescence lifetime (usually 2-20 ns) corresponds to the excited state lifetime ($\tau_f = \tau_{S1}$), as non-radiative transitions are typically slower than fluorescence. The fluorescence quantum yield φ_f provides information about competing relaxation pathways. A higher value of φ_f approaching 1 indicates a lesser chance of competing non-radiative transitions.[20]

For triplet excited states t_1, the quantum yield of intersystem crossing φ_{ISC} is crucial. Due to the unallowed spin-crossing, triplet states are long-lived (μs to ms), so there is no temporal competition through relaxation to the ground state in bimolecular reactions. However, φ_{ISC} must be as high as possible so that a large proportion of the excited molecules are in the triplet state rather than the singlet state. This helps to exclude competing relaxation pathways from the excited singlet state s_1 to the ground state s_0. In reaction systems where the excited triplet state is desired, the oxygen-containing atmosphere must also be considered, as molecular oxygen also naturally occurs in its triplet ground state. This means that either the reaction must be carried out under oxygen exclusion, or the reaction design must be adjusted with incorporation of O_2 into the system.[20]

2.1.3 Electrochemical considerations

For photochemical electron transfer reactions, it is advantageous to know not only the redox potentials of the involved reactants in the ground state but also their corresponding potentials in their excited states. The same principles as for classical redox chemistry apply here. For a potentially successful reduction, the excited-state reducing agent must have a more negative potential $E(M^*/M^{+\cdot})$ than the substrate in the ground state $E(S/S^{-\cdot})$. Conversely, for a potentially successful oxidation, the excited-state oxidizing agent must have a more positive potential $E(M^*/M^{-\cdot})$ than the substrate in the ground state $E(S/S^{+\cdot})$.[20]

2.2 Types of Photochemical Reactions

Generally, one can distinguish between several types of photoinduced reactions. In general, three subgroups can be distinguished: direct photoexcitation, reactions proceeding *via* an electron-donor-acceptor (EDA) complex intermediate, and reactions conducted with the involvement of a photocatalyst. However, there are also hybrid systems, such as dual catalysis, that incorporate other catalytic methods such as organocatalysis.

2.2.1 Direct Photoexcitation

Direct photoexcitation is the oldest and most straightforward method to initiate a photochemical reaction (Scheme 6). The substrate gets irradiated with photons and is consequently excited to the singlet state. From there, it can either react directly or undergo intersystem crossing to transition to the longer-living excited triplet state. From the excited state, it can undergo either pericyclic or, more commonly, radical reactions. In the case of radical reactions, the excited compound can either react directly in a radical fashion, as often observed in photochemical carbonyl chemistry[21], or it can first undergo a decomposition into multiple subcomponents, at least one of which is a radical, leading to subsequent reactions with a corresponding reactant.[15,22]

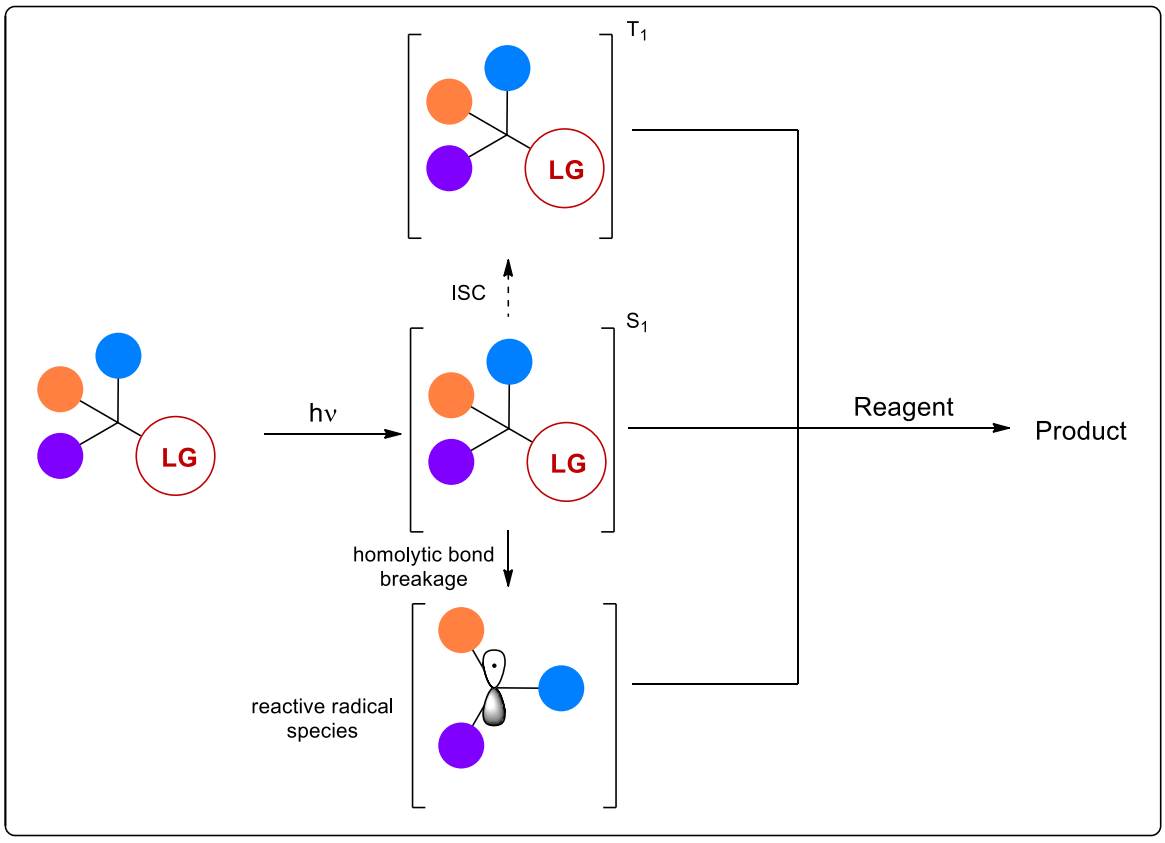

Scheme 6: General scheme for direct photoexcitation.[22]

Even if this method is the oldest and, therefore, most extensively studied approach, it continues to play a crucial role in the synthesis of otherwise difficult-to-access four-membered ring systems, such as cyclobutanes and oxetanes (Scheme 7). The latter can be synthesized through the well-known Paterno-Büchi reaction, where the component containing the carbonyl group gets irradiated, so the excited state can then react with an olefin. This mechanism can proceed either through a pericyclic [2+2] cycloaddition or a radical pathway. Depending on whether the carbonyl group is in the excited singlet or triplet state, different products can be obtained. While the reaction in the triplet state is regioselective, the reaction in the singlet state is stereospecific. The photochemical synthesis of these ring systems plays till these days an important role, which is why the Paterno-Büchi reaction and other photoinduced [2+2] cycloadditions remain relevant in research.[15,21,23,24]

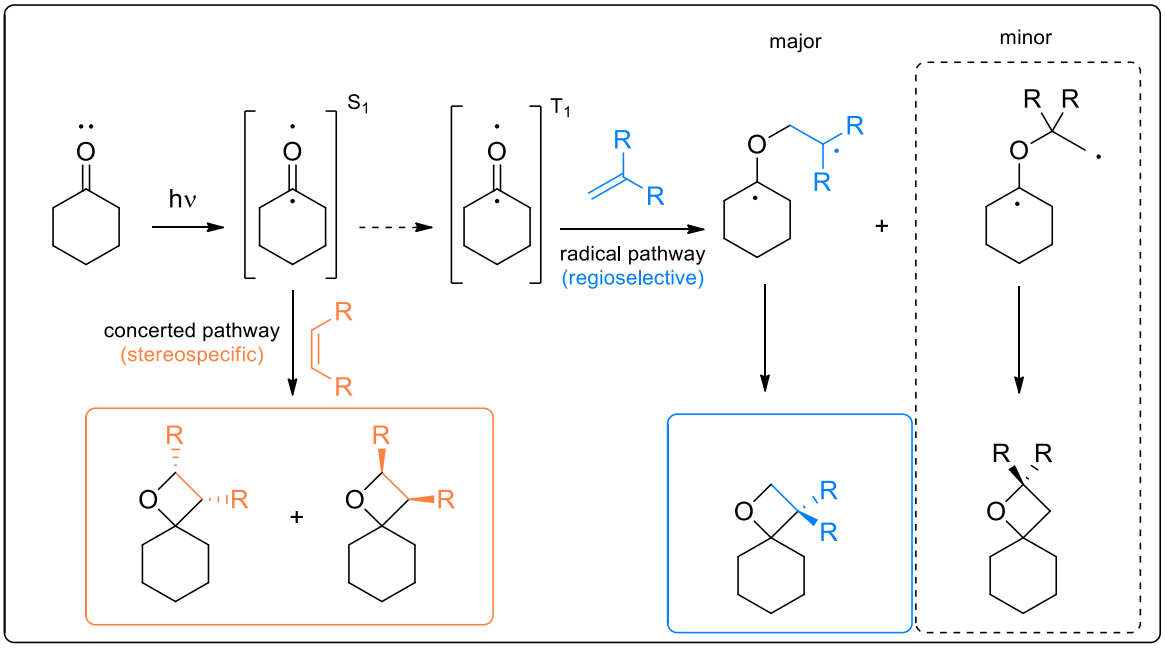

Scheme 7: General mechanistical principle of the Paterno-Büchi reaction.[21]

However, the Paterno-Büchi reaction is not the only important classical representative of this subgroup. In general, the photochemistry of the carbonyl group is considered one of the longest-studied disciplines in this subclass, and well-known reactions, such as the Norrish type I & II reactions, are still used in the synthesis of complex natural products (Scheme 8).[21,25]

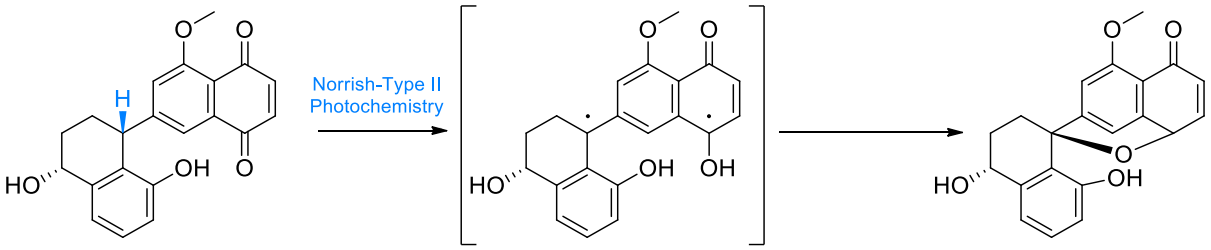

Scheme 8: Building block synthesis (total synthesis of Spiroxin C) *via* Norrish-Type II photochemistry.[25]

One major limitation of direct photoexcitation is that many substrates, such as olefins or carbonyls, are often unable to absorb light in the visible region due to their small chromophore systems, so light with higher energy is often required. Therefore, UV radiation is usually required to achieve quantitative excitation levels. In the context of sustainable chemistry, there is an increasing trend toward designing reactions that can take place in the visible range.[15,22]

Many modern methods employ a reaction system where the substrate already possesses an extensive chromophore system, thereby enabling it to absorb light in the visible region. The excited substrate then undergoes a bond breakage, and the *in situ*-formed radical can, subsequently, react directly with a second added reactant to form the desired product.[22]

One example is represented in Barton *et al.*'s work (Scheme 9A), demonstrating an interesting deprotection-cascade-alkylation reaction approach from carboxylic acid precursors.[22] Furthermore, Melchiorre *et al.*[26] (Scheme 9B), and Schröder *et al.*[27] (Scheme 9C) showed that Hantzsch esters can be excellent and readily accessible starting materials for photochemical provision of reactive radical species than can be used in hydroalkylations[26] and hydroacylations.[27] These reactions, along with many other examples, present interesting possibilities for C-C bond formation[28] and offer the advantage of avoiding transition metal catalysts, which often require/incorporate expensive elements such as palladium or platinum and are nowadays most frequently used in C-C coupling reactions.

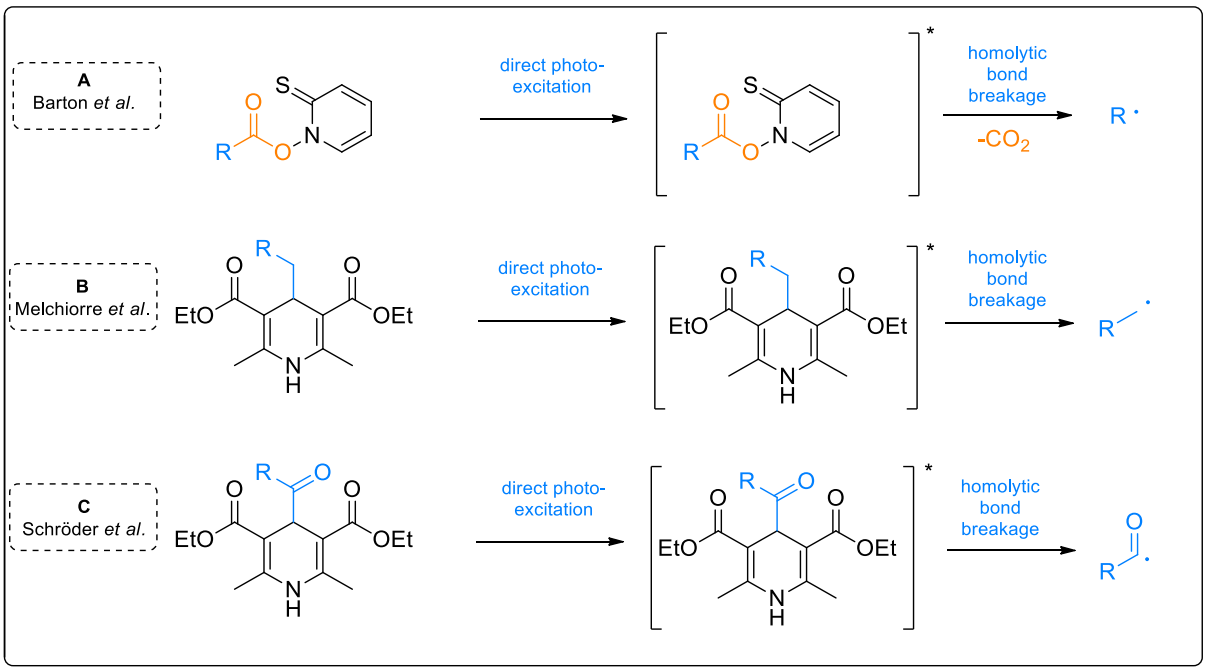

Scheme 9: Representatives for the principle of direct photoexcitation followed by homolytic bond breakage, providing a reactive alkyl- (A & B) or acyl- (C) radical species.[22,26,27]

Another emerging trend is the combination of direct photoexcitation with organocatalysis. For example, Melchiorre demonstrated in 2015 that the alkylation of aldehydes and ketones is photochemically feasible if firstly a conversion to a reactive, excitable enamine intermediate is done *in situ* (Scheme 10).[29]

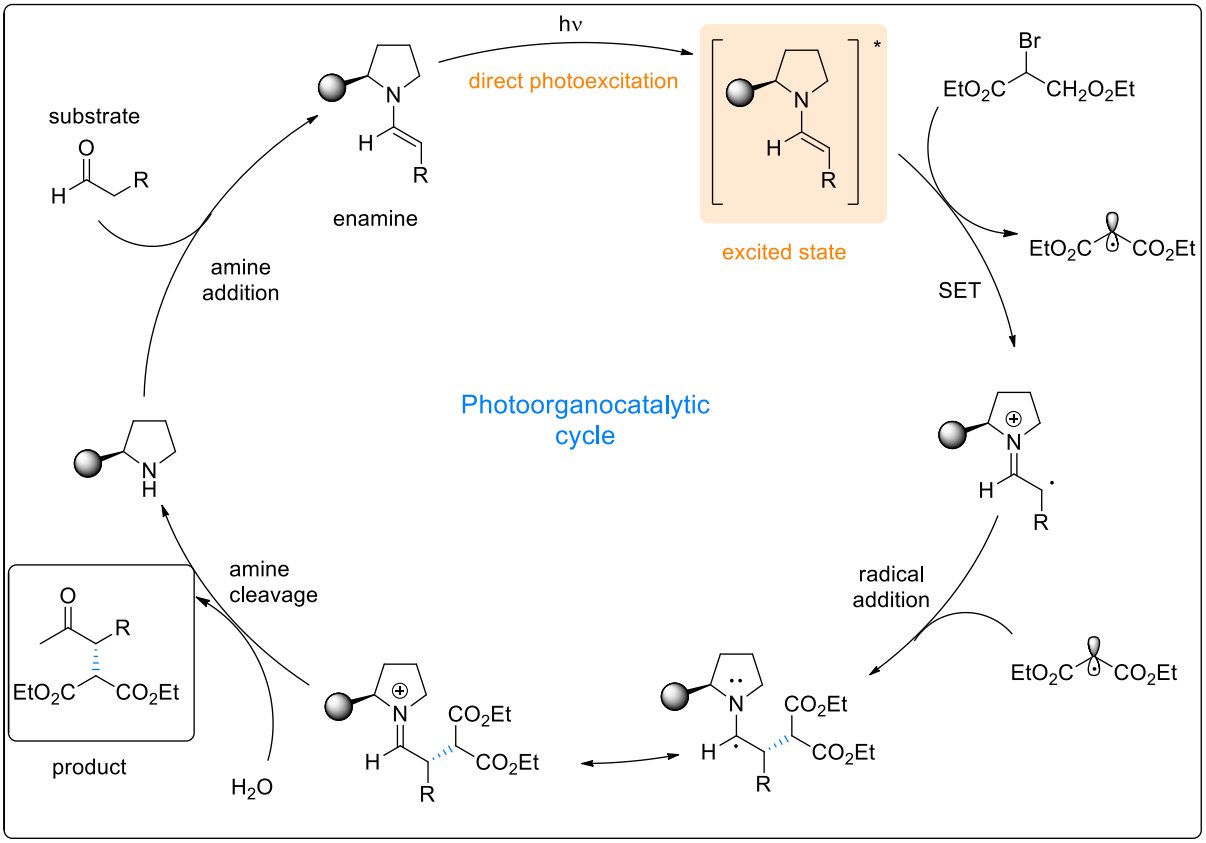

Scheme 10: Proposed mechanism for the organocatalytic α-alkylation of aldehydes *via* direct photoexcitation.[29]

2.2.2 Electron-donor-acceptor Complexes

An alternative to classical direct photoexcitation is the utilization of electron-donor-acceptor (EDA) complexes. The advantage of this methodology lies in the fact that two molecules, which individually would not be capable of absorbing light in the visible spectrum, can expand their chromophore system by forming such a complex. As a result, the *in situ*-formed colored complex can absorb light in the visible region. The excited complex then undergoes a single electron transfer (SET), wherein an electron from the donor molecule is transferred to the acceptor molecule, leading to the formation of reactive radical-ion species that can engage in subsequent reactions with other reactants to yield the desired product (Scheme 11).[22,30]

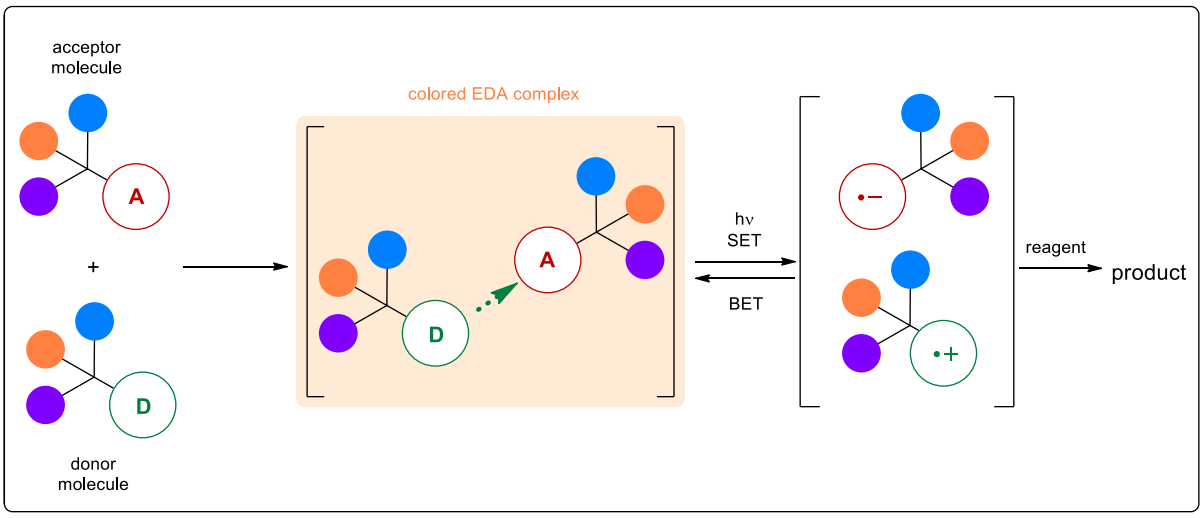

Scheme 11: General scheme for photochemical EDA-complex strategy.[22,30]

A commonly encountered issue is the back electron transfer (BET) from the charged radical species leading to the backformation of the complex, which often competes kinetically with the radical follow-up reaction. In many cases, a leaving group is attached to one of the starting molecules to circumvent this problem. After the SET has occurred, the leaving group can undergo irreversible detachment, thereby preventing any reverse reaction or BET.[22,30]

Although Mulliken *et al*. already investigated the formation of EDA complexes in his quantum chemical studies in 1961,[31] there were only very few synthetic applications of EDA complexes. This is likely due to the fact that photochemistry in the visible range generally had a niche character before the 1980s due to limited setups and equipment. Furthermore, the groundbreaking discoveries in the field of photocatalysis seemed to overshadow EDA complexes as potential alternatives. It was only in 2013, led by the work of Melchiorre *et al*., that this research branch experienced a renaissance and has since garnered increasing interest within the research community.[22,30]

Melchiorre demonstrated a photochemical organocatalyzed α-alkylation of aldehydes and ketones, which proceeds through the formation of an EDA complex (Scheme 12). This method offers the advantage, compared to the direct photoexcitation method (demonstrated in Scheme 10), that the used enamines do not need to be capable of absorbing visible light themselves. Instead, the formation of an EDA complex with an appropriate acceptor molecule takes on this role. Upon excitation of the colored complex, the formation of the radical ion pair occurs through a SET. The acceptor radical anion subsequently undergoes detachment of its leaving group (Scheme 12, marked in red), followed by the addition of the formed radical to the radical cationic enamine species. Conversion of the enamine to the aldehyde or ketone leads to the final formation of the product.[32]

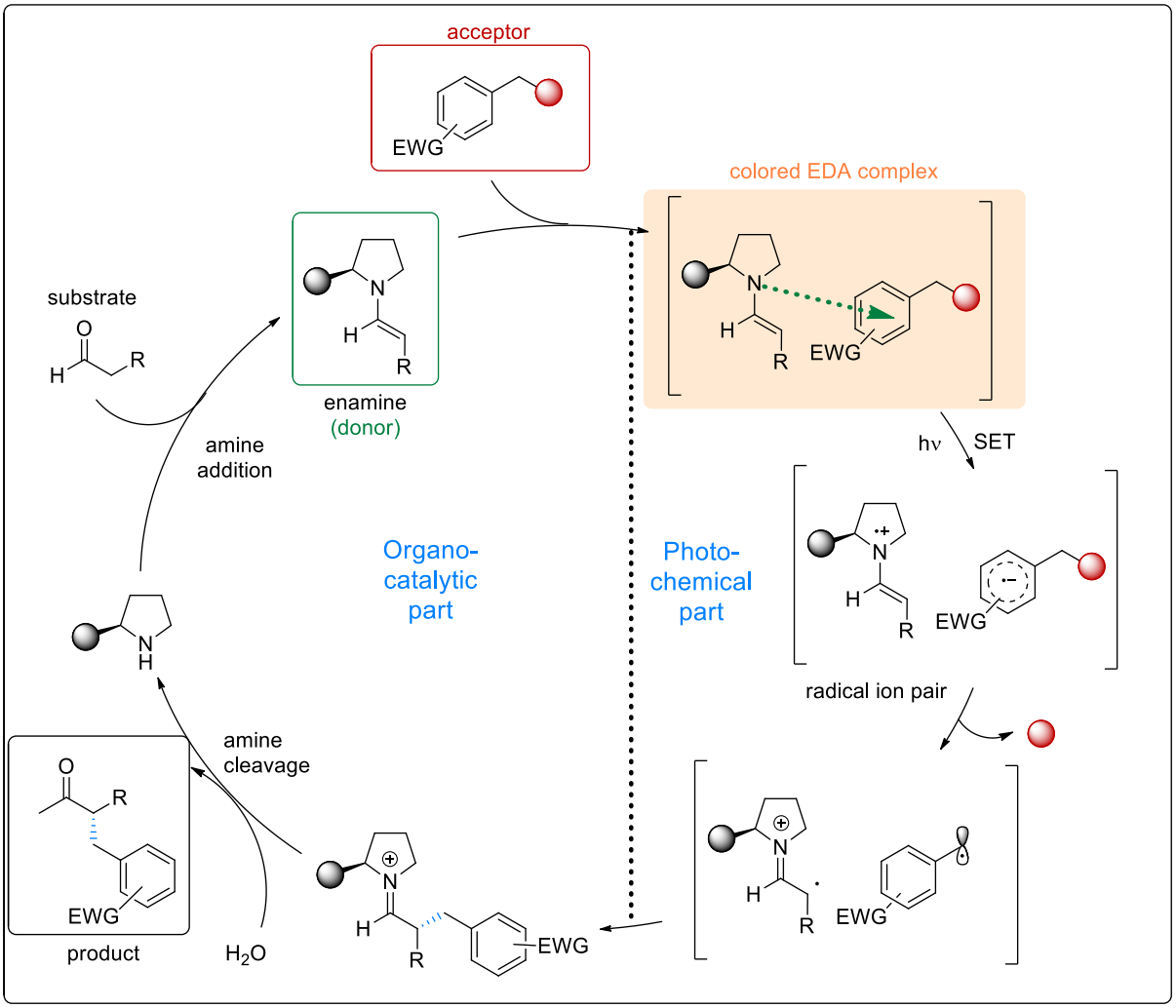

Scheme 12: Proposed mechanism for the organocatalytic α-alkylation of aldehydes *via* photochemical EDA-complex formation stragety.[31]

2.2.3 Photoredox Catalysis

Although both direct photoexcitation and the EDA-complex strategy represent groundbreaking areas in photochemistry and have yielded remarkable results in recent decades, photoredox catalysis is considered the field of photochemistry that has emerged most rapidly in the last decades. Presumably, this can be attributed to several advantages that this branch possesses over the other two sub-types. The two other methods have the major drawback that, in the case of direct photoexcitation, a substrate or, in the case of EDA complexes, a suitable donor-acceptor molecular pair, is required, capable of absorbing light in the visible range, which imposes a strong restriction on the use of corresponding components.

In contrast, the use of photocatalysts allows the conversion of the problem into a catalytically active molecule that can be employed for this purpose, which is used sub-stoichiometrically, and, therefore, does not require the other components, which are involved in the reaction to possess corresponding photophysical and photochemical properties. Additionally, this approach enables better fine-tuning of the catalytically active species to meet the specific needs of the reaction setups in terms of their photophysical and electrochemical properties, such as quantum yield and redox potentials.[20,33]

Photoredox catalysis has been an area of research since the 1980s, as evidenced by the experimental findings of Deronzier *et al.*[34] and Okada *et al.*[35]. However, it took another two decades until the work of MacMillan, Yoon, and Stephenson propelled the field of photocatalysis forward, presumably due to the fact that photoreaction setups were atypical and, therefore, less common in research laboratories. Additionally, the idea of controllable radical chemistry was an unconventional thought in the world of classical polarity-based chemistry at this time.[22,33]

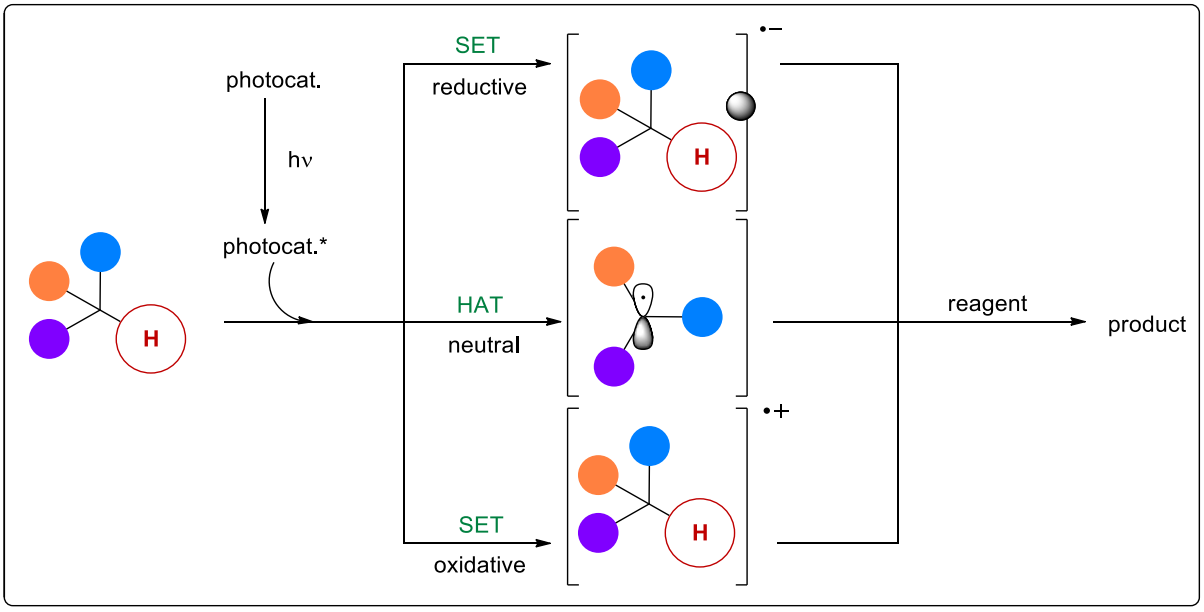

Scheme 13: General scheme for photo(redox)-catalysis.[22,36]

In 2008, MacMillan successfully developed a dual catalytic system for the α-functionalization of aldehydes and ketones (Scheme 14). The *in situ*-formed enamine reacts with the also *in situ*-formed functionalized alkyl radical in an addition reaction. The resulting radical intermediate then undergoes a single electron transfer (SET) with the excited ruthenium catalyst, forming a cationic imine intermediate, which can subsequently be cleaved with water, regenerating the desired product and the organocatalyst. This method shows the advantage in comparison to the similar already mentioned α-alkylation approaches (Scheme 10 & 12), that no stoichiometric co-component must be used, and either no specific adjustments of the amine catalyst or the substrate has to be done in terms of photophysical properties for excitation purposes.[37]

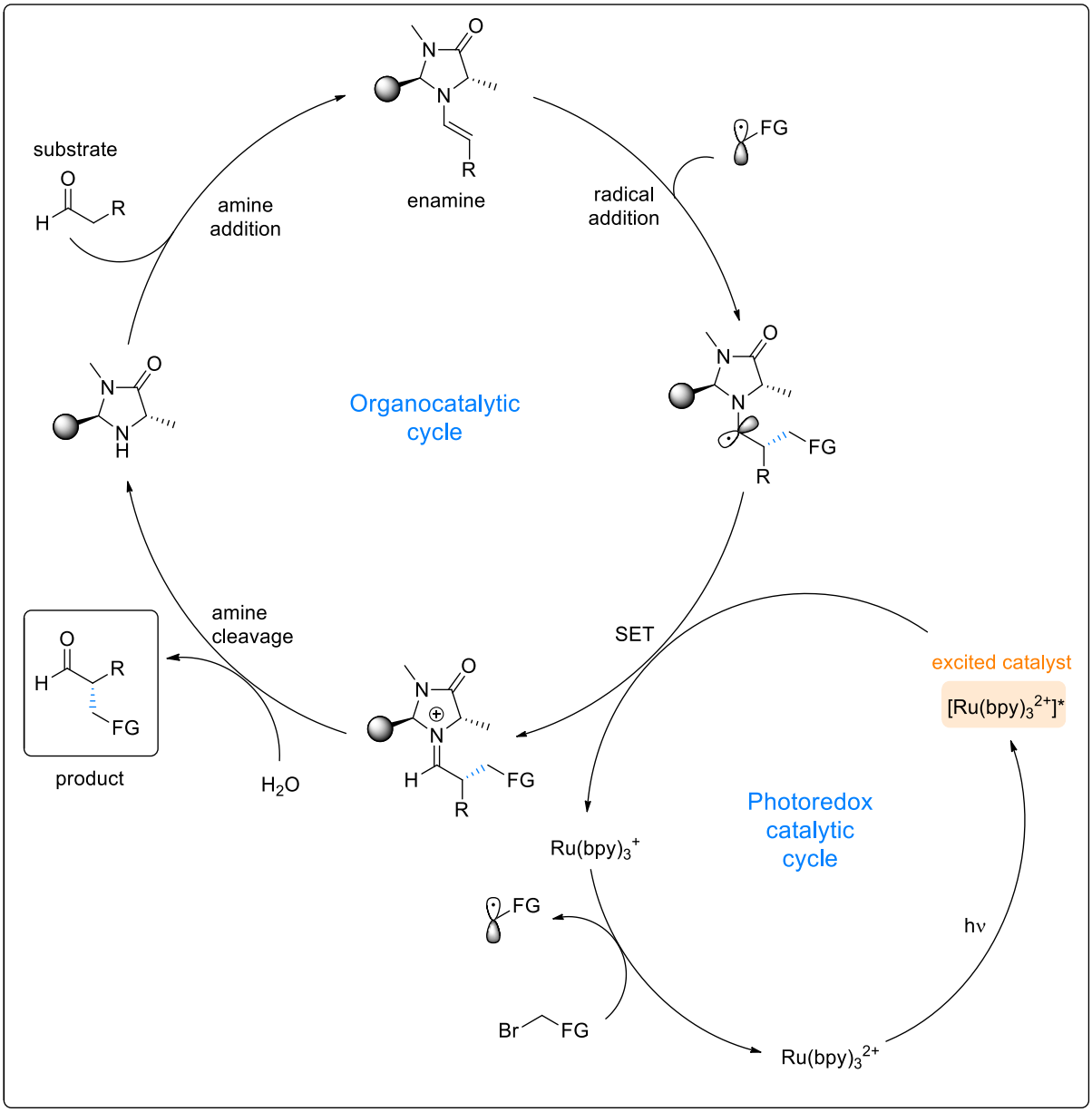

Scheme 14: Proposed mechanism for the dual photo- and organocatalytic α-functionalization of aldehydes.[37]

When a photoredox catalyst is used, it assumes the role of photon absorption. Depending on the redox system, the excited catalyst is capable of either reducing or oxidizing the substrate *via* a SET, with the catalyst itself being reversibly quenched by the substrate in an oxidative or reductive manner. The radical ionic intermediate is then either restored to its original oxidation state by a sacrificial agent or by a reactant involved in the system, initiating a new catalytic cycle[20] (Scheme 15).

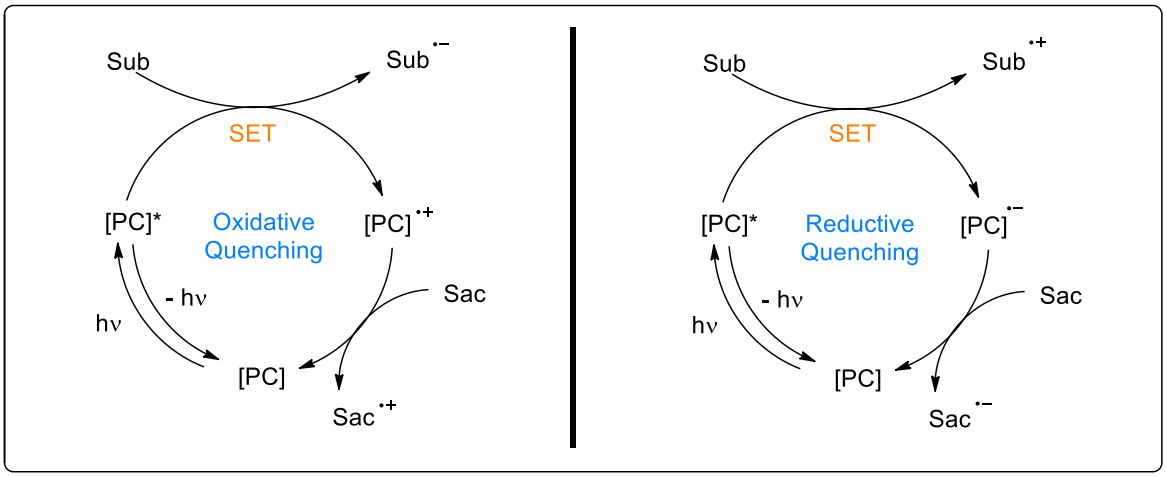

Scheme 15: Basic principle of a photoredox-catalytic cycle.[20]

Due to the rapid development in this research field, several common catalytic systems have emerged in recent decades (Figure 4), with the most common variations based on ruthenium or iridium, typically derived from the original $Ru(bpy)_3$ catalyst. However, today there are also a variety of organic photocatalysts, which often serve as cost-effective alternatives. For example, cyanoarenes are excellent photooxidants, while quinones are similar good photoreductants. Also, more complex xanthene systems are regularly employed nowadays.[20,22,33]

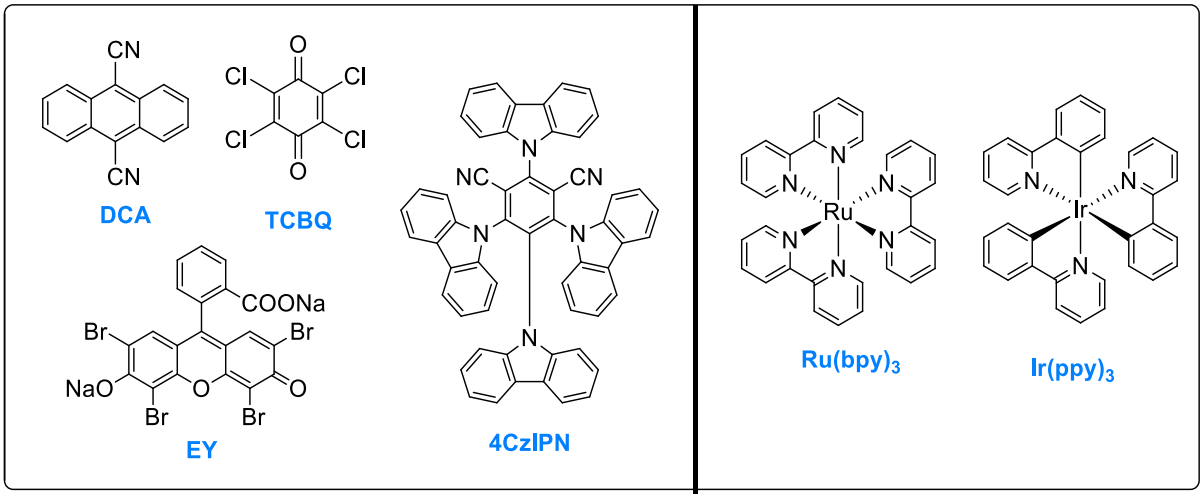

Figure 4: Commonly used photocatalysts (organic compounds, left; metalorganic compounds, right).[20,33]

In addition to classical SET-based photoredox chemistry, another subcategory of photocatalysis has been gaining increasing attention in recent years, in which hydrogen atom transfer (HAT) reactions participate in key steps of the catalytic cycle (Scheme 16). These cycles can proceed exclusively *via* HAT (direct HAT) or involve SET intermediate reaction steps (indirect HAT). What makes these types of reactions so interesting is the fact that they enable reliable and selective C-H activations, which generally pose one of the greatest challenges in classical organic synthesis, making this reaction type currently a subject of much attention.[36]

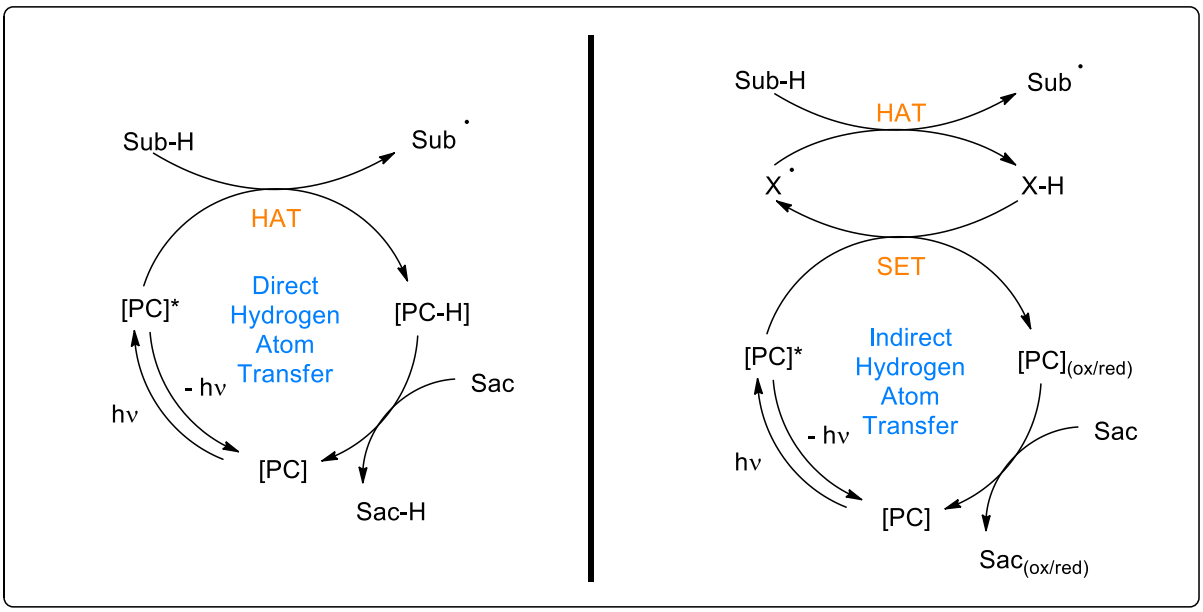

Scheme 16: Basic principle of a photocatalytic cycle involving HAT. (PC = photocatalyst; Sub = substrate; Sac = sacrificial agent).[36]

2.3 Photochemical Hydrocarboxylations

As mentioned earlier, the synthesis of carboxylic acids from olefins represents an economically and ecologically interesting reaction type, which holds significant importance for both academia and industry, as alkenes are often inexpensive and readily available bulk materials.[3,4]

Already discussed in the preceding sections, toxic carbon monoxide still remains the most popular C1 source for carboxylation reactions in the industry, despite the challenges associated with this reagent. In classical thermally driven transition metal catalysis, very harsh conditions are often required to efficiently incorporate CO into the olefin structure.

However, the development of photochemical (hydro-)carboxylations over the last decade offers a variety of alternative approaches, with the advantage that milder conditions and alternative C1 sources, such as formic acid, formates, or CO_2, can often be employed instead.

2.3.1 Photochemical Hydrocarboxylation with CO_2 as the C_1 Source

In the field of photochemical hydrocarboxylations, the utilization of CO_2 as the C1 source has particularly attracted attention, thus resulting in the majority of publications in this field in the recent decade being centered around this molecule. CO_2 offers the advantage of being a non-toxic, inexpensive, and readily available greenhouse gas, which is currently in the spotlight due to climate change concerns. The idea of efficiently incorporating CO_2 into industrially relevant reaction setups is a very attractive option for many researchers as sustainable chemistry and the reduction of CO_2 emissions gain increasing prominence both in media and science.[38,39]

The idea of using CO_2 as C1 source in carboxylations is not restricted to photochemistry; there have been several research reports on the development of thermally driven reaction setups for carboxylations using CO_2. Nevertheless, these methods often suffer from the disadvantage of requiring high temperatures, which contradicts the principle of energy efficiency in the context of sustainability. Additionally, metallic or organometallic reducing agents, such as Mn, Zn, or $AlEt_3$, are frequently used in stoichiometric quantities. In contrast, photochemical approaches can often be conducted under milder conditions and with greater atom economy.[38,39]

In recent years, photochemical visible-light-driven hydrocarboxylations have been developed, achieving regioselective formation of both Markovnikov and anti-Markovnikov products. For instance, in 2017, Iwasawa *et al.*[40] demonstrated a Marknovnikov hydrocarboxylation of styrenes through dual catalysis (Rh(I) transition metal catalysis / $Rh(bpy)_3$ photocatalysis) (Scheme 17A), while Jamison *et al.*[41] achieved a *p*-terphenyl photocatalyzed anti-Markovnikov hydrocarboxylation of similar compounds (Scheme 17B).

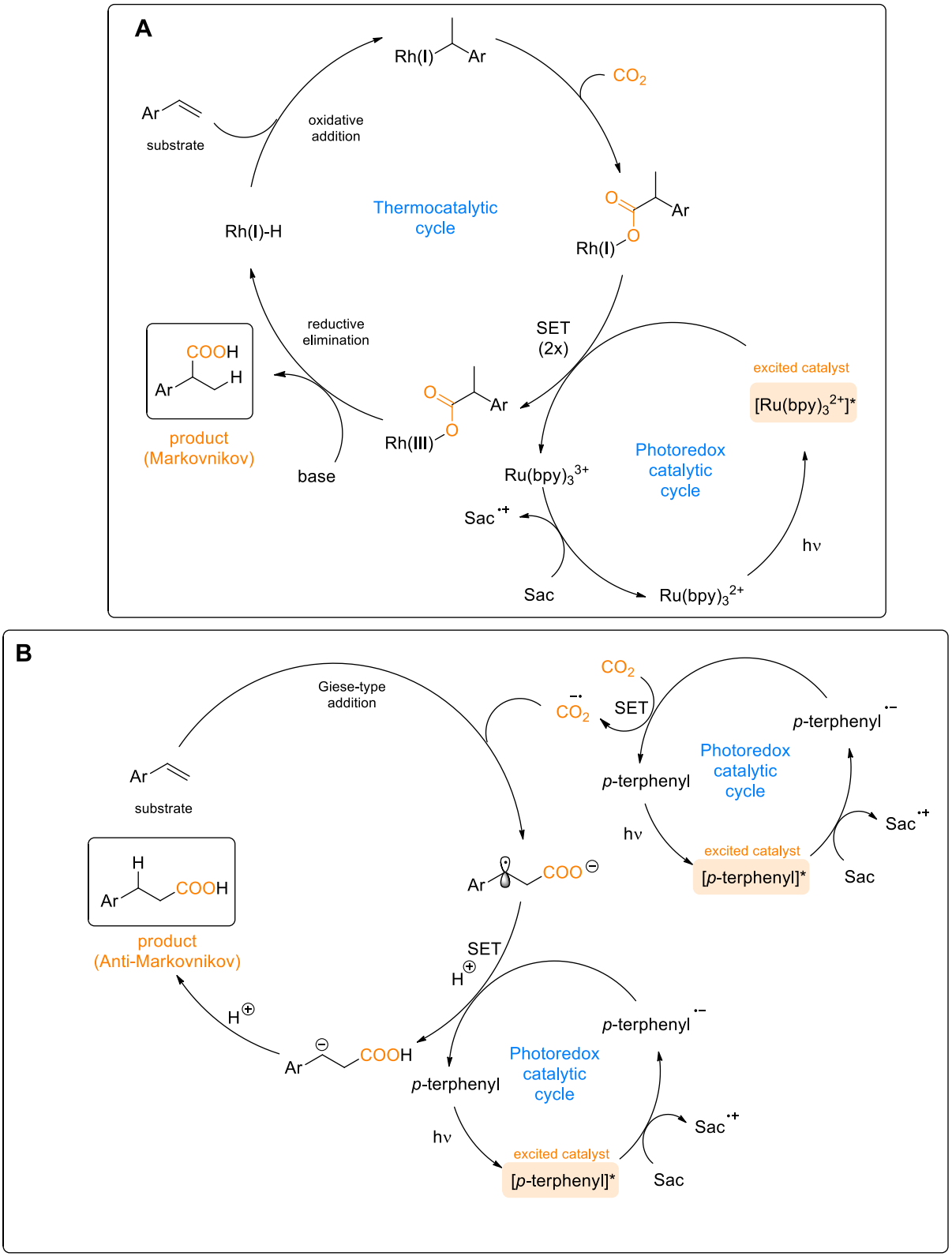

Scheme 17: Proposed mechanism for (A) Markovnikow hydrocarboxylation[40] & (B) anti-Markovnikow hydrocarboxylation.[41]

In addition to classical hydrocarboxylations, other carboxylation variants with similar reaction principles allow for difunctionalization of the olefin. For example, Yu *et al*. and Wu *et al*. enabled photocatalytic thio-,[42] silylo-,[43] and phosphocarboxylations[44] (Scheme 18).

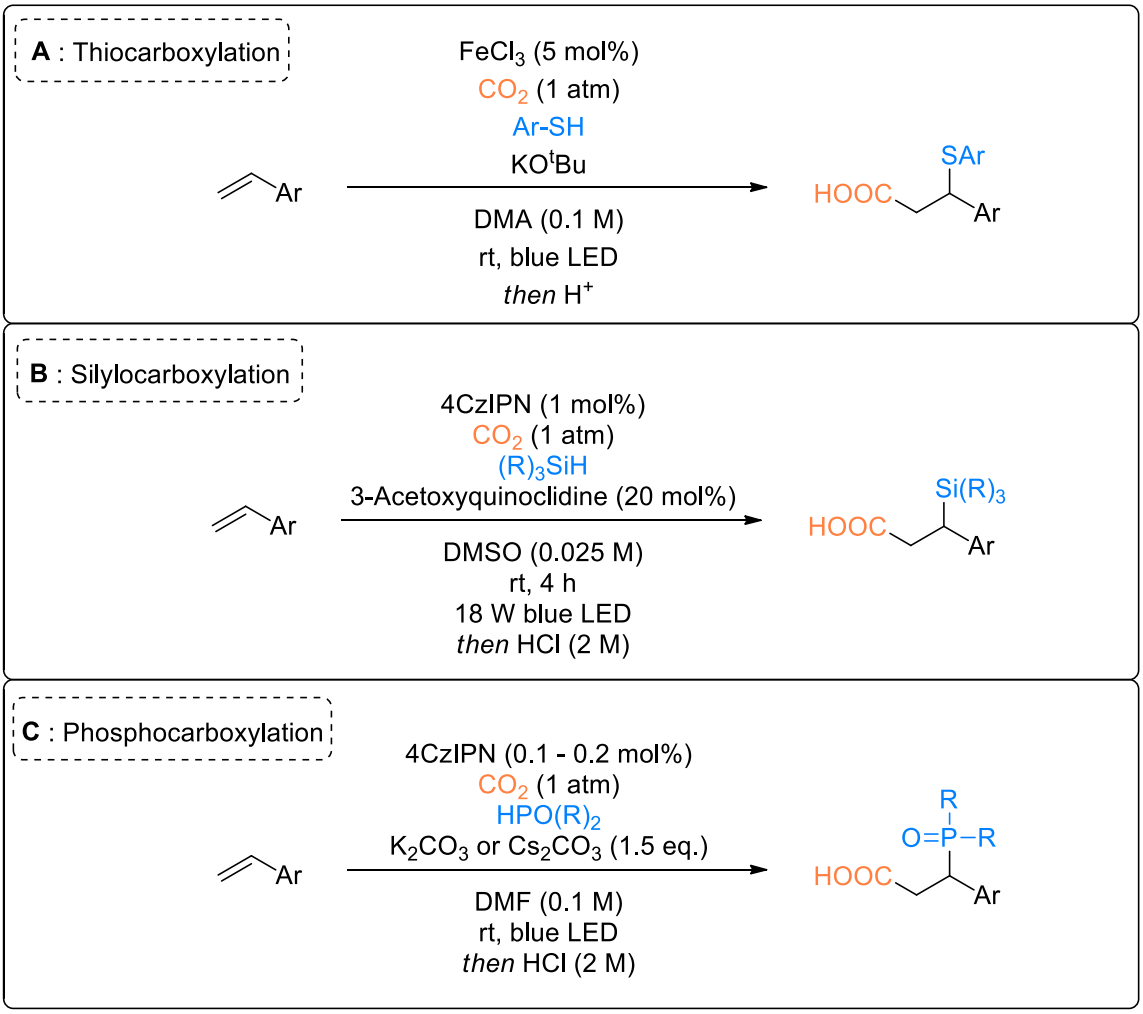

Scheme 18: Photocatalytic carboxylation methods with CO_2. (A) Thiocarboxylation (B) Silylocarboxylation (C) Phosphocarboxylation.[38]

Mechanistically, there are two distinct approaches. The first variant aims to activate CO_2 through SET, converting it into the reactive CO_2 radical anion, which then undergoes a Giese-type addition to the olefin, as exemplified in Scheme 17B. The second variant seeks to convert the alkene into a carbanion, which is then capable of attacking CO_2. For instance, Martin et al.[45] demonstrated this through a photocatalyzed carboxylation of styrenes, using CF_3SO_2Na as the second carbon source (Scheme 19). Instead of a CO_2 radical anion, a styrene carbanionic intermediate is formed *via* single electron transfer with the iridium photocatalyst.[46]

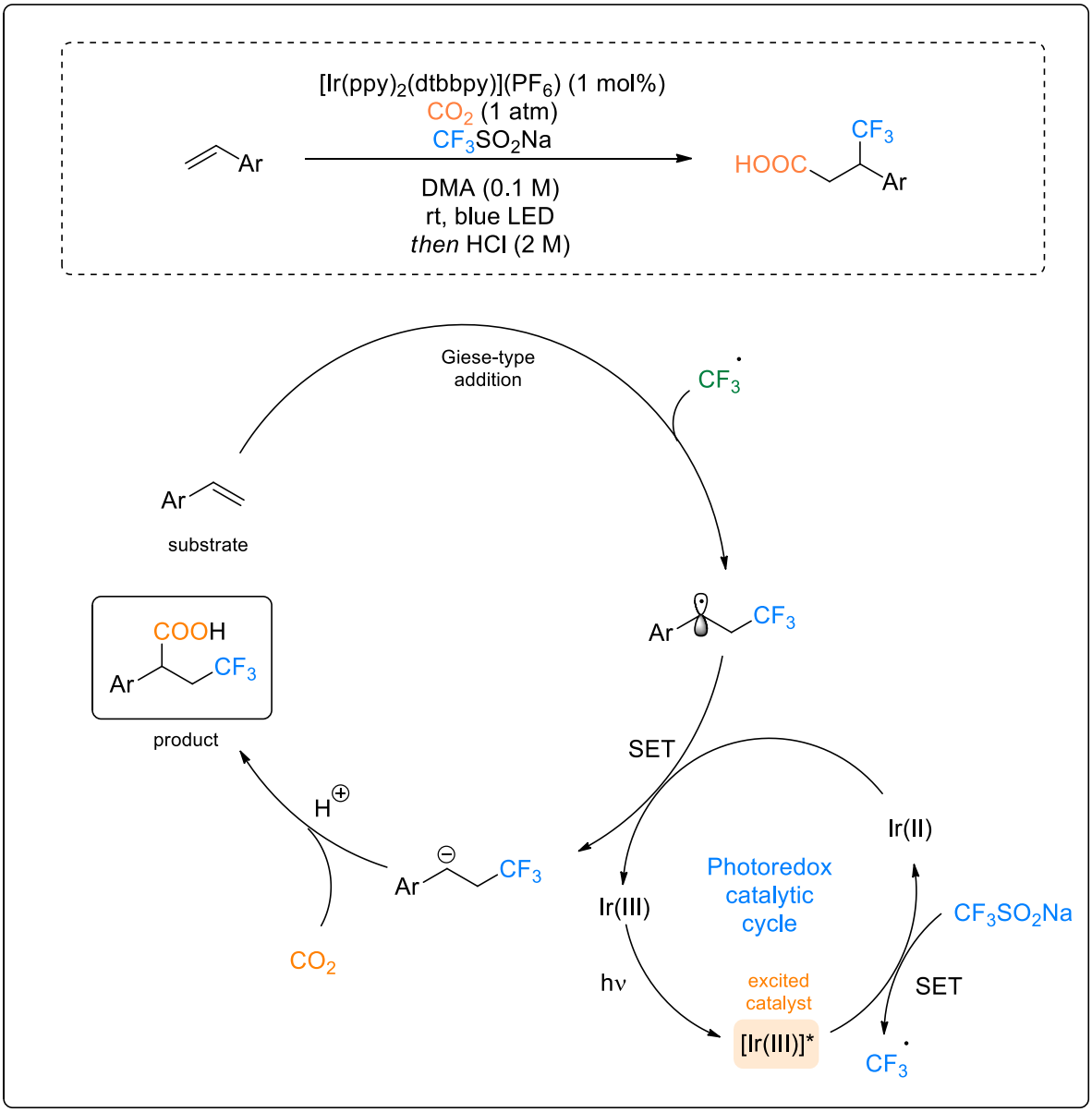

Scheme 19: Proposed mechanism for photocatalytic carboxylation.[45]

While most (hydro-)carboxylations proceed *via* a classical photoredox cycle, where predominantly iridium or ruthenium-based photocatalysts, and occasionally organic photocatalysts, such as 4CzIPN, are employed (Scheme 18B-C), there are indeed other approaches, though less common, that utilize the other two alternative principles of direct photoexcitation[39] or the formation of EDA / CT complexes.[47]

For instance, Yu *et al*. developed a method for anti-Markovnikov hydrocarboxylation of styrenes in 2020, which proceeds through a CT complex intermediate formed by π-π interactions between the styrene ring and the thiophenol ring, enabling a SET (Scheme 20A).[47] Also, due to the work of Yu *et al*. in 2021, a catalyst-free photochemical carboxylation of alkenes could be developed, proceeding through the excitation of the used Hantzsch esters, which act as alkyl radical donors (Scheme 20B).[39]

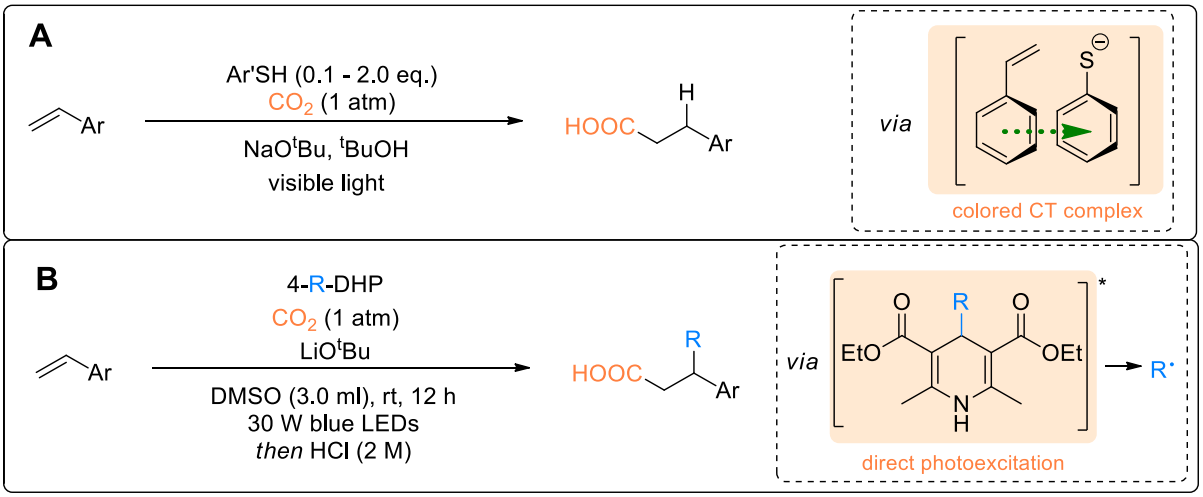

Scheme 20: Photochemical carboxylation reactions with (A) CT-complex formation[47] & (B) direct photoexcitaton.[39]

One of the greatest challenges in photochemical hydrocarboxylation with CO_2 remains the limitation to specific substrates, often requiring activated olefins, such as (ring-substituted) styrenes. Just recently, a photocatalytic hydrocarboxylation of inactivated olefins could be achieved for the first time; however, the exact mechanism behind this process remains to be elucidated (Scheme 21).[48]

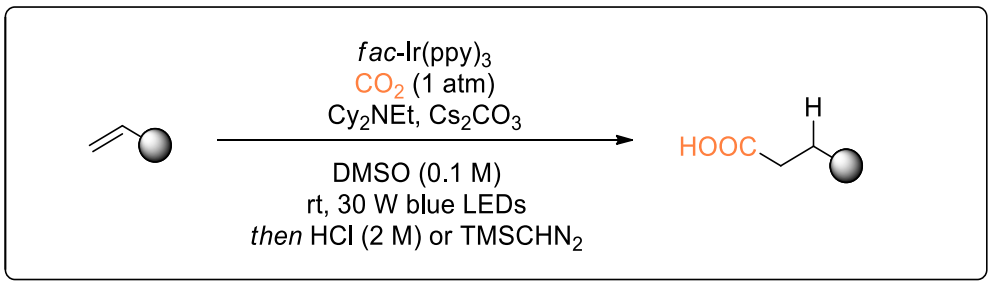

Scheme 21: Photocatalytic hydrocarboxylation of inactivated olefins with CO_2.[48]

2.3.2 Photochemical Hydrocarboxylation with HCOOH as a C1 Source

In contrast to CO_2, significantly less photochemical hydrocarboxylations using formic acid and its salt derivatives instead are known. The examples mentioned in section 2.4.1 represent groundbreaking scientific achievements in the field of photocatalysis, by utilizing a favorable, readily available, and non-toxic gas of such global importance. But even if this offers many advantages, the use of HCOOH also presents some benefits over CO_2 as a C1 source.[49]

As mentioned in Section 1, many industrial systems are generally designed for the use of solid and liquid components, thereby rendering CO_2 gas incompatible with the existing setups/systems. Another issue is that the generation of reactive CO_2 radical anionic species requires strong reducing conditions due to the thermodynamic stability of CO_2 ($E_{1/2}(CO_2/CO_2^-$ = - 2.2 V vs SCE). This fact significantly limits the number of catalytic systems capable of facilitating the necessary SET reaction.[49]

In contrast, HCOOH / HCOO- has the advantage of already being in the appropriate oxidation state, eliminating the need for a SET in this regard. Instead, HAT reagents/catalysts can take on the task of forming the activated radical anion. Furthermore, the presence of a hydrogen atom provides an internal hydrogen source for the respective hydrocarboxylation, thereby rendering the introduction of external reagents unnecessary. These factors make HCOOH a highly undervalued hydrocarboxylation reagent.[49]

Nevertheless, the use of HCOOH as a C1 source for photochemical hydrocarboxylations has also been reported in literature. For instance, *Li et al.*[50] developed, in 2001, a photo-catalyzed hydrocarboxylation of alkenes (especially styrenes and acrylates) using Eosin B as a photocatalyst (Scheme 22A). Mita *et al.*[51] achieved a photocatalytic dearomatizing hydrocarboxylation, in 2023, including substrates such as indoles and benzofurans (Scheme 22B). Additionally, in 2023, Wickens *et al.*[52] successfully developed the first photocatalytic hydrocarboxylation of inactivated alkenes, involving thiols as HAT promoters, thus providing an alternative to Yu's photo-catalyzed hydrocarboxylation of inactivated olefins by using CO_2[48] (Scheme 22C).

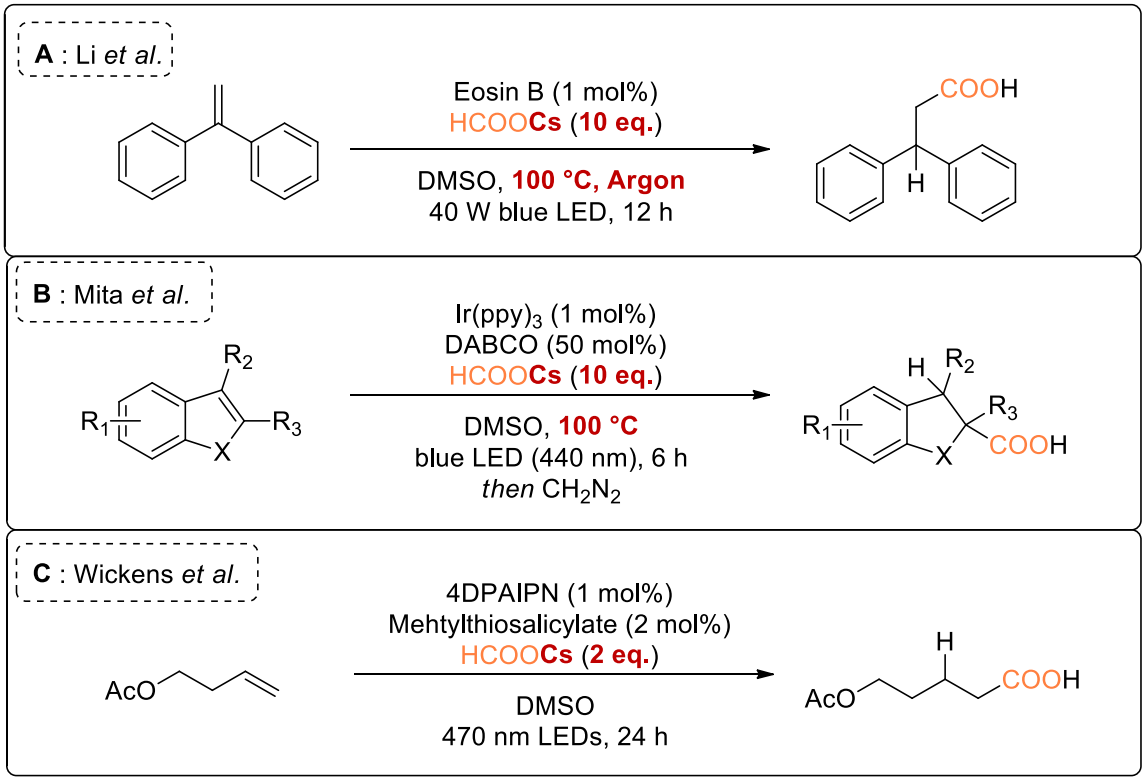

Scheme 22: Photocatalytic carboxylation methods with HCOOCs.[50–52]

3. Aim of the Thesis

The field of photochemistry, especially photocatalysis, has gained significant attention in recent decades. Reactions that were inconceivable under classical thermal or transition metal-catalyzed conditions have become achievable thanks to photochemistry.

One of these approaches is the photochemical hydrocarboxylation of olefins, which holds high relevance both in the industry and in academia, especially as there is a growing desire to move away from cumbersome and toxic chemicals, such as CO.

Although some methods for this purpose are known in the literature, a large portion of them focus on CO_2 as an alternative C1 source, overlooking formic acid and its formate salts along with its advantages. The limited existing literature that utilizes $HCOO^-$ salts usually comes with significant limitations concerning the reaction conditions. Often, large quantities of expensive cesium formates (2.0 - 10.0 eq.) must be used (Scheme 22) since the cheaper potassium or sodium formate salts frequently exhibit solubility issues. Moreover, high temperatures are often required to ensure the desired conversions.

Another problem is the strong substrate class restriction. Most approaches use only electron-rich substrates, such as styrenes. Successful hydrocarboxylation of inactivated and electron-deficient olefins is quite rare.

The aim of the thesis is to address these problems. The pursued goal is the development of a photocatalytic hydrocarboxylation strategy for electron-deficient olefins, allowing for direct use of formic acid under mild reaction conditions and temperatures.

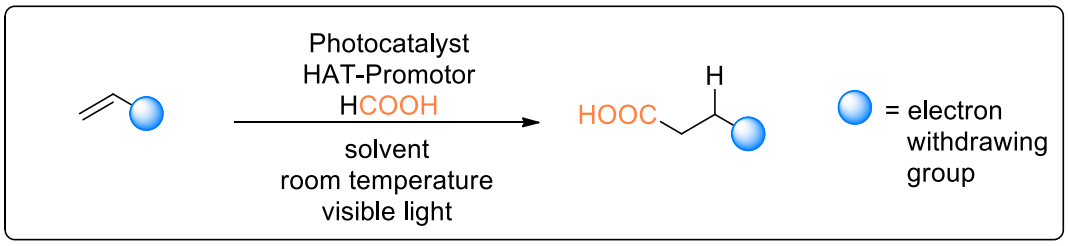

Scheme 23: Proposed photocatalytic hydrocarboxylation approach.

4. Results & Discussion

4.1 Reaction Design

One aim behind the proposed reaction design was to generate a CO_2 radical anion directly from formic acid, which can subsequently undergo a Giese-type addition with the electron-deficient olefin. Consequently, a hydrogen atom transfer (HAT) promoter had to be selected, fulfilling a dual role in the system (Scheme 24).

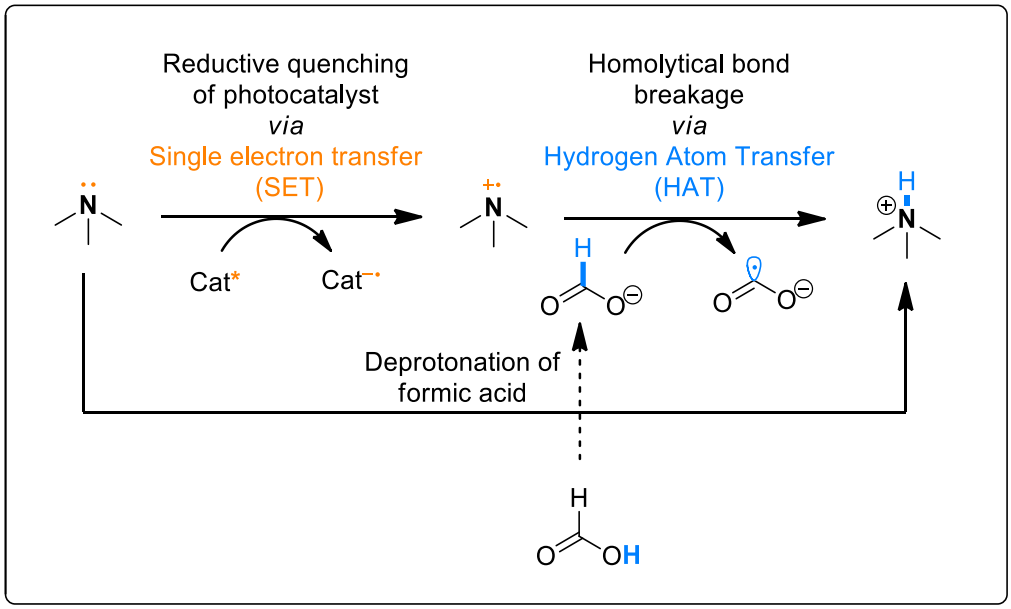

Scheme 24: Desired dual role of the used HAT-promoter.

Firstly, the HAT promoter needed to possess the property of generating a formate anionic salt *in situ* and, therefore, being non-nucleophilic to not undergo addition reactions itself. Secondly, it must be able to perform the hydrogen atom transfer, converting the formate into the CO_2 radical anion. Since common bases in organic synthesis, such as amine bases, are not capable of performing a radical HAT themselves without any help, they firstly need to be converted into a reactive radical species to initiate this reaction step.

To accomplish this, a photocatalyst had to be employed, which activates the amine base by undergoing a reductive quenching cycle following light irradiation. This activated amine base should then be able to undergo a HAT with the formate salt generated from formic acid, resulting in the production of the reactive CO_2 radical anion, which can subsequently react with the olefin.

The initial substrate chosen was benzyl acrylate, primarily because acrylates are one of the few electron-deficient substrate classes that have been investigated for photocatalytic hydrocarboxylation,[47] making it an excellent "proof-of-concept substrate" (Scheme 25). Additionally, benzyl acrylate offers practical advantages, such as availability, low volatility, and good UV detectability for chromatographic analysis due to its attached aromatic ring system.

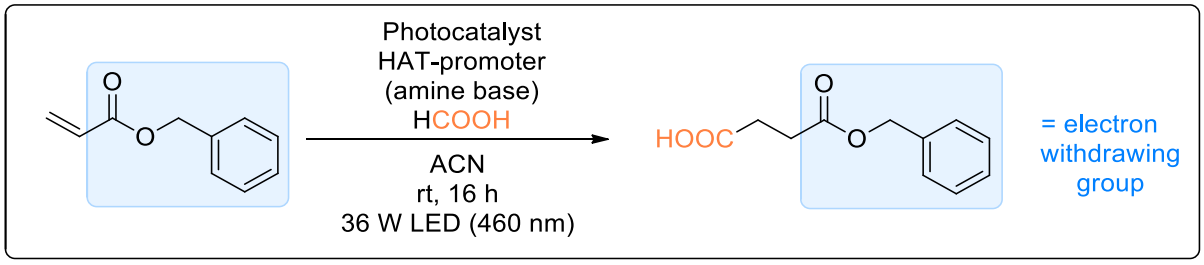

Scheme 25: Initial reaction setup.

Furthermore, an aprotic polar solvent was used, as protic solvents could stabilize both the substrate salt and the base through hydrogen bonding, which would hinder the generation of the reactive species and, thus, be undesirable. On the other hand, apolar solvents are unable to solubilize the substrates used. Hence, acetonitrile was chosen as it is frequently used in photocatalytic hydrocarboxylation reactions.

4.2 Parameter Screening

4.2.1 Catalyst Screening

Before embarking on the design of an entirely new photocatalyst for the developed system, common catalysts that have already been employed in similar systems were used to determine if any of the selected candidates could perform the desired transformation (Table 1).[20,33] A suitable catalyst was found in $(Ir[dF(CF_3)ppy]_2(dtbpy))PF_6$ (Table 1, entry 4, referred as **Ir-1**), which achieved quantitative conversions (over 99%). Nevertheless, also common organic photocatalysts were tested, as they are significantly cheaper than iridium-based catalysts. However, these organic photocatalysts either did not lead to any conversion or achieved negligible conversion rates (Table 1, entry 1-3).

Table 1: Catalyst screening.

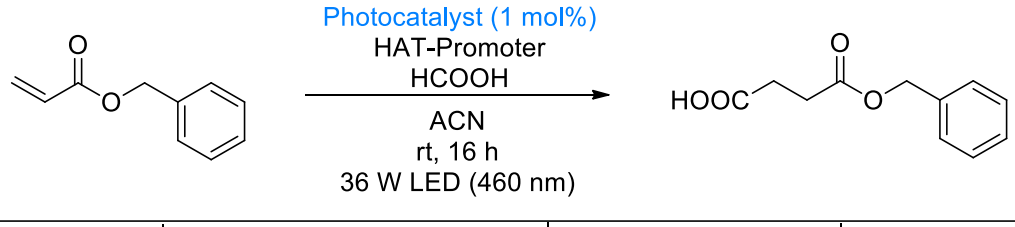

Entry[a]	Structure	Name	Conversion[b]
1	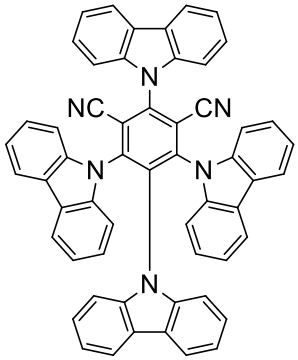	4CzIPN	traces
2	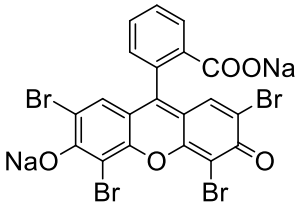	Eosin Y	n.d.
3	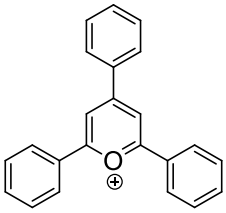	TPT^+	n.d.
4	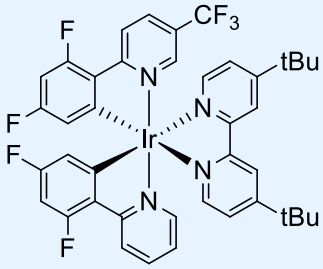	Ir-1	> 99%

[a]Performed with 0.2 mmol (1 eq.) benzyl acrylate, 2.0 µmol (1 mol%) photocatalyst, 1.0 mmol (5.0 eq.) formic acid and 2.0 mmol (10 eq.) DABCO as HAT-promoter in 2 ml of ACN for 16 h at room temperature under continuous irradiation at 460 nm. [b]Determined *via* ^{1}H-NMR analysis of the crude product using TCE as internal standard.

4.2.2 HAT-Promoter Screening

Besides thiols,[52] amine bases are a frequently used HAT-promoter class. Since a general acid-base reaction precedes the formation of the formate salt during the HAT, common amine bases were tested for organic reactions (Table 2).

Table 2: HAT-promoter screening.

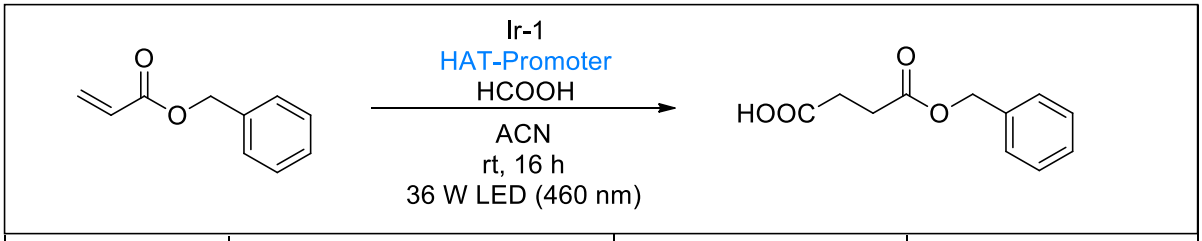

Entry[a]	Structure	Name	Conversion[b]
1	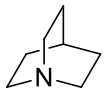	Quinuclidine	95%
2	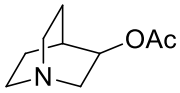	3-Acetoxy-quinuclidine	90%
3	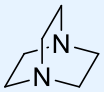	DABCO	> 99%
4	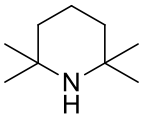	TMP	n.d.
5	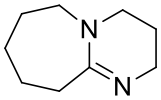	DBU	n.d.
6	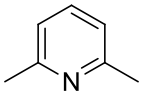	2,6-Lutidine	n.d.
7	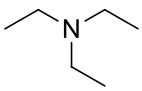	Triethyl amine	n.d.
8	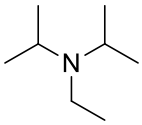	Hünig's Base	n.d.

[a]Performed with 0.2 mmol (1 eq.) benzyl acrylate, 2.0 µmol (1 mol%) Ir-1 catalyst, 1.0 mmol (5.0 eq.) formic acid and 2.0 mmol (10 eq.) HAT-promoter in 2 ml of ACN for 16 h at room temperature under continuous irradiation at 460 nm. [b]Determined *via* ^{1}H-NMR analysis of the crude product using TCE as internal standard.

Based on available literature data,[53] the results were not particularly surprising. Firstly, the choice of amine bases is limited to tertiary amines, as secondary amines (e.g., Table 2, entry 4) tend to prefer aza-Michael type reactions with the olefin substrate instead of deprotonating formic acid. Furthermore, commonly used bases, such as triethylamine or Hünig's base (Table 2, entry 7-8), cannot be used in this system as they tend to undergo α-hydrogen abstractions, leading to undesired side reactions.[54]

Only quinuclidine-like structures achieved considerable conversions (Table 2, entry 1-3). The rigid bridge structure prevents α-hydrogen radical formation. Also, the formed quinuclidine radical cation has the advantage of high electrophilicity, facilitating a HAT with the formate salt.[53] Among the quinuclidine bases used, DABCO yielded the best results (Table 2, entry 3).

4.2.3 Optimization of reaction conditions

According to the literature,[50–52] an excess of formate is used in general (typically 2.0 - 10.0 eq.). So, for the initial reaction setup, 5 eq. of formic acid were used. The use of an excess of formate is justified as the *in situ* generated CO_2 radical anion is a strong reducing agent, capable of reducing olefins to alkanes instead of undergoing a Giese-type addition[55] (Scheme 26).

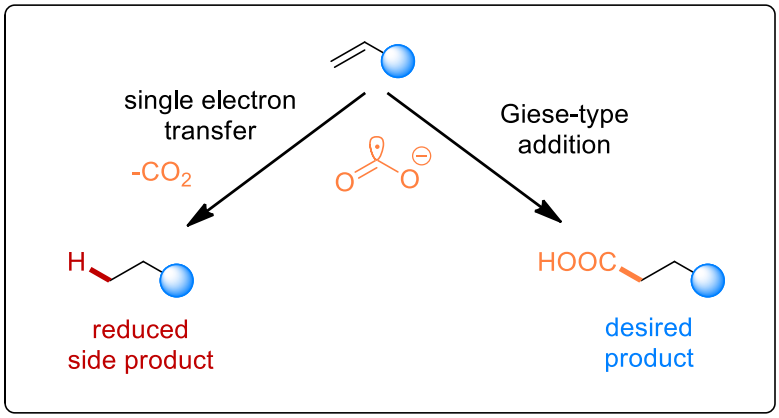

Scheme 26: Concurrent reaction pathways that the CO_2 radical anion can undergo with the olefin.[55]

As already mentioned, DABCO has the dual role of deprotonating formic acid and converting it to the corresponding DABCO-formate salt, as well as performing the HAT transfer. Both tasks cannot be achieved by a single DABCO molecule at once, which makes an excess of DABCO necessary. Therefore, twice the equivalent amount (relative to formic acid) was initially employed which also led to the best results (Table 3, entry 1).

Table 3: Ratio / amount screening.

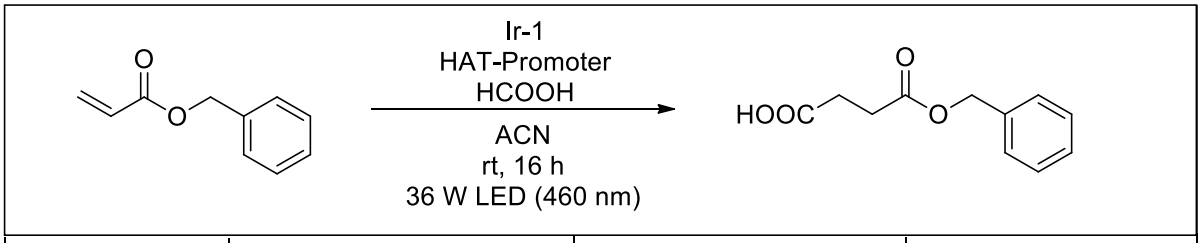

Entry[a]	DABCO eq.	Formic Acid eq.	Conversion[b]
1	10.0	5.0	> 99%[c]
2	8.5	5.0	> 99%[d]
3	6.0	5.0	99%
4	5.5	5.0	88%
5	4.4	4.0	62%
6	3.3	3.0	53%

[a]Performed with 0.2 mmol (1 eq.) benzyl acrylate and 2.0 µmol (1 mol%) photocatalyst in 2 ml of ACN with the given ratios of formic acid and DABCO for 16 h at room temperature under continuous irradiation at 460 nm. [b]Determined *via* ^{1}H-NMR analysis of the crude product using TCE as internal standard. [c]Isolated yield 67%. [d]Isolated yield 53%

Reducing the relative amount of DABCO to formic acid did not decrease conversion. However, based on the isolated product amounts, it was observed that significantly less of the desired addition product was formed (Table 3, entry 2), which indicates that more of the reduced alkane side product was formed instead. Adjusting the absolute amount led to a decreasing conversion trend (Table 3, entry 5-6), which further confirms the necessity of using excess quantities of at least 5.0 eq. formic acid.

4.3 Mechanistic Studies

4.3.1 Control Experiments

With optimized conditions in hand, several control experiments were conducted to gain a better understanding of the underlying mechanism (Table 4). To verify whether the mechanism indeed proceeds *via* a radical intermediate, TEMPO, a typical radical scavenger, was employed. As evident from the low yield (Table 4, entry 1), a TEMPO-radical complex must have formed, confirming the suspicion of at least one radical-intermediate formation.[56]

Furthermore, a reaction was performed in darkness to investigate whether a light source and, hence, a photocatalyst are essential for initiating the reaction sequence. As no conversion was observed, this indeed verifies the occurrence of a photoredox cycle being crucial for the reaction (Table 4, entry 2).

Table 4: Control experiments.

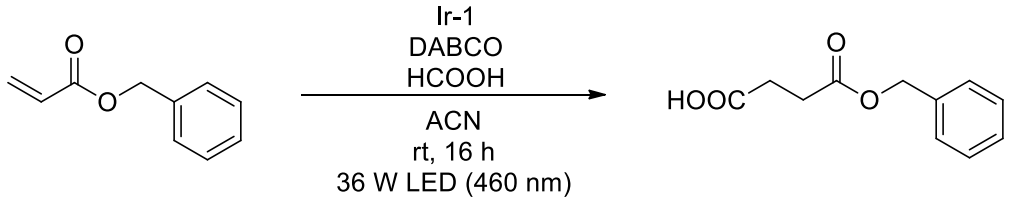

Entry	Conditions	Conversion[c]
1[a]	TEMPO addition (1.1 eq.)	10%
2[a]	Reaction in dark	n.d.
3[a]	Water addition (10 eq.)	> 99%
4[b]	Air atmosphere	85%
5[b]	Argon atmosphere	78%

[a]Performed with 0.2 mmol (1 eq.) benzyl acrylate, 2.0 µmol (1 mol%) Ir-1 catalyst, 1.0 mmol (5.0 eq.) formic acid and 2.0 mmol (10 eq.) DABCO in 2 ml of ACN for 16 h at room temperature under continuous irradiation at 460 nm. [b] Reaction duration (8 h). [c] Determined *via* ^{1}H-NMR analysis of the crude product using TCE as internal standard.

As one of the main goals of the project was to develop a reaction setup that can be performed under simple and mild conditions, sensitivity to moisture and atmospheric oxygen was also examined. The former was simulated by adding 10 eq. of water to the reaction system (Table 4, entry 3), which did not lead to any reduction in the conversion. This observation suggests that the reaction system exhibits a certain degree of moisture resistance, thus specific water exclusion measures are not necessary and do not need to be implemented.

Results regarding atmospheric oxygen were particularly interesting (Table 4, entry 4-5). As triplet oxygen can be an interfering factor in many photocatalytic reactions[57] and lead to byproducts, reactions are often conducted under oxygen exclusion. To investigate if this is also the case here, two reaction setups were compared, one under argon atmosphere and the other under standard air atmosphere. A slight increase in NMR conversion could be observed under the standard atmosphere, indicating that oxygen may even play a supportive role in the reaction system. For instance, in some catalytic cycles, oxygen (in the form of a superoxide radical anion) is known to induce a SET which can assist in the regeneration of the photocatalyst.[58] However, to support this claim for this system, further studies would be necessary. Nevertheless, it can be asserted that the developed system runs, at least independently or maybe even more optimal, under oxygen-containing air atmosphere instead of under argon atmosphere. For this reason, all syntheses were subsequently carried out under air atmosphere. This not only has the advantage to possibly result in better conversions but also eliminates the need for elaborate inert reaction setups and the use of expensive inert gases, such as argon.

4.3.2 Alternating Light and Darkness Impact

To gain a more precise understanding of the occurring mechanism, a light on/off experiment was conducted (Figure 5). This experiment was carried out within 180 min, with alternating periods of 30 minutes each between light and dark period. After each period, the NMR was recorded, and the conversion was calculated. No significant increase in conversion occurred during the dark phases, indicating that the mechanism is catalyst-controlled. If a radical-chain mechanism would be operative, a substantial increase in conversion during the dark phases would also be observable. Therefore, it is not expected that long-living radicals contribute in this system, and, hence self-propagation is unlikely to occur.[59]

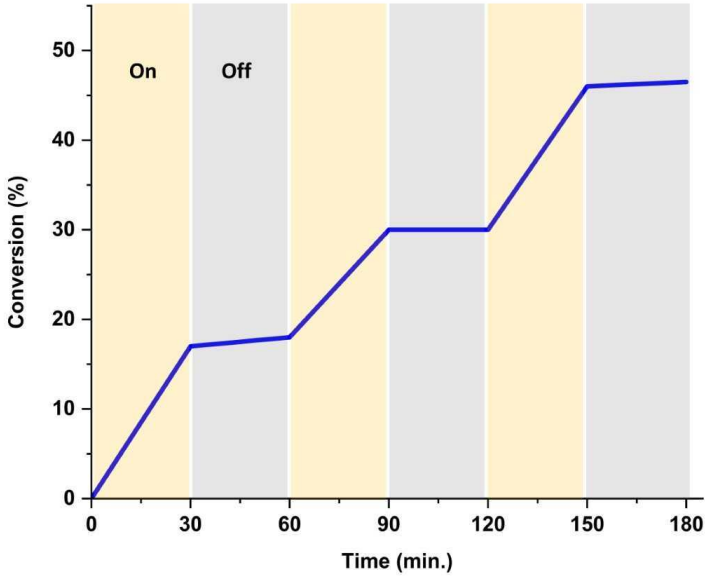

Figure 5: Light on/off experiment.

4.3.3 Quantum Yield Determination

Another, much more reliable method to determine whether the mechanism proceeds through self-propagation or radical coupling is the determination of the quantum yield (φ). In an ideally efficient photoreaction, where one photon leads to the formation of one product molecule, the quantum yield is equal to 1. Results that exceed this value imply a radical-chain mechanism since more molecules are converted than the number of photons absorbed by the reaction system. On the other hand, values where $\varphi < 1$ suggest the likelihood of a radical coupling mechanism, i.e., a catalyst-controlled reaction.[59]

To determine the photon flux, which is needed for the calculation of the quantum yield φ, ferrioxalate actinometry was conducted in accordance with literature.[60]

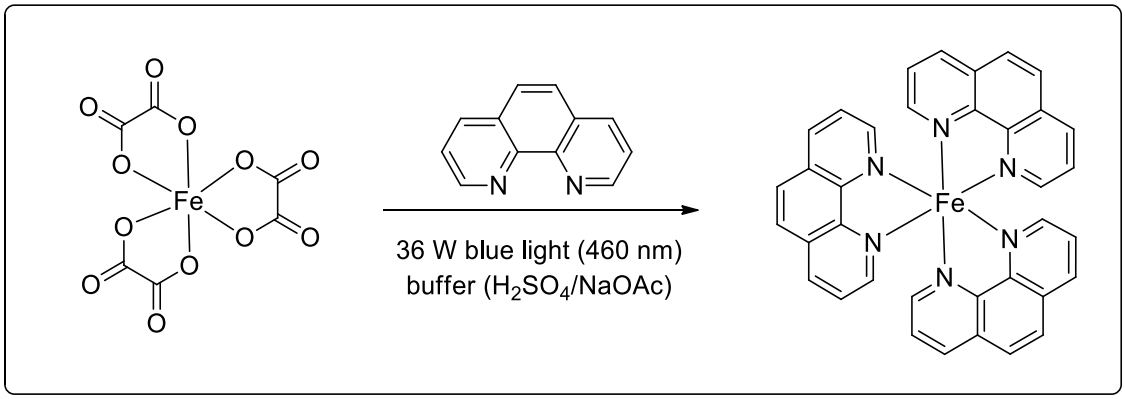

Scheme 27: Photodecomposition of the Fe(III) complex and re-complexation of the reduced Fe(II) species with 1,10-phenanthroline.

In this method, ferrioxalate is irradiated with the light source used in the reaction system, which leads to its decomposition, due to the photolability of the oxalate complex, and re-complexation with 1,10-phenanthroline. The formed complex can then be quantified/detected *via* UV/Vis spectrometry at 510 nm. By measuring the absorption intensity, the amount of formed iron-phenanthroline complex can be inferred, which in turn correlates with the decomposition rate of the ferrioxalate complex, thus enabling a quantitative determination of the photon flux of the irradiation source.

Determination of the Photon Flux

1 ml of the ferrioxalate solution was added to three 8 ml screw-cap vials each, which were then irradiated for 10 seconds. Subsequently, the irradiated solutions were transferred, along with three additional non-irradiated samples, into separate 10 ml volumetric flasks. To each flask, 0.5 ml of phenanthroline solution and additional 2 ml of buffer solution were added, followed by dilution with Milli-Q water to the 10-ml mark. Subsequently, the amount of formed iron(II) species was determined by UV-Vis spectrometry (Figure 6), and the photon flux was calculated. The medians of the non-irradiated and irradiated samples were used for the calculations**.** The photon flux was calculated according to equation 1. (For preparation of the reaction solutions, see section 5.4)

$$Photon\ flux = \frac{mol\ Fe^{2+}}{\Phi * t * f} = 4.40 * 10^{-8}\ einstein\ s^{-1} \text{ (equation 1)}$$

where $\Phi =$ quantum yield of ferrioxalate actinometer solution at 460 nm, $t =$ irradiation time**,** $f =$ fraction of light absorbed at 460 nm by the ferrioxalate solution.

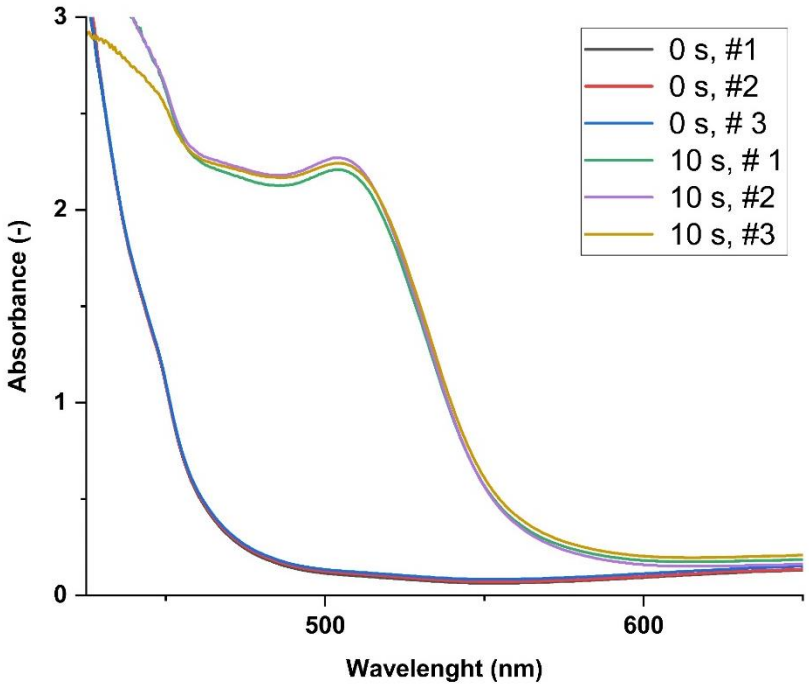

Figure 6: UV-vis spectra of irradiated and non-irradiated ferrioxalate solutions.

Determination of the Quantum Yield

Three photocatalytic hydrocarboxylation reactions were carried out in parallel for 1 h under continuous irradiation by the 36 W lamp at 460 nm, from which the photon flux was calculated. (see section 5.4) Then the samples were analyzed by ^{1}H NMR spectroscopy and the average conversion was calculated to be 35%. With this information available, the quantum yield could be calculated.

$$\Phi = \frac{mol\ product}{photon\ flux * t * f} = 0.44 \text{ (equation 2)}$$

where Φ = quantum yield, t = irradiation time, f = amount of incident photons absorbed at 460 nm by the reaction mixture.

As the calculated quantum yield for the applied reaction setup is φ = 0.44 (see section 5.4), this supports the previous conjecture made during the light on/off experiment that the mechanism proceeds without self-propagation and instead occurs in a catalyst-controlled manner.[59]

4.3.4 Deuterium Labeling Experiments

Furthermore, deuterium labeling studies were performed to determine which components of the system are responsible for the hydrogen transfer, leading to the aliphatic carboxylic acid product. It was observed that using deuterated acetonitrile alone did not result in significant deuterium incorporation in the product (Scheme 28A). However, with the additional use of deuterated formic acid in deuterated acetonitrile, 75% deuterium labeling was found at the β-carbon of the added carboxyl group (Scheme 28B). This indicates that the *in situ*-formed DABCO-formate salt is the main source of the corresponding hydrogen transfer.

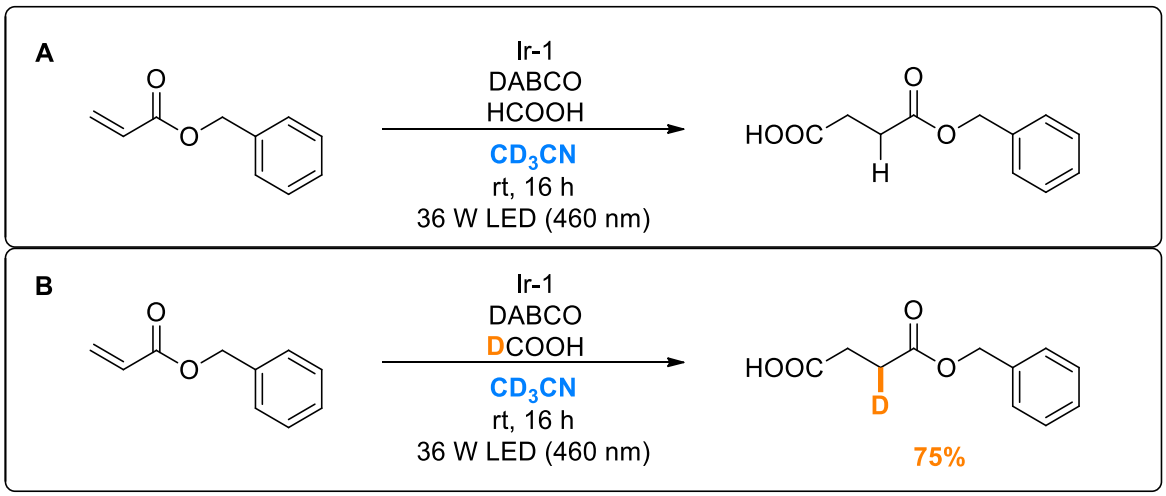

Scheme 28: Deuterium labeling studies.

4.3.5 Proposed Mechanism

Based on these results, the following mechanism can be proposed (Scheme 29). The Ir-1 catalyst is irradiated with blue light and transitions to its excited state. From there, it undergoes a reductive quenching mechanism, initiated through a SET to a DABCO molecule, which converts DABCO into a radical cation species. Formic acid, already converted into the corresponding DABCO-formate salt (**I**) by another DABCO molecule, subsequently reacts with the DABCO radical cation *via* a hydrogen-atom transfer, leading to the formation of the key intermediate, the CO_2 radical anion (**II**). This intermediate reacts with the electron-deficient olefin in a Giese-type addition, yielding the corresponding radical anionic-addition intermediate (**III**). This intermediate is then converted into the carbanionic species (**IV**) through another SET, thus closing the photocatalytic cycle. The SET can occur either directly through the Ir-1 catalyst (Scheme 29A) or indirectly through oxygen (Scheme 29B), which is transformed into a reactive superoxide radical-anion species by the catalyst. This could explain the slightly improved conversion compared to the reaction under argon atmosphere, but further analyses are required to confirm this assumption. Nevertheless, in both scenarios, the Ir-1 catalyst returns to its initial oxidation state, and a new catalytic cycle can start again. The carbanionic intermediate is finally reprotonated by a DABCO formate salt (**V**). This suggestion is supported by the deuterium labeling studies. Ultimately, the carboxylate species is acidified, leading to the desired hydrocarboxylation product at the end (**VI**).

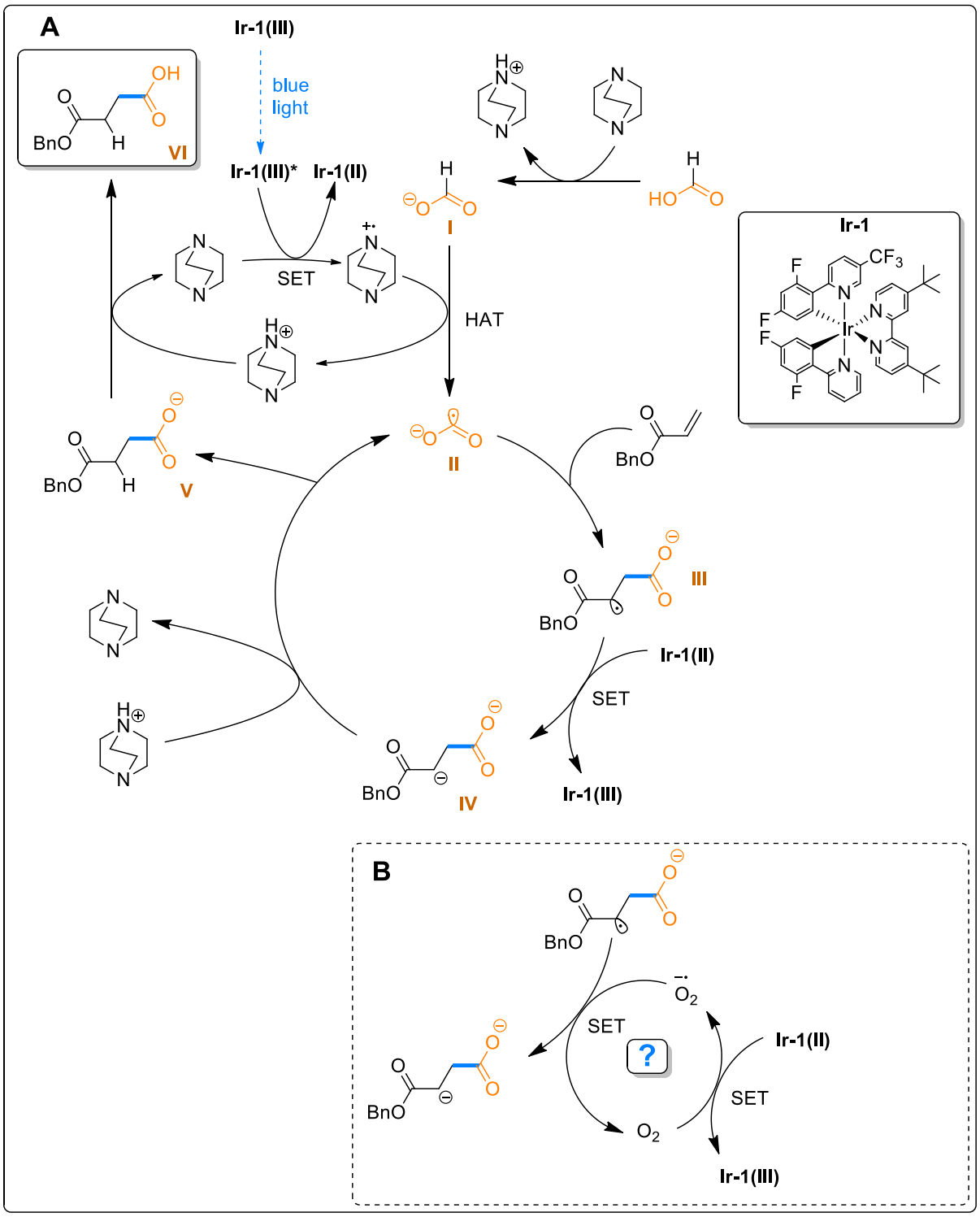

Scheme 29: Proposed mechanism for the photochemical hydrocarboxylation with HCOOH as C_1 source.

4.3.6 Scope and Limitations

After completion of the mechanistic studies, the potential substrate scope was tested. All reactions were conducted under optimized conditions (Scheme 30), including room temperature and atmospheric air. Various groups of electron-deficient olefins were tested.

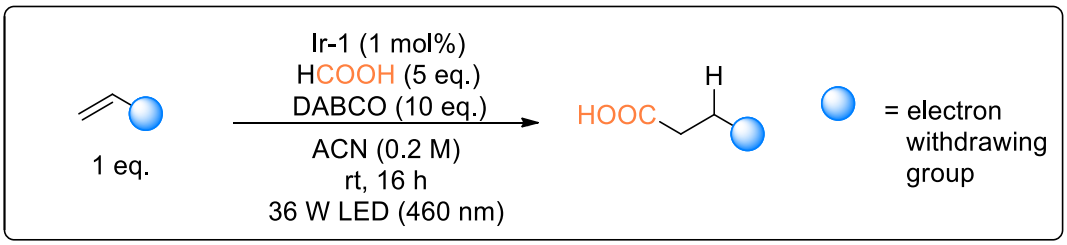

Scheme 30: Optimized reaction conditions.

The investigation began with (mostly) commercially available acrylates, which, in most cases, yielded good to very good conversions (Table 5). It was concluded that substrates with either bulky or long ester groups resulted in significantly poorer outcomes (Table 5, entry 6-7) compared to acrylates with more compact and/or flexible residues (Table 5, entry 2-3).

Table 5: Substrate scope part I.

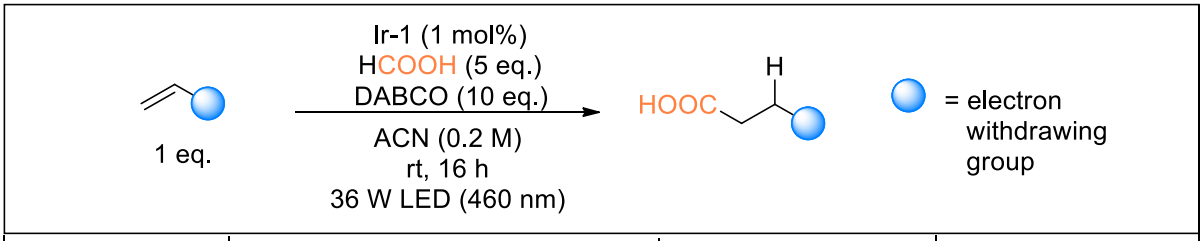

Entry[a]	Substrate	Conversion[b]	Isolated Yield
1[c]	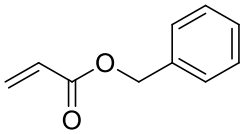	> 99%	67%
2	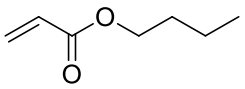	74%	60%
3	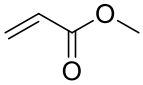	91%	62%
4	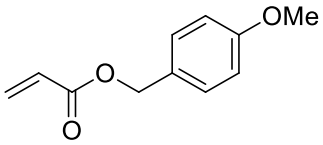	76%	39%
5	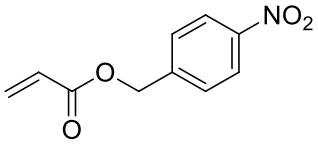	88%	8%
6	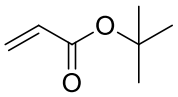	60%	23%
7	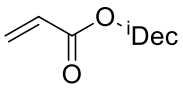	n.d.	n.d.
8[d]	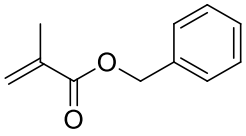	> 99%	53%

[a]Performed with 0.2 mmol (1 eq.) substrate, 2.0 µmol (1 mol%) Ir-1 catalyst, 1.0 mmol (5.0 eq.) formic acid and 2.0 mmol (10 eq.) DABCO in 2 ml of ACN for 16 h at room temperature under continuous irradiation at 460 nm. [b]Determined *via* ^{1}H-NMR analysis of the crude product using TCE as internal standard. [c]Isolation of reduced by-product with 25% yield. [d]Isolation of oxetane by-product with 25% yield.

It should be noted that, in all cases, the conversion was significantly higher compared to the isolated yield. This can be mainly attributed to the side-reduction pathway (Scheme 26), which competes strongly with the desired addition pathway. This side reaction is often thermodynamically favored due to the formation of stable CO_2 gas. Additionally, as already mentioned, the CO_2 radical anion exhibits a very strong reduction potential, leading to a preference for the reduction pathway, particularly when using highly electron-deficient substrates, which counteracts Giese-type additions. This effect is particularly evident in substrates with very strong electron- withdrawing groups (Table 5, entry 5), where a high conversion corresponds to a low yield of the addition product.

To confirm this assumption, the benchmark substrate, benzyl acrylate, was tested (Table 5, entry 1), resulting in a conversion of > 99%. Approximately 67% of the addition product (4-(benzyloxy)-4-oxobutanoic acid) and 25% of the reduced product (benzyl propionate) were isolated, leaving about only 7% of the remaining conversion not directly identifiable, which could be attributed to the formation of minor by-products or losses during workup.

A notable result was obtained for the conversion of benzyl methacrylate (Table 5, entry 8). It produced surprisingly low yields of the linear hydrocarboxylation product compared to benzyl acrylate (53% *vs.* 67%). During the workup, an additional by-product, an oxetane, was unexpectedly isolated with a significant yield of 25% (Scheme 31).

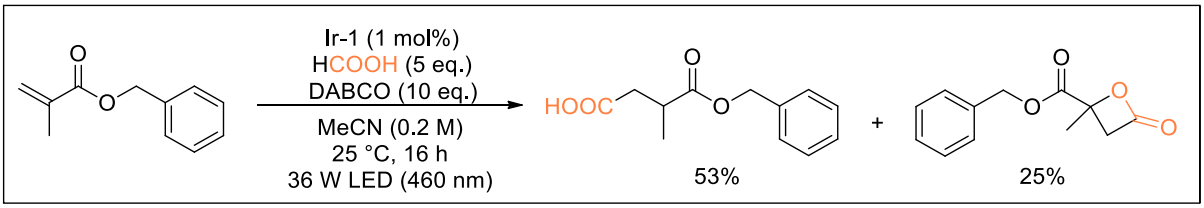

Scheme 31: Formation of an oxetane byproduct (right) using benzyl methacrylate as starting material.

To determine the structure of the oxetane product definitively, additional NMR experiments were conducted. In addition to the classical ^{1}H NMR spectrum, a ^{13}C APT, as well as 2D NMR spectra (HSQC, COSY, and HMBC) were also recorded.

Even the otherwise less informative COSY spectrum reveals that the chemically distinguishable hydrogen atoms in the molecule are separated from each other, either by an oxygen or a quaternary carbon atom. This is evident as, apart from the coupling of the two hydrogen atoms at 2.73 ppm and 2.57 ppm, no other H-H couplings occur. The large, identical coupling constants (J = 15.8) and the coupling pattern of both signals to each other, showing mirror symmetry, lead to the suggestion that the two hydrogen atoms belong to the same carbon atom.

This assumption is confirmed by the HSQC spectrum, in which both signals couple with the same carbon atom (C_{12}) at 44.69 ppm. The chemical distinguishability of both hydrogen atoms, indicated by the large signal shift relative to each other, is also a strong indication of the cyclic structure of the investigated fragment of the molecule. The HSQC spectrum also allows for the assignment of the other hydrogen atom signals to the corresponding carbon atom signals in the APT spectrum.

However, crucial for a successful structure elucidation in this particular case is the HMBC spectrum (Figure 7). Since the ^{13}C NMR APT spectrum exhibits two signals in the region typical for carbonyls, an unambiguous assignment of both signals (lactone or ester) is essential. This was accomplished by examining the hydrogen atom signal at 5.17-5.05 ppm (attached to C_7 at 65.50 ppm), which couples with the quaternary carbon atom of the open ester at 174.44 ppm (C_9) *via* a ^3J coupling. However, the same hydrogen atom is too far away to couple with the other carbonyl carbon at 171.70 ppm, clearly assigning it to the quaternary lactone carbon (C_{13}). This is further confirmed by the hydrogen atoms at 1.35 ppm of the methyl group (attached to C_{16} at 26.07 ppm), which couple with C_9 *via* a ^3J coupling but not with C_{13}, as this would require a ^4J coupling, which normally does not occur for non-aromatic fragments.

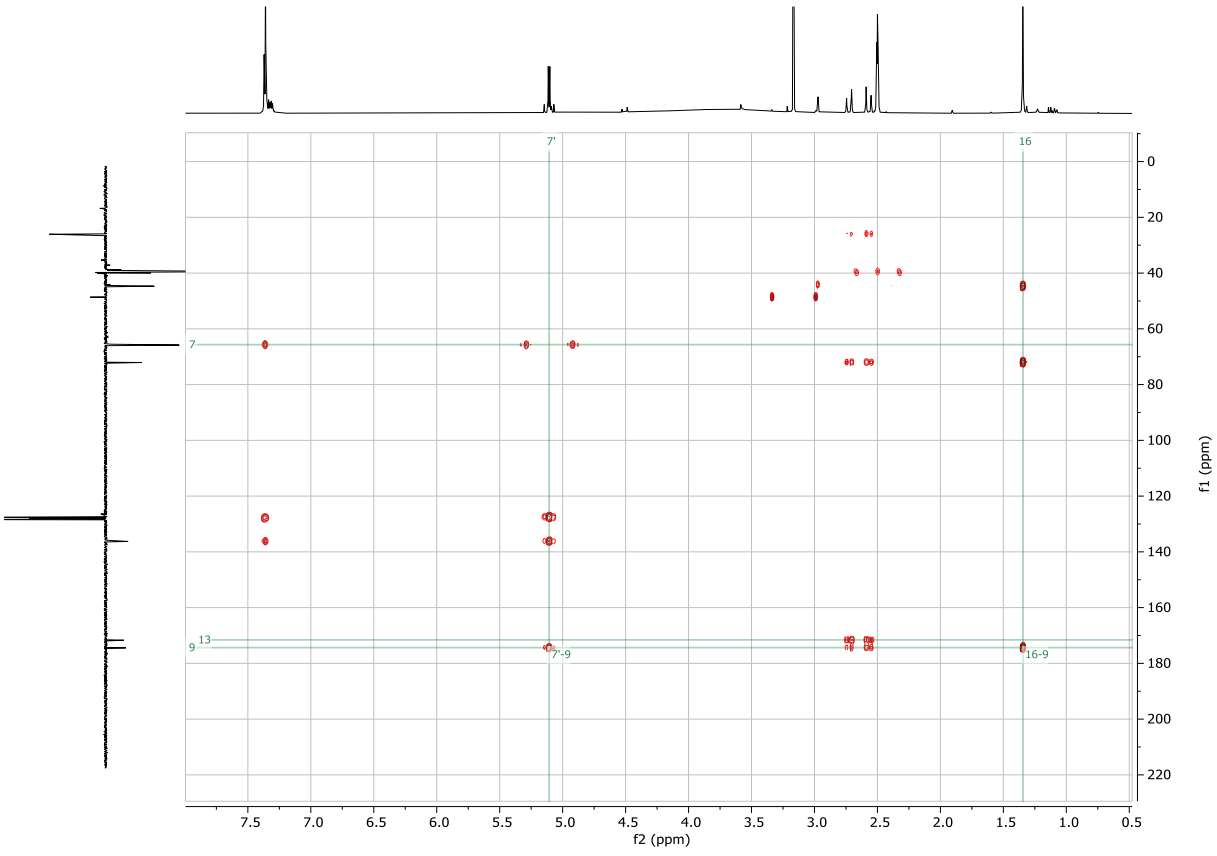

Figure 7: HMBC spectrum of the oxetane byproduct.

The latter information also confirms the presented regiochemistry: If O_{14} would be connected to C_{12} instead of C_{10} and therefore C_{13} with C_{10} instead of C_{12} (Figure 8), an additional ^{3}J coupling signal would occur for the hydrogen atoms of the C_{16} methyl group with C_{13}, resulting in two coupling signals in the ^{13}C carbonyl region of the HMBC spectrum for these hydrogen atoms. Since this is not the case, only one regioisomer is formed selectively.

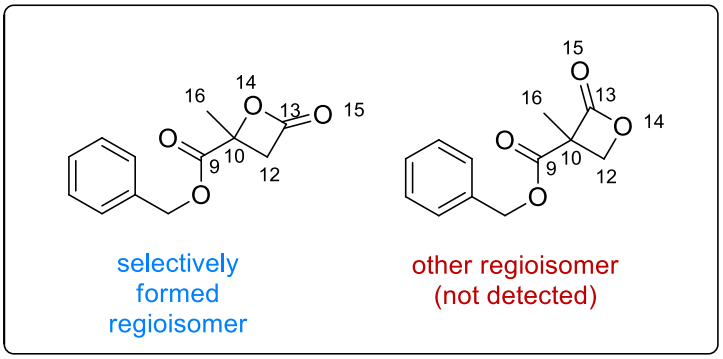

Figure 8: Selective formation of one regioisomer (left).

The mechanistic basis of this product formation is unclear, and no photocatalytic methods for oxetane synthesis from olefins have been reported in the literature thus far. Therefore, an investigation into the synthesis of this product class would be highly desirable. It is suspected that the methyl group of the olefin may have a crucial role on the product formation, potentially allowing at least one additional or competitive mechanistic step due to the formation of a more stable radical intermediate (stabilized by the methyl group), which was not observed in the other substrates and leads to a side pathway resulting in the formation of the oxetane ring. To verify this hypothesis, further methacrylates should be tested to observe if oxetane formation also occurs.

In addition to acrylates, anilides, sulfoanilides, and a sulfonamide were also successfully tested, with conversions always exceeding 90% (Table 6). The isolated hydrocarboxylation products of the anilides were obtained in moderate yields (Table 6, entry 9-11), while the significantly more electron-deficient corresponding sulfoanilides had noticeably lower product yields (Table 6, entry 12-13). This suggests that the unwanted reduction pathway is more favored for sulfoanilides compared to the anilide pendants, as evidenced by the similarly high NMR conversions.

Table 6: Substrate scope part II.

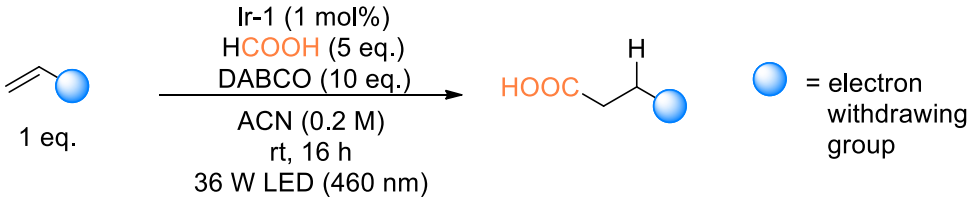

Entry[a]	Substrate	Conversion[b]	Isolated Yield
9	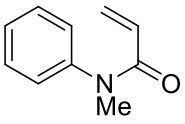	95%	41%
10	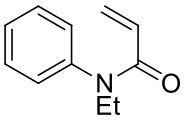	99%	48%
11	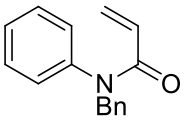	99%	36%
12	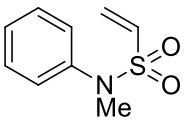	95%	20%
13	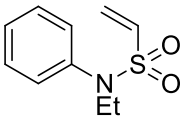	98%	16%
14	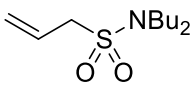	98%	38%

[a]Performed with 0.2 mmol (1 eq.) substrate, 2.0 µmol (1 mol%) Ir-1 catalyst, 1.0 mmol (5.0 eq.) formic acid and 2.0 mmol (10 eq.) DABCO in 2 ml of ACN for 16 h at room temperature under continuous irradiation at 460 nm.
[b]Determined *via* ^{1}H-NMR analysis of the crude product using TCE as internal standard.

There was also one exception to this trend (Table 6, entry 14), where the starting material, being a sulfonamide, led to surprisingly high yields. This suggests that flexible systems may exhibit different product ratios concerning reduction and addition compared to aromatic systems. However, to confirm this assumption, further investigation with non-aromatic amides and sulfonamides would be required.

Among the substrate classes tested successfully, there were some that did not lead to any successful product formation (Figure 9). Phenyl esters and phenyl sulfonesters decomposed into their corresponding phenol counterparts. It is presumed that the basic conditions were unsuitable for phenyl (sulfon)esters, which can be highly labile and prone to decomposition when exposed to strong pH changes.[61]

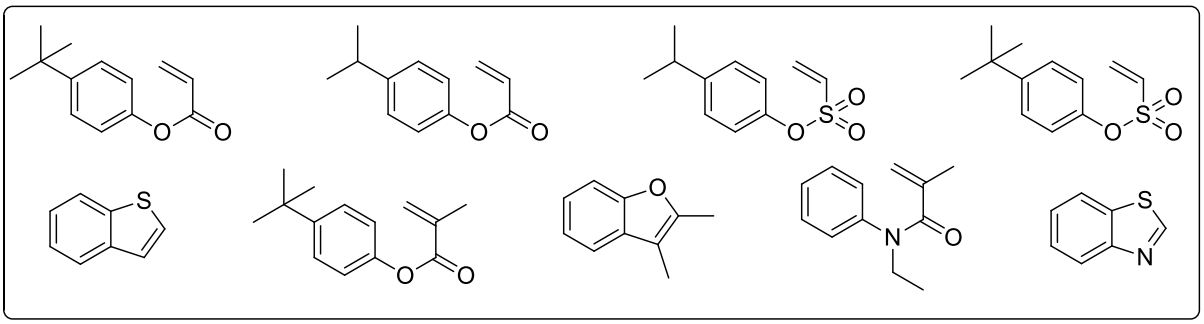

Figure 9: Substrates that did not yield any desired product.

Heteroaromatic systems, as used in Mita *et al*'s work,[51] also did not work with this reaction setup. It appears that the olefinic bonds in aromatic compounds are too stable to undergo the desired reaction with the conditions used in this method, indicating that high temperatures may be essential for the conversion of this substrate type.

4.3.7 Conclusions and Outlook

In the context of this master thesis, a new method for the photocatalytic hydrocarboxylation of olefins has been developed. This method offers the option to conduct photocatalytic hydrocarboxylations of olefins under a simple reaction setup due to the possibility to run it under air atmosphere and, also, enables the usage of mild reaction conditions as it can be performed at room temperature.

The developed method represents the first successful photocatalytic hydrocarboxylation of olefins using formic acid directly, as in this method the formate salt is formed *in situ* with the amine base, which is an elegant and much cheaper alternative to other formate variants, such as cesium formate.

Another achievement reported herein is the successful conversion of electron-deficient olefin substrates, which posed a significant challenge due to the competition with the reduction pathway. With the developed method, 13 different electron-deficient olefins, including acrylates and (sulfon)anilides/-amides, were successfully converted into the desired hydrocarboxylated products.

Mechanistic studies have been carried out to acquire a better understanding of the underlying mechanism. All data support the hypothesis that this method proceeds through a photochemically-induced radical mechanism, where no chain-growth takes place. Instead, the reaction is catalyst controlled, so no long-living radicals are formed during the reaction.

Despite all the mentioned positive aspects, the main challenge remains that the CO_2 radical anion still tends to preferentially reduce highly electron-deficient olefins rather than undergoing a carboxylation-addition with them. Therefore, it remains an exciting prospect for future research to explore/investigate how to overcome this issue in the field of the photocatalytic hydrocarboxylation of electron-deficient olefins.

5. Experimental

5.1 Materials & Methods

All purchased chemicals from commercial suppliers were used without further purification, unless otherwise specified. Dry solvents were pre-distilled and desiccated on aluminum oxide columns (PURESOLV, Innovative Technology). Column chromatography was performed on standard manual glass columns, using Merck (40-60 μm) silica gel, with pre-distilled solvents. For TLC analysis, pre-coated aluminum-backed plates were purchased from Merck (silica gel 60 F_{254}). UV-active compounds were detected at 254 nm. Non-UV-active compounds were detected using standard bromocresol green, phosphomolybdic acid or permanganate stains.

^{1}H & ^{13}C NMR spectra were recorded on a Bruker Avance UltraShield 200 MHz, 400 MHz or 600 MHz spectrometer and chemical shifts were reported in ppm using TMS as internal standard. Coupling constants (*J*) are given in Hz. For NMR purposes, the following abbreviations are used: s (singlet), d (doublet), t (triplet), q (quartet), p (pentet), hept (heptet), m (multiplet).

HR-MS analysis was performed using HTC PAL system auto sampler, an Agilent 1100/1200 HPLC and Agilent 6230 AJS ESI-TOF mass spectrometer. Melting points above room temperature were measured on an automated melting system OPTI MELT of Stanford Research Systems and were uncorrected, Infrared spectra were recorded on a Perkin-Elmer Spectrum 65 FT IR spectrometer equipped with a specac MK II Golden Gate Single Reflection ATR unit, UV/Vis spectra were recorded at 297 K on a Shimadzu UV/Vis 1800 spectrometer using 1 cm path length quartz cuvettes.

5.2 Substrate Synthesis for Hydrocarboxylation

5.2.1 Acrylanilide Synthesis

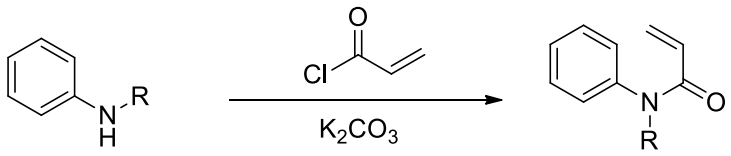

R = Et (**1**)
R = Me (**2**)
R = Bn (**3**)

Compounds **1-3** were prepared according to literature procedures[62] with slight modifications. K_2CO_3 (23.0 mmol, 2.3 eq.) was added to a solution of the corresponding aniline (10.0 mmol, 1.0 eq.) in THF (23 ml) and the mixture was stirred at room temperature. Then it was cooled to 0 °C and acryloylchloride (12.0 mmol, 1.2 eq.) was added dropwise. Subsequently, the reaction mixture was stirred for another 15 min at room temperature, extracted with EtOAc and washed with $NaHCO_3$ followed by H_2O, 1 M HCl, H_2O and brine. The organic layer was separated, dried over Na_2SO_4 and concentrated *in vacuo* (20 mbar).

***N*-ethyl-*N*-Phenylacrylamide (1)**

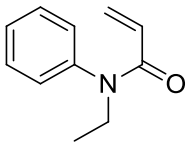

1

In accordance to the general procedure of 5.2.1, *N*-ethylaniline (1259 µl, 10.0 mmol, 1.0 eq.), K_2CO_3 (3110 mg, 23.0 mmol, 2.3 eq.) and acryloylchloride (975 µl, 12.0 mmol, 1.2 eq.) were used. The product was obtained as a clear yellow oil (1426 mg, 8.1 mmol. 81%).

^{1}H NMR (400 MHz, $CDCl_3$) δ 7.46 – 7.38 (m, 2H), 7.37 – 7.31 (m, 1H), 7.18 – 7.11 (m, 2H), 6.35 (dd, *J* = 16.8, 2.1 Hz, 1H), 5.98 (dd, *J* = 16.8, 10.3 Hz, 1H), 5.49 (dd, *J* = 10.3, 2.0 Hz, 1H), 3.84 (q, *J* = 7.1 Hz, 2H), 1.15 (t, *J* = 7.1 Hz, 3H).

^{13}C NMR (151 MHz, $CDCl_3$) δ 165.47 (s), 142.04 (s), 129.85 (s), 129.19 (s), 128.69 (s), 128.08 (s), 127.63 (s), 44.64 (s), 13.27 (s).

Analytical data was in agreement with literature.[62]

***N*-Methyl-*N*-phenylacrylamide (2)**

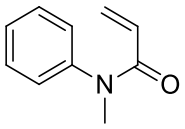

2

In accordance to the general procedure of 5.2.1, *N*-methylaniline (1084 µl, 10.0 mmol, 1.0 eq.), K_2CO_3 (3110 mg, 23.0 mmol, 2.3 eq.) and acryloylchloride (975 µl, 12.0 mmol, 1.2 eq.) were used. The product was obtained as light-yellow crystals (1166 mg, 7.2 mmol, 72%).

^{1}H NMR (600 MHz, $CDCl_3$) δ 7.45 – 7.37 (m, 2H), 7.36 – 7.31 (m, 1H), 7.21 – 7.14 (m, 2H), 6.36 (dd, *J* = 16.8, 2.0 Hz, 1H), 6.06 (dd, *J* = 16.8, 10.3 Hz, 1H), 5.51 (dd, *J* = 10.3, 1.9 Hz, 1H), 3.36 (s, 3H).

^{13}C NMR (151 MHz, $CDCl_3$) δ 166.08 (s), 143.73 (s), 129.92 (s), 128.81 (s), 127.93 (s), 127.75 (s), 127.62 (s), 37.75 (s).

Analytical data was in agreement with literature.[63]

***N*-Benzyl-*N*-phenylacrylamide (3)**

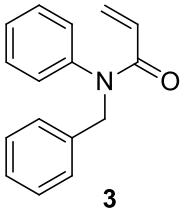

3

In accordance to the general procedure of 5.2.1, *N*-benzylaniline (1833 mg, 10.0 mmol, 1.0 eq.), K_2CO_3 (3110 mg, 23.0 mmol, 2.3 eq.) and acryloylchloride (975 µl, 12.0 mmol, 1.2 eq.) were used. The product was obtained as beige crystals (2207 mg, 9.3 mmol, 93%).

^{1}H NMR (400 MHz, $CDCl_3$) δ 7.36 – 7.19 (m, 8H), 7.03 – 6.98 (m, 2H), 6.43 (dd, *J* = 16.8, 2.0 Hz, 1H), 6.04 (dd, *J* = 16.8, 10.3 Hz, 1H), 5.54 (dd, *J* = 10.3, 2.1 Hz, 1H), 4.98 (s, 2H).

Analytical data was in agreement with literature.[64]

5.2.2 Synthesis of Ring-Substituted Benzyl Acrylates

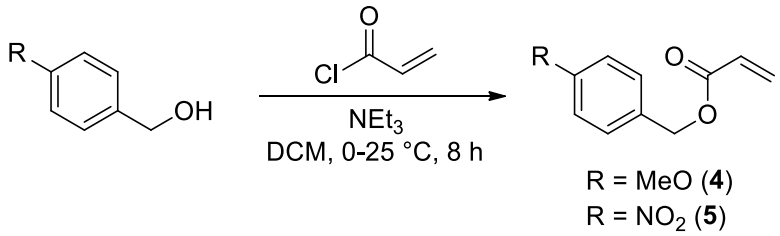

Compounds **4-5** were prepared according to literature procedures[65] with slight modifications. Triethylamine (7.5 mmol, 1.5 eq.) was added into a solution of the corresponding benzyl alcohol (5.0 mmol, 1.0 eq.) in DCM (10 ml) and the mixture was stirred at room temperature. Then it was cooled to 0 °C, acryloylchloride (6.0 mmol, 1.2 eq.) was added dropwise and the reaction mixture was stirred for another 8 h at room temperature. The mixture was quenched with distilled water (10 ml) and transferred into a separation funnel. After decanting the water phase, the organic layer was washed 2× with water (10 ml), followed by 2× with NH_4Cl solution (10 ml). The organic layer was separated, dried over Na_2SO_4 and concentrated *in vacuo* (20 mbar).

4-Methoxybenzyl acrylate (4)

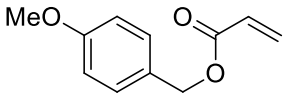

4

In accordance to the general procedure of 5.2.2, (4-methoxyphenyl)methanol (612 µl, 5.0 mmol, 1.0 eq.), NEt_3 (1040 µl, 7.5 mmol, 1.5 eq.) and acryloylchloride (975 µl, 6.0 mmol, 1.2 eq.) were used. The product was obtained as a brown liquid (572 mg, 3.0 mmol, 60%).

^{1}H NMR (600 MHz, $CDCl_3$) δ 7.34 – 7.30 (m, 2H), 6.92 – 6.87 (m, 2H), 6.43 (dd, *J* = 17.3, 1.4 Hz, 1H), 6.14 (dd, *J* = 17.3, 10.4 Hz, 1H), 5.83 (dd, *J* = 10.4, 1.4 Hz, 1H), 5.14 (s, 2H), 3.81 (s, 3H).

^{13}C NMR (151 MHz, $CDCl_3$) δ 166.46 (s), 159.97 (s), 131.31 (s), 130.48 (s), 128.73 (s), 128.25 (s), 114.26 (s), 66.50 (s), 55.61 (s).

Analytical data was in agreement with literature.[66]

4-Nitrobenzyl acrylate (5)

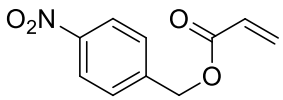

5

In accordance to the general procedure of 5.2.2, (4-nitrophenyl)methanol (766 mg, 5.0 mmol, 1.0 eq.), NEt_3 (1040 µl, 7.5 mmol, 1.5 eq.) and acryloylchloride (975 µl, 6.0 mmol, 1.2 eq.) were used. The product was obtained as a brown-yellowish solid (873 mg, 4.2 mmol, 84%).

^{1}H NMR (400 MHz, $CDCl_3$) δ 8.27 – 8.20 (m, 2H), 7.57 – 7.51 (m, 2H), 6.50 (dd, *J* = 17.3, 1.3 Hz, 1H), 6.20 (dd, *J* = 17.3, 10.4 Hz, 1H), 5.92 (dd, *J* = 10.4, 1.3 Hz, 1H), 5.30 (s, 2H).

^{13}C NMR (101 MHz, $CDCl_3$) δ 165.77 (s), 143.28 (s), 132.13 (s), 128.51 (s), 127.87 (s), 123.98 (s), 64.94 (s).

Analytical data was in agreement with literature.[66]

5.2.3 Synthesis of Ring-Substituted Phenylacrylates

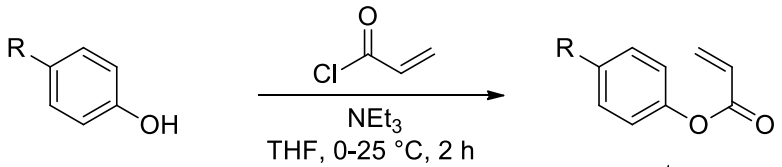

R = ^{t}Bu (**6**)
R = ^{i}Pr (**7**)

Compounds **6-7** were prepared according to literature procedures[67] with slight modifications. NEt_3 (20.0 mmol, 2.0 eq.) was added into a solution of the corresponding phenol (10.0 mmol, 1.0 eq.) in THF (20 ml) wand the mixture was stirred at room temperature. Then it was cooled to 0 °C, acryloylchloride (10.0 mmol, 1.0 eq.) was added dropwise over 20 min and the reaction mixture was stirred for another 2 h at room temperature. The reaction mixture was concentrated *in vacuo* (20 mbar) and the remaining residue was dissolved in EtOAc and transferred into a separation funnel. The organic layer was washed with distilled water, followed by brine. After drying over Na_2SO_4, the crude product was concentrated *in vacuo* (20 mbar). Purification was done by column chromatography.

4-(*tert*-Butyl)phenyl acrylate (6)

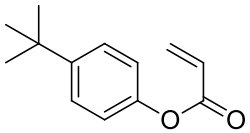

6

In accordance to the general procedure of 5.2.3, 4-(*tert*-butyl)phenol (1502 mg, 10.0 mmol, 1.0 eq.), NEt_3 (2773 µl, 20.0 mmol, 2.0 eq.) and acryloylchloride (812 µl, 10.0 mmol, 1.0 eq.) were used. Purification was done by column chromatography (5% Et_2O / PE, visualization *via* UV detection + $KMnO_4$ stain). The product was obtained as a colorless oil (693 mg, 3.4 mmol, 34%).

^{1}H NMR (600 MHz, $CDCl_3$) δ 7.44 – 7.37 (m, 2H), 7.08 – 7.02 (m, 2H), 6.60 (dd, *J* = 17.3, 1.2 Hz, 1H), 6.33 (dd, *J* = 17.3, 10.5 Hz, 1H), 6.00 (dd, *J* = 10.5, 1.2 Hz, 1H), 1.33 (s, 9H).

^{13}C NMR (151 MHz, $CDCl_3$) δ 165.10 (s), 149.00 (s), 148.51 (s), 132.74 (s), 128.38 (s), 126.68 (s), 121.13 (s), 34.82 (s), 31.75 (s).

Analytical data was in agreement with literature.[68]

4-Isopropylphenyl acrylate (7)

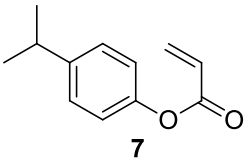

7

In accordance to the general procedure of 5.2.3, 4-isopropylphenol (1362 mg, 10.0 mmol, 1.0 eq.), Net_3 (2773 µl, 20.0 mmol, 2.0 eq.) and acryloylchloride (812 µl, 10.0 mmol, 1.0 eq.) were used. Purification was done by column chromatography (5% Et_2O / PE, visualization *via* UV detection + $KMnO_4$ stain). The product was obtained as a colorless oil (1084 mg, 5.7 mmol, 57%).

^{1}H NMR (400 MHz, $CDCl_3$) δ 7.26 – 7.23 (m, 2H), 7.07 – 7.02 (m, 2H), 6.60 (dd, *J* = 17.3, 1.3 Hz, 1H), 6.32 (dd, *J* = 17.3, 10.5 Hz, 1H), 6.00 (dd, *J* = 10.5, 1.2 Hz, 1H), 2.92 (hept, *J* = 6.9 Hz, 1H), 1.25 (d, *J* = 6.9 Hz, 6H).

^{13}C NMR (151 MHz, $CDCl_3$) δ 164.92 (s), 148.57 (s), 146.53 (s), 132.54 (s), 128.17 (s), 127.49 (s), 121.29 (s), 33.76 (s), 24.18 (s).

HRMS (ESI) calc. for $C_{12}H_{15}O_2$ $[M+H]^+$ 191.1067, found 191.1069.

IR (ν_{max}/cm^{-1}) 3071 (C-H vin.), 2953 (C-H), 1735 (C=O), 1141 (C-O), 986 (C=C), 848 (C-H arom.).

5.2.4 Synthesis of Ethenylsulfoanilides

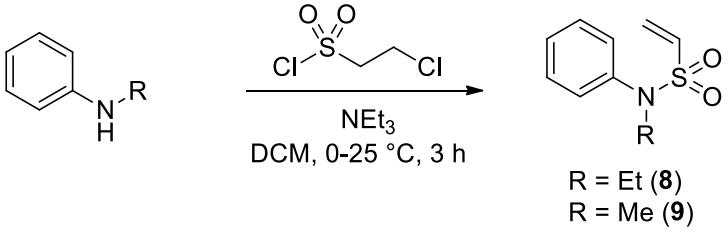

R = Et (**8**)
R = Me (**9**)

Compounds **8-9** were prepared according to literature procedures[69] with slight modifications. NEt_3 (30.0 mmol, 3.0 eq.) was added into a solution of the corresponding aniline (10.0 mmol, 1.0 eq.) in DCM (20 ml) and the mixture was stirred at room temperature. Then it was cooled to 0 °C, 2-chloroethylsulfonylchloride (11.0 mmol, 1.1 eq.) was added dropwise and the reaction mixture was stirred for another 3 h at room temperature. Subsequently, it was quenched with 10 ml distilled water and afterwards transferred into a separation funnel. The organic layer was washed 3× with brine (60 ml), dried over Na_2SO_4 and concentrated *in vacuo* (20 mbar).

***N*-Ethyl-*N*-phenylethenesulfonamide (8)**

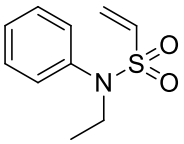

8

In accordance to the general procedure of 5.2.4, *N*-ethylaniline (1259 µl, 10.0 mmol, 1.0 eq.), NEt_3 (4159 µl, 30.0 mmol, 3.0 eq.) and 2-chloroethylsulfonylchloride (1149 µl, 11.0 mmol, 1.1 eq.) were used. The product was obtained as a brown viscous oil (1819 mg, 8.6 mmol, 86%).

^{1}H NMR (600 MHz, $CDCl_3$) δ 7.40 – 7.27 (m, 5H), 6.53 (dd, *J* = 16.6, 10.0 Hz, 1H), 6.16 (d, *J* = 16.6 Hz, 1H), 5.95 (d, *J* = 9.9 Hz, 1H), 3.64 (q, *J* = 7.1 Hz, 2H), 1.13 (t, *J* = 7.1 Hz, 3H).

^{13}C NMR (151 MHz, $CDCl_3$) δ 139.00 (s), 134.36 (s), 129.60 (s), 129.31 (s), 128.41 (s), 127.64 (s), 46.17 (s), 14.64 (s), 13.66 (s), 1.36 (s).

Analytical data was in agreement with literature.[70]

***N*-Methyl-*N*-phenylethenesulfonamide (9)**

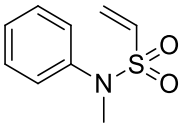

9

In accordance to the general procedure of 5.2.4, *N*-methylaniline (542 µl, 5.0 mmol, 1.0 eq.), NEt_3 (2076 µl, 15.0 mmol, 3.0 eq.) and 2-chloroethylsulfonylchloride (575 µl, 5.5 mmol, 1.1 eq.) were used. The product was obtained as a yellow-whitish solid (470 mg, 2.4 mmol, 48%).

^{1}H NMR (600 MHz, $CDCl_3$) δ 7.39 – 7.34 (m, 2H), 7.34 – 7.31 (m, 2H), 7.30 – 7.27 (m, 1H), 6.45 (dd, *J* = 16.6, 10.0 Hz, 1H), 6.20 (d, *J* = 16.6 Hz, 1H), 6.02 (d, *J* = 10.0 Hz, 1H), 3.24 (s, 3H).

^{13}C NMR (151 MHz, $CDCl_3$) δ 141.51 (s), 132.49 (s), 129.48 (s), 128.82 (s), 127.82 (s), 126.95 (s), 38.40 (s).

Analytical data was in agreement with literature.[70]

5.2.5 Synthesis of Ring-Substituted Phenylethenylsulfonesters

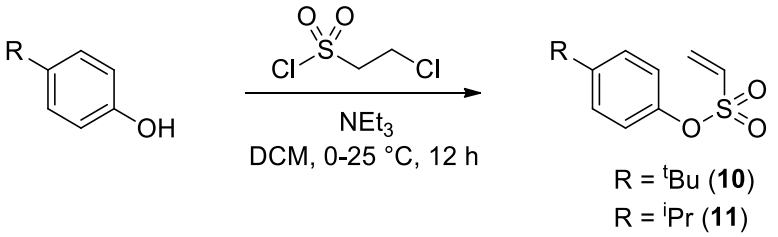

Compounds **10-11** were prepared according to literature procedures[69] with slight modifications. To a solution of the corresponding phenol (5.0 mmol, 1.0 eq.) in DCM (20 ml) NEt_3 (15.0 mmol, 3.0 eq.) was added and the mixture was stirred at room temperature. Then it was cooled to 0 °C, 2-chloroethylsulfonylchloride (6.0 mmol, 1.2 eq.) was added dropwise and the reaction mixture was stirred for another 12 h at room temperature. The reaction mixture was quenched with 10 ml distilled water and afterwards transferred into a separation funnel. The organic layer was washed 3× with brine (60 ml), dried over Na_2SO_4 and concentrated *in vacuo* (20 mbar).

4-(*tert*-Butyl)phenylethenesulfonate (10)

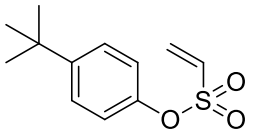

10

In accordance to the general procedure of 5.2.4, 4-(*tert*-butyl)phenol (751 mg, 5.0 mmol, 1.2 eq.), NEt_3 (2076 µl, 15.0 mmol, 3.0 eq.) and 2-chloroethylsulfonylchloride (627 µl, 6.0 mmol, 1.2 eq.) were used. The product was obtained as a black solid (1118 mg, 4.9 mmol, 98%).

^{1}H NMR (400 MHz, $CDCl_3$) δ 7.41 – 7.36 (m, 2H), 7.17 – 7.11 (m, 2H), 6.67 (dd, *J* = 16.6, 10.0 Hz, 1H), 6.38 (dd, *J* = 16.7, 0.6 Hz, 1H), 6.15 (dd, *J* = 10.0, 0.6 Hz, 1H), 1.31 (s, 9H).

^{13}C NMR (151 MHz, $CDCl_3$) δ 150.54 (s), 147.17 (s), 132.23 (s), 131.65 (s), 126.90 (s), 121.75 (s), 34.75 (d, *J* = 2.8 Hz), 31.45 (d, *J* = 3.7 Hz).

Analytical data was in agreement with literature.[71]

4-Isopropylphenylethenesulfonate (11)

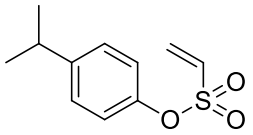

11

In accordance to the general procedure of 5.2.4, 4-isopropylphenol (681 mg, 5.0 mmol, 1.2 eq.), NEt_3 (2076 µl, 15.0 mmol, 3.0 eq.) and 2-chloroethylsulfonylchloride (627 µl, 6.0 mmol, 1.2 eq.) were used. The product was obtained as white pasty solid (883 mg, 3.9 mmol, 78%).

Melting point 76 – 77 °C.

^{1}H NMR (600 MHz, $CDCl_3$) δ 7.24 – 7.21 (m, 2H), 7.14 (d, *J* = 8.7 Hz, 2H), 6.67 (dd, *J* = 16.7, 10.0 Hz, 1H), 6.37 (dd, *J* = 16.6, 0.7 Hz, 1H), 6.16 (dd, *J* = 10.0, 0.7 Hz, 1H), 2.91 (hept, *J* = 6.9 Hz, 1H), 1.23 (d, *J* = 6.9 Hz, 6H).

^{13}C NMR (151 MHz, $CDCl_3$) δ 148.25 (s), 147.42 (s), 132.21 (s), 131.67 (s), 127.89 (s), 122.13 (s), 33.78 (s), 24.08 (s).

HRMS (ESI) calc. for $C_{11}H_{15}O_3S$ $[M+H]^+$ 227.0736, found 227.0738.

IR (ν_{max}/cm^{-1}) 3079 (C-H vin.), 2964 (C-H), 1359 (S=O), 1176 (S=O), 987 (C=C), 848 (C-H arom.).

5.2.6 Synthesis of 4-(*tert*-butyl)phenyl methacrylate (12)

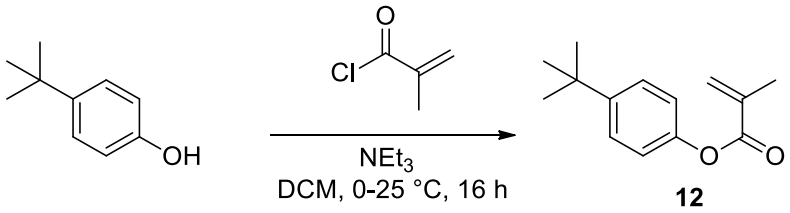

Compound **12** was prepared according to literature procedures[72] with slight modifications.

To a solution of 4-(*tert*-butyl)phenol (1362 mg, 10.0 mmol, 1.0 eq.) in DCM (25 ml) NEt_3 (1663 µl, 12.0 mmol, 1.2 eq.) was added and the mixture was stirred at room temperature. Then it was cooled to 0 °C, methacryloylchloride (1172 µl, 12.0 mmol, 1.2 eq.) was added dropwise and the reaction mixture was stirred for another 16 h at room temperature. Afterwards, $NaHCO_3$ (25 ml) was added slowly and the mixture was transferred into a separation funnel. After separating the aqueous and organic phase, the aqueous phase was extracted 3× with DCM (50 ml). The combined organic layers were then washed 2× with 2 M HCl (25 ml), 2× with water (25 ml) and 2× with brine (25 ml). After drying over $NaSO_4$, the crude product was concentrated *in vacuo* (20 mbar). Purification was done by column chromatography (2% Et_2O / PE, visualization *via* UV detection + $KMnO_4$ stain). The product was obtained as colorless crystals (1266 mg, 5.8 mmol, 58%).

Melting point 31 – 33 °C.

^{1}H NMR (600 MHz, $CDCl_3$) δ 7.42 – 7.37 (m, 2H), 7.07 – 7.01 (m, 2H), 6.34 (t, *J* = 1.2 Hz, 1H), 5.74 (p, *J* = 1.6 Hz, 1H), 2.06 (dd, *J* = 1.6, 1.0 Hz, 3H), 1.32 (s, 9H).

^{13}C NMR (151 MHz, $CDCl_3$) δ 166.22 (s), 148.64 (s), 148.61 (s), 136.07 (s), 127.27 (s), 126.46 (s), 121.00 (s), 34.61 (s), 31.55 (s), 18.60 (s).

HRMS (ESI) calc. for $C_{14}H_{19}O_2$ $[M+H]^+$ 219.1441, found 219.1384.

IR (ν_{max}/cm^{-1}) 2964 (C-H), 1726 (C=O), 1297 (C-O), 1173 (C=O), 875 (C=C), 809 (C-H arom.).

5.2.7 Synthesis of *N*-ethyl-*N*-phenylmethacrylamide (13)

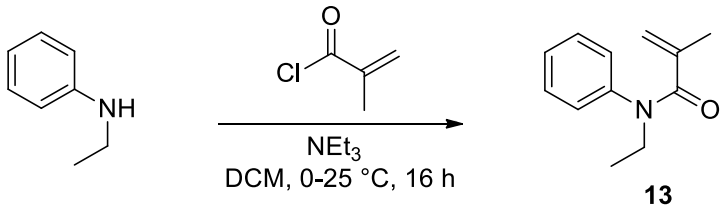

13

Compound **13** was prepared according to literature procedures[72] with slight modifications.

To a solution of *N*-ethylaniline (1259 µl, 10.0 mmol, 1.0 eq.) in DCM (25 ml) NEt_3 (1663 µl, 12.0 mmol, 1.2 eq.) was added and the mixture was stirred at room temperature. Then it was cooled to 0 °C, methacryloylchloride (1172 µl, 12.0 mmol, 1.2 eq.) was added dropwise and the reaction mixture was stirred for another 16 h at room temperature. Afterwards, $NaHCO_3$ (25 ml) was added slowly and the mixture was transferred into a separation funnel. After separating the aqueous and organic phase, the aqueous phase was extracted 3× with DCM (50 ml). The combined organic layers were then washed 2× with 2 M HCl (25 ml), 2× with water (25 ml) and 2× with brine (25 ml). After drying over $NaSO_4$, the crude product was concentrated *in vacuo* (20 mbar). Purification was done by column chromatography (wet loaded, 1:4 EtOAc / PE, visualization *via* UV detection + $KMnO_4$ stain). The product was obtained as a light-yellow liquid (1090 mg, 5.8 mmol, 58%).

^{1}H NMR (600 MHz, $CDCl_3$) δ 7.37 – 7.32 (m, 2H), 7.29 – 7.25 (m, 1H), 7.13 – 7.09 (m, 2H), 5.01 – 4.98 (m, 1H), 4.96 (d, *J* = 1.6 Hz, 1H), 3.83 (q, *J* = 7.1 Hz, 2H), 1.74 (s, 3H), 1.14 (t, *J* = 7.1 Hz, 3H).

^{13}C NMR (151 MHz, $CDCl_3$) δ 171.87 (s), 143.22 (s), 141.35 (s), 129.49 (s), 127.95 (s), 127.40 (s), 119.41 (s), 44.90 (s), 20.72 (s), 13.26 (s).

Analytical data was in agreement with literature.[73]

5.3 Photocatalytic Hydrocarboxylation of Electron-Deficient Olefins

5.3.1 General Reaction Setup

All photo reactions were carried out in 8 ml screw-cap vials and mixing was performed with/using a magnetic stirrer. As irradiation source, a 36 W Kessil PR160L LED lamp (460 nm) was used at a distance of 6 cm from the reaction vials employing maximum intensity (100%). To make sure that every reaction vessel receives the same light intensity with identical penetration depth, a maximum of three reaction vials were simultaneously positioned parallel to each other, at a distance of 6 cm from the light source.

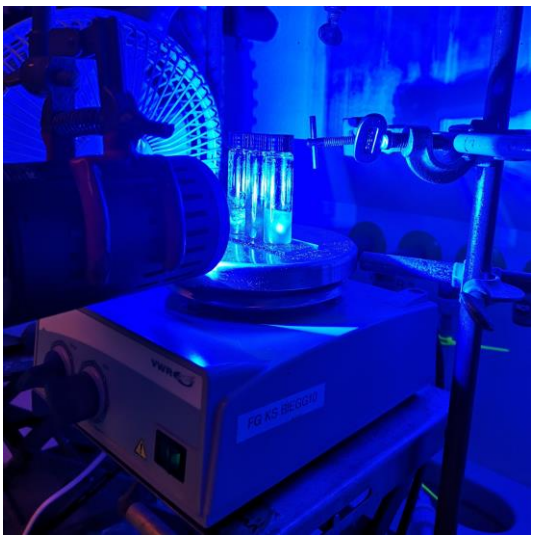

Figure 10: Reaction setup

5.3.2 General Reaction Procedure

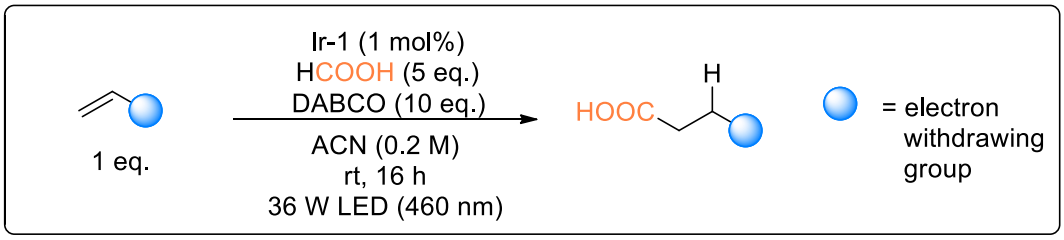

All reactions were performed under atmospheric conditions. The iridium catalyst (Ir-1) (2.0 µmol, 1 mol%) was weighted into an 8 ml screw-cap vial, followed by DABCO (2.0 mmol, 10.0 eq.) and the substrate (0.2 mmol, 1 eq.), if it was solid. Liquid substrates were added after addition of solvent and formic acid. The mixture was dissolved in ACN (0.2 M, 2 ml) and formic acid was added (1.0 mmol, 5.0 eq.). The reaction mixture was stirred for 16 h under continuous irradiation at 460 nm. After reaction completion, the solvent was removed *in vacuo*. The crude matrix was dissolved in $CDCl_3$ and TCE (0.2 mmol, 1 eq.) was added as an internal standard to control conversion *via* ^1H NMR. If the reaction was successful, the solvent and TCE were evaporated and workup was performed. Depending on the substrate, different workup methods were used.

Workup method A (preferred method)

The crude solid was suspended in EtOAc (5 ml) and 2 M HCl was added until the pH of the solution reached 1-2. Afterwards, the clear solution was extracted 3× with EtOAc (5 ml). The organic layers were combined, dried over Na_2SO_4 and concentrated *in vacuo.* Purification was done with column chromatography. Lastly, the obtained product was dried under high vacuum (0.1 mbar) overnight.

Workup method B (for pH-stable substrates, advantage of no column)

The crude solid was suspended in EtOAc (5 ml) and a minimum amount of 2 M NaOH was added till the pH was 11-12. Afterwards, it was washed 2× with EtOAc (5ml) and then, the aqueous phase was reacidified by adding a minimum amount of 2 M HCl until the pH got to 1-2. The product was back extracted from the aqueous phase by using 3× EtOAc (5 ml). The combined organic layers were dried over Na_2SO_4 and concentrated *in vacuo* (20 mbar). No further purification had to be performed with this workup method. Lastly, the obtained product was dried under high vacuum (0.1 mbar) overnight.

Workup method C (for volatile substrates)

The same procedure as in workup method A was performed with the exception of the final purification step. Instead of purifying the product with column chromatography, the compound was redissolved in a minimum amount of Et_2O and filtered through a Pasteur column, filled with silica. The obtained product was concentrated *in vacuo* (20 mbar).

5.2.3 Analytical Data of Hydrocarboxylated Products

4-(Benzyloxy)-4-oxobutanoic acid (14)

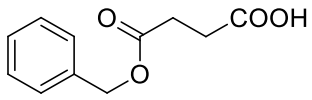

14

In accordance to the general procedure of 5.3.2, benzyl acrylate (30.6 µl, 0.2 mmol, 1.0 eq.), DABCO (224.4 mg, 2.0 mmol, 10.0 eq.), HCOOH (37.7 µl, 1.0 mmol, 5.0 eq.) and Ir-1 (2.24 mg, 2.0 µmol, 1 mol%) were used. Workup method **A** & **B** were used.

^{1}H NMR conversion (using TCE as internal standard): > 99%

Workup method A: Purification was done by column chromatography (1:6 → 1:1 EtOAc / PE, visualization *via* UV detection + phosphomolybdic acid stain). The product was isolated as colorless crystals (27.90 mg, 0.134 mmol, 67%).

Workup method B: The product was isolated as a yellowish solid (10.41 mg, 0.050 mmol, 25%).

^{1}H NMR (400 MHz, $CDCl_3$) δ 7.38 – 7.33 (m, 5H), 5.15 (s, 2H), 2.75 – 2.65 (m, 4H).

^{13}C NMR (101 MHz, $CDCl_3$) δ 178.39 (s), 172.12 (s), 135.79 (s), 128.69 (s), 128.42 (s), 128.33 (s), 66.78 (s), 29.06 (s), 29.00 (s).

Analytical data was in agreement with literature.[74]

Isolation of benzyl propionate (reduced side product) (15)

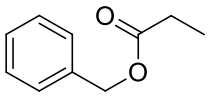

15

Workup method A: Purification was done by column chromatography (1:6 EtOAc / PE isocratic, visualization *via* UV detection + phosphomolybdic acid stain). The product was isolated as a colorless liquid (8.21 mg, 0.050 mmol, 25%).

^{1}H NMR (600 MHz, $CDCl_3$) δ 7.40 – 7.34 (m, 5H), 5.12 (s, 2H), 2.39 (q, J = 7.6 Hz, 2H), 1.17 (t, J = 7.6 Hz, 3H).

Analytical data was in agreement with literature.[75]

4-(Benzyloxy)-3-methyl-4-oxobutanoic acid (16)

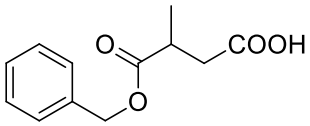

16

In accordance to the general procedure of 5.3.2, benzyl methacrylate (33.9 µl, 0.2 mmol, 1.0 eq.), DABCO (224.4 mg, 2.0 mmol, 10.0 eq.), HCOOH (37.7 µl, 1.0 mmol, 5.0 eq.) and Ir-1 (2.24 mg, 2.0 µmol, 1 mol%) were used. Workup method **A** was used.

^{1}H NMR conversion (using TCE as internal standard): > 99%

Workup method A: Purification was done by column chromatography (3:7 → 1:1 EtOAc / PE, visualization *via* UV detection + bromocresol green). The product was isolated as colorless crystals (22.56 mg, 0.106 mmol, 53%).

^{1}H NMR (600 MHz, DMSO) δ 7.39 – 7.30 (m, 5H), 5.09 (d, *J* = 1.5 Hz, 2H), 2.86 – 2.77 (m, 1H), 2.56 (dd, *J* = 16.9, 8.5 Hz, 1H), 2.41 (dd, *J* = 16.8, 5.5 Hz, 1H), 1.13 (d, *J* = 7.2 Hz, 3H).

^{13}C NMR (151 MHz, DMSO) δ 174.79 (s), 172.93 (s), 136.32 (s), 128.46 (s), 127.95 (s), 127.65 (s), 65.50 (s), 37.15 (s), 35.34 (s), 16.76 (s).

Analytical data was in agreement with literature.[76]

Isolation of benzyl 2-methyl-4-oxooxetane-2-carboxylate (side product) (17)

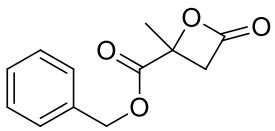

17

Workup method A: Purification was done by column chromatography (3:7 → 1:1 EtOAc / PE, visualization *via* UV detection + bromocresol green). The product was isolated as colorless oil. (11.01 mg, 0.050 mmol, 25%).

^{1}H NMR (400 MHz, DMSO) δ 7.40 – 7.28 (m, 5H), 5.17 – 5.05 (m, 2H), 2.73 (d, *J* = 15.8 Hz, 1H), 2.57 (d, *J* = 15.8 Hz, 1H), 1.35 (s, 3H).

^{13}C NMR (101 MHz, DMSO) δ 174.44 (s), 171.70 (s), 136.27 (s), 128.42 (s), 127.94 (s), 127.62 (s), 72.08 (s), 65.81 (s), 44.69 (s), 26.07 (s).

HRMS (ESI) calc. for $C_{12}H_{14}O_5Na$ $[M+H_2O+Na]^+$ 261.0739, found 261.0800.

IR (ν_{max}/cm^{-1}) 2982 (C-H), 1726 (C=O), 1188 (C-O), 1111 (C-O), 740 (C-H arom.).

4-((4-Methoxybenzyl)oxy)-4-oxobutanoic acid (18)

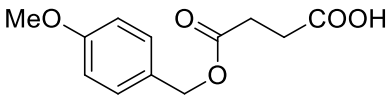

18

In accordance to the general procedure of 5.3.2, 4-methoxybenzyl acrylate (38.44 mg, 0.2 mmol, 1.0 eq.), DABCO (224.4 mg, 2.0 mmol, 10.0 eq.), HCOOH (37.7 µl, 1.0 mmol, 5.0 eq.) and Ir-1 (2.24 mg, 2.0 µmol, 1 mol%) were used. Workup method **A** was used.

^{1}H NMR conversion (using TCE as internal standard): 76%

Workup method A: Purification was done by column chromatography (1:2 EtOAc / PE, visualization *via* UV detection + phosphomolybdic acid stain). The product was isolated as a white-yellowish solid (18.58 mg, 0.078 mmol, 39%).

^{1}H NMR (600 MHz, MeOD) δ 7.30 – 7.24 (m, 2H), 6.90 – 6.83 (m, 2H), 5.04 (s, 2H), 3.77 (s, 3H), 2.62 – 2.55 (m, 4H).

^{13}C NMR (151 MHz, MeOD) δ 176.00 (s), 174.10 (s), 161.11 (s), 131.07 (s), 129.48 (s), 114.82 (s), 67.24 (s), 55.66 (s), 30.08 (s), 29.71 (s).
Analytical data was in agreement with literature.[74]

4-((4-Nitrobenzyl)oxy)-4-oxobutanoic acid (19)

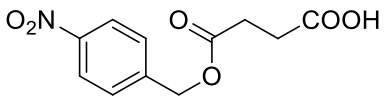

19

In accordance to the general procedure of 5.3.2, 4-nitrobenzyl acrylate (41.43 mg, 0.2 mmol, 1.0 eq.), DABCO (224.4 mg, 2.0 mmol, 10.0 eq.), HCOOH (37.7 µl, 1.0 mmol, 5.0 eq.) and Ir-1 (2.24 mg, 2.0 µmol, 1 mol%) were used. Workup method **A** was used.

^{1}H NMR conversion (using TCE as internal standard): 88%

Workup method A: Purification was done by column chromatography (1:4 → 100% EtOAc / PE, visualization *via* UV detection + phosphomolybdic acid stain + bromocresol green stain). The product was isolated as a white solid (4.05 mg, 0.016 mmol, 8%).

^{1}H NMR (600 MHz, MeOD) δ 7.37 – 7.33 (m, 4H), 5.12 (s, 2H), 2.63 (ddd, *J* = 7.4, 5.8, 1.3 Hz, 2H), 2.58 (ddd, *J* = 7.0, 5.8, 1.3 Hz, 2H).

^{13}C NMR (151 MHz, MeOD) δ 176.99 (s), 174.23 (s), 168.88 (s), 137.62 (s), 129.51 (s), 129.09 (d, *J* = 7.0 Hz), 67.30 (s), 45.51 (s), 30.45 (d, *J* = 9.7 Hz).

Analytical data was in agreement with literature.[74]

4-Methoxy-4-oxobutanoic acid (20)

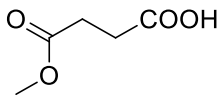

20

In accordance to the general procedure of 5.3.2, methyl acrylate (18.13 µl, 0.2 mmol, 1.0 eq.), DABCO (224.4 mg, 2.0 mmol, 10.0 eq.), HCOOH (37.7 µl, 1.0 mmol, 5.0 eq.) and Ir-1 (2.24 mg, 2.0 µmol, 1 mol%) were used. Workup method **C** was used.

^{1}H NMR conversion (using TCE as internal standard): 91%

Workup method C: The product was isolated as a light yellow solid (16.35 mg, 0.124 mmol, 62%).

^{1}H NMR (400 MHz, $CDCl_3$) δ 3.70 (s, 3H), 2.69 (ddd, *J* = 6.8, 5.6, 1.7 Hz, 2H), 2.65 – 2.60 (m, 2H).

^{13}C NMR (151 MHz, DMSO) δ 172.77 (s), 171.98 (s), 50.75 (s), 27.98 (s), 27.83 (s).
Analytical data was in agreement with literature.[77]

4-Butoxy-4-oxobutanoic acid (21)

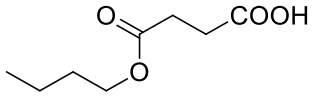

21

In accordance to the general procedure of 5.3.2, butyl acrylate (28.49 µl, 0.2 mmol, 1.0 eq.), DABCO (224.4 mg, 2.0 mmol, 10.0 eq.), HCOOH (37.7 µl, 1.0 mmol, 5.0 eq.) and Ir-1 (2.24 mg, 2.0 µmol, 1 mol%) were used. Workup method **C** was used.

^{1}H NMR conversion (using TCE as internal standard): 74%

Workup method C: The product was isolated as a white-yellowish solid (20.90 mg, 0.120 mmol, 60%).

^{1}H NMR (400 MHz, $CDCl_3$) δ 4.09 (t, *J* = 6.7 Hz, 2H), 2.67 (ddd, *J* = 6.9, 5.6, 1.7 Hz, 2H), 2.64 – 2.58 (m, 2H), 1.60 (ddt, *J* = 8.9, 7.9, 6.5 Hz, 2H), 1.41 – 1.31 (m, 2H), 0.91 (t, *J* = 7.4 Hz, 3H).

^{13}C NMR (101 MHz, $CDCl_3$) δ 178.32 (s), 172.36 (s), 64.87 (s), 30.69 (s), 29.11 (s), 29.03 (s), 19.19 (s), 13.77 (s).

Analytical data was in agreement with literature.[78]

4-(*tert*-Butoxy)-4-oxobutanoic acid (22)

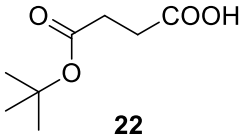

22

In accordance to the general procedure of 5.3.2, *tert*-butyl acrylate (29.14 µl, 0.2 mmol, 1.0 eq.), DABCO (224.4 mg, 2.0 mmol, 10.0 eq.), HCOOH (37.7 µl, 1.0 mmol, 5.0 eq.) and Ir-1 (2.24 mg, 2.0 µmol, 1 mol%) were used. Workup method **C** was used.

^{1}H NMR conversion (using TCE as internal standard): 60%

Workup method C: The product was isolated as a white-yellowish solid (8.01 mg, 0.046 mmol, 23%).

^{1}H NMR (600 MHz, DMSO) δ 2.42 – 2.37 (m, 4H), 1.38 (s, 9H).

^{13}C NMR (151 MHz, DMSO) δ 173.53 (d, *J* = 9.6 Hz), 171.40 (d, *J* = 5.2 Hz), 79.73 (s), 29.84 (d, *J* = 7.8 Hz), 28.82 (d, *J* = 5.8 Hz), 27.74 (d, *J* = 2.4 Hz).

Analytical data was in agreement with literature. [49]

4-(Methyl(phenyl)amino)-4-oxobutanoic acid (23)

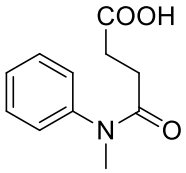

23

In accordance to the general procedure of 5.3.2, *N*-methyl-*N*-phenylacrylamide (32.24 mg, 0.2 mmol, 1.0 eq.), DABCO (224.4 mg, 2.0 mmol, 10.0 eq.), HCOOH (37.7 µl, 1.0 mmol, 5.0 eq.) and Ir-1 (2.24 mg, 2.0 µmol, 1 mol%) were used. Workup method **A** & **B** were used.

^{1}H NMR conversion (using TCE as internal standard): 95%

Workup method A: Purification was done by column chromatography (1:4 → 100% EtOAc / PE, visualization *via* UV detection + phosphomolybdic acid stain). The product was isolated as a yellow-brownish oil (16.58 mg, 0.080 mmol, 40%).

Workup method B: The product was isolated as a dark green oil (17.41 mg, 0.084 mmol, 42%).

^{1}H NMR (400 MHz, MeOD) δ 7.48 (t, *J* = 7.6 Hz, 2H), 7.43 – 7.36 (m, 1H), 7.36 – 7.29 (m, 2H), 3.24 (s, 3H), 2.53 (t, *J* = 6.5 Hz, 2H), 2.33 (t, *J* = 6.6 Hz, 2H).

^{13}C NMR (101 MHz, MeOD) δ 176.35 (s), 173.88 (s), 145.04 (s), 131.02 (s), 129.27 (s), 128.52 (s), 37.76 (s), 30.12 (d, *J* = 5.2 Hz), 20.73 (s).

Analytical data was in agreement with literature.[79]

4-(Ethyl(phenyl)amino)-4-oxobutanoic acid (24)

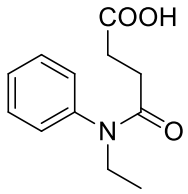

24

In accordance to the general procedure of 5.3.2, *N*-ethyl-*N*-phenylacrylamide (35.05 mg, 0.2 mmol, 1.0 eq.), DABCO (224.4 mg, 2.0 mmol, 10.0 eq.), HCOOH (37.7 µl, 1.0 mmol, 5.0 eq.) and Ir-1(2.24 mg, 2.0 µmol, 1 mol%) were used. Workup method **B** was used.

^{1}H NMR conversion (using TCE as internal standard): 99%

Workup method B: The product was isolated as a yellow oil (21.24 mg, 0.096 mmol, 48%).

^{1}H NMR (400 MHz, MeOD) δ 7.49 (dd, *J* = 8.3, 6.7 Hz, 2H), 7.44 – 7.38 (m, 1H), 7.32 – 7.27 (m, 2H), 3.73 (q, *J* = 7.2 Hz, 2H), 2.51 (dd, *J* = 7.4, 5.8 Hz, 2H), 2.28 (dd, *J* = 7.4, 5.8 Hz, 2H), 1.10 (t, *J* = 7.2 Hz, 3H).

^{13}C NMR (101 MHz, MeOD) δ 176.33 (s), 173.27 (s), 143.26 (s), 130.94 (s), 129.60 (s), 129.39 (s), 45.31 (s), 30.47 (s), 30.08 (s), 13.19 (s).

HRMS (ESI) calc. for $C_{11}H_{16}NO_3$ $[M+H]^+$ 222.1125, found 222.1130.

IR (ν_{max}/cm^{-1}) 2973 (O-H), 2957 (C-H), 1696 (C=O), 1333 (C-N), 771 (C-H arom.).

4-(Benzyl(phenyl)amino)-4-oxobutanoic acid (25)

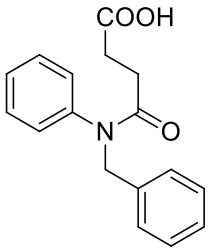

25

In accordance to the general procedure of 5.3.2, *N*-ethyl-*N*-phenylacrylamide (47.46 mg, 0.2 mmol, 1.0 eq.), DABCO (224.4 mg, 2.0 mmol, 10.0 eq.), HCOOH (37.7 µl, 1.0 mmol, 5.0 eq.) and Ir-1 (2.24 mg, 2.0 µmol, 1 mol%) were used. Workup method **B** was used.

^{1}H NMR conversion (using TCE as internal standard): 99%

Workup method B: The product was isolated as a yellow oil (20.40 mg, 0.072 mmol, 36%).

^{1}H NMR (400 MHz, MeOD) δ 7.40 – 7.30 (m, 4H), 7.29 – 7.21 (m, 4H), 7.20 – 7.16 (m, 2H), 7.14 – 7.09 (m, 2H), 4.90 (s, 2H), 2.57 (dd, *J* = 7.4, 5.6 Hz, 2H), 2.35 (dd, *J* = 7.4, 5.6 Hz, 2H).

^{13}C NMR (101 MHz, MeOD) δ 176.33 (s), 173.84 (s), 143.23 (s), 138.59 (s), 130.70 (s), 129.65 (s), 129.60 (s), 129.40 (s), 129.35 (s), 128.41 (s), 54.00 (s), 30.40 (s), 30.13 (s).

Analytical data was in agreement with literature.[80]

3-(*N*-Methyl-*N*-phenylsulfamoyl)propanoic acid (26)

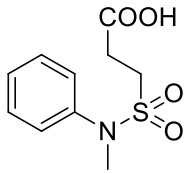

26

In accordance to the general procedure of 5.3.2, *N*-methyl-*N*-phenylethenesulfonamide (39.45 mg, 0.2 mmol, 1.0 eq.), DABCO (224.4 mg, 2.0 mmol, 10.0 eq.), HCOOH (37.7 µl, 1.0 mmol, 5.0 eq.) and Ir-1 (2.24 mg, 2.0 µmol, 1 mol%) were used. Workup method **B** was used.

^{1}H NMR conversion (using TCE as internal standard): 95%

Workup method B: The product was isolated as a yellow-brownish powder (9.73 mg, 0.040 mmol, 20%).

^{1}H NMR (400 MHz, MeOD) δ 7.46 – 7.35 (m, 5H), 3.41 – 3.37 (m, 2H), 3.33 (s, 3H), 2.72 (dd, *J* = 7.8, 7.1 Hz, 2H).

^{13}C NMR (101 MHz, MeOD) δ 173.76 (s), 142.88 (s), 130.32 (s), 128.49 (s), 127.83 (s), 45.96 (s), 38.90 (s), 29.04 (s).

Analytical data was in agreement with literature.[81]

3-(*N*-Ethyl-*N*-phenylsulfamoyl)propanoic acid (27)

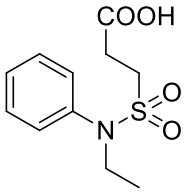

27

In accordance to the general procedure of 5.3.2, *N*-ethyl-*N*-phenylethenesulfonamide (42.26 mg, 0.2 mmol, 1.0 eq.), DABCO (224.4 mg, 2.0 mmol, 10.0 eq.), HCOOH (37.7 µl, 1.0 mmol, 5.0 eq.) and Ir-1 (2.24 mg, 2.0 µmol, 1 mol%) were used. Workup method **B** was used.

^{1}H NMR conversion (using TCE as internal standard): 99%

Workup method B: The product was isolated as a dark orange oil (8.23 mg, 0.032 mmol, 16%).

^{1}H NMR (400 MHz, MeOD) δ 7.42 dd, *J* = 7.5 Hz, 1.7 Hz, 5H), 3.76 (q, *J* = 7.1 Hz, 2H), 3.38 (dd, *J* = 7.8, 7.1 Hz, 2H), 2.75 (dd, *J* = 7.8, 7.1 Hz, 2H), 1.09 (t, *J* = 7.1 Hz, 3H).

^{13}C NMR (101 MHz, MeOD) δ 173.88 (s), 140.18 (s), 130.43 (s), 130.33 (s), 129.17 (s), 47.27 (d, *J* = 1.9 Hz), 45.58 (s), 29.25 (s), 14.83 (s).

HRMS (ESI) calc. for $C_{11}H_{15}NO_4SNa$ $[M+Na]^+$ 280.0614, found 280.0615.

IR (ν_{max}/cm^{-1}) 2973 (O-H), 2935 (C-H), 1721 (C=O), 1379 (C-N), 1171 (S=O), 702 (C-H arom.).

3-(*N*,*N*-Dibutylsulfamoyl)propanoic acid (28)

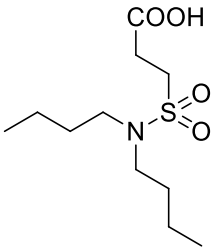

28

In accordance to the general procedure of 5.3.2, *N*,*N*-dibutylethenesulfonamide (43.89 mg, 0.2 mmol, 1.0 eq.), DABCO (224.4 mg, 2.0 mmol, 10.0 eq.), HCOOH (37.7 µl, 1.0 mmol, 5.0 eq.) and Ir-1 (2.24 mg, 2.0 µmol, 1 mol%) were used. Workup method **B** was used.

^{1}H NMR conversion (using TCE as internal standard): 98%

Workup method B: No further purification done. The product was isolated as a colorless oil (20.17 mg, 0.076 mmol, 38%).

^{1}H NMR (400 MHz, MeOD) δ 3.35 – 3.26 (m,2H), 3.26 – 3.17 (m, 4H), 2.74 (t, *J* = 7.4 Hz, 2H), 1.60 (tdd, *J* = 9.1, 6.9, 5.3 Hz, 4H), 1.42 – 1.31 (m, 4H), 0.97 (t, *J* = 7.4 Hz, 6H).

^{13}C NMR (101 MHz, MeOD) δ 174.01 (s), 48.88 (s), 47.60 (s), 32.37 (s), 29.25 (s), 20.90 (s), 14.06 (s).

HRMS (ESI) calc. for $C_{11}H_{24}NO_4S$ $[M+H]^+$ 266.1421, found 266.1417.

IR (ν_{max}/cm^{-1}) 2970 (O-H), 1712 (C=O), 1332 (C-N), 1166 (S=O).

5.4 Quantum Yield Determination

Solution Preparation for Photon Flux Determination (Made and stored in Dark):

1) Ferrioxalate solution (0.012 M): 147.4 mg of potassium ferrioxalate trihydrate (freshly prepared) and 69.5 µL of sulfuric acid (96%) was weighted into a 25 mL volumetric flask and filled with Milli-Q water.

2) Phenanthroline solution (0.2 wt%): 100 mg 1,10-phenanthroline was weighted into a 50 mL volumetric flask and filled with Milli-Q water.

3.) Buffer solution: 4.94 g NaOAc and 1.0 mL sulfuric acid (96%) were weighted into a 100 mL volumetric flask which was filled with Milli-Q water.

Practical Procedure for Quantum Yield Determination

Three reactions were carried out in parallel. The iridium catalyst (2.24 mg, 2.0 µmol, 1 mol%) was weighed into an 8 ml screw-cap vial, followed by DABCO (224.4 mg, 2.0 mmol, 10.0 eq.) and benzyl acrylate (30.6 µl, 0.2 mmol, 1 eq.). The mixture was dissolved in CD_3CN (0.2 M, 2 ml) and formic acid was added (37.7 µl, 1.0 mmol, 5.0 eq.). Subsequently, the mixture was stirred for 1 h under continuous irradiation by a 36 W lamp at 460 nm, from which the photon flux was calculated. Then the samples were analyzed by ^1H NMR spectroscopy and the average conversion was calculated. (See section 4.3.3)

6. NMR Spectra

6.1 Structure elucidation of the oxetane byproduct (17)

Benzyl 2-methyl-4-oxooxetane-2-carboxylate (17), ^{1}H NMR spectrum (600 MHz, DMSO)

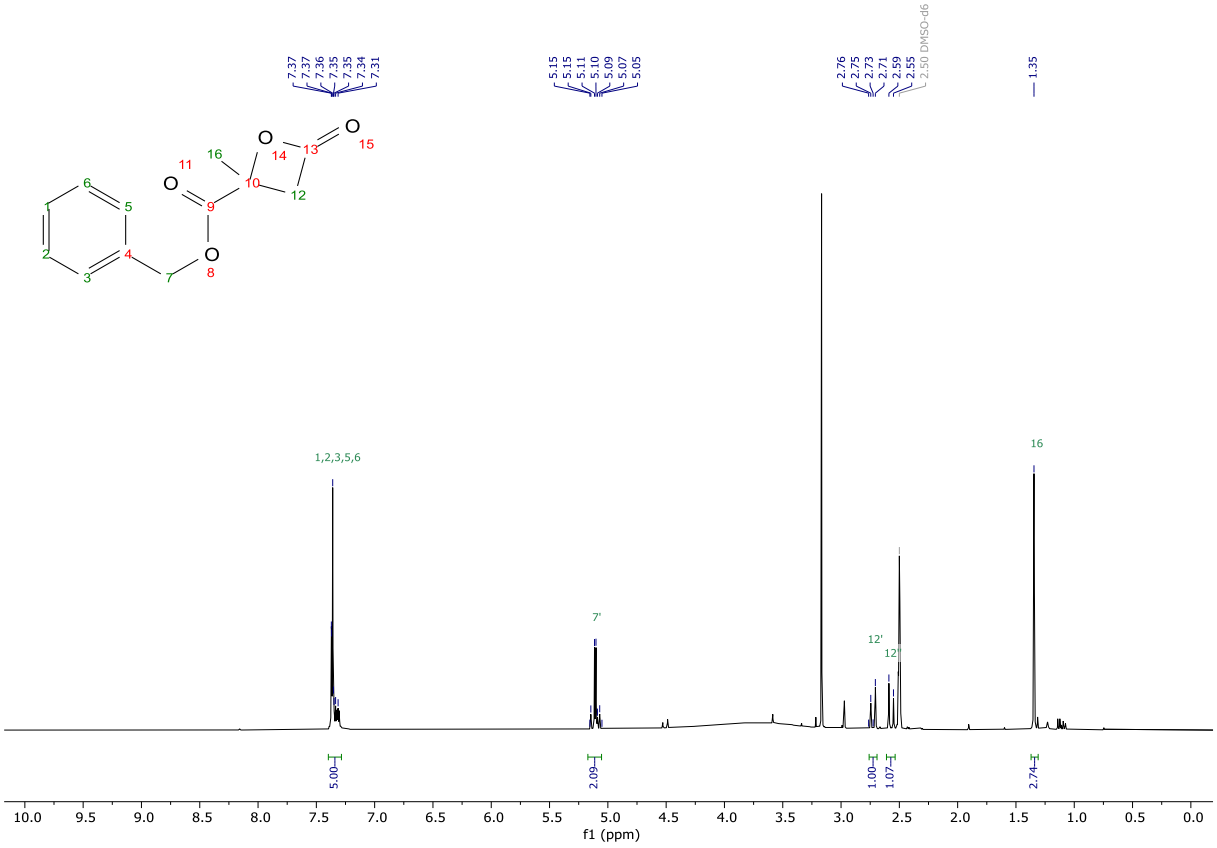

Benzyl 2-methyl-4-oxooxetane-2-carboxylate (17), ^{13}C NMR APT spectrum (151 MHz, DMSO)

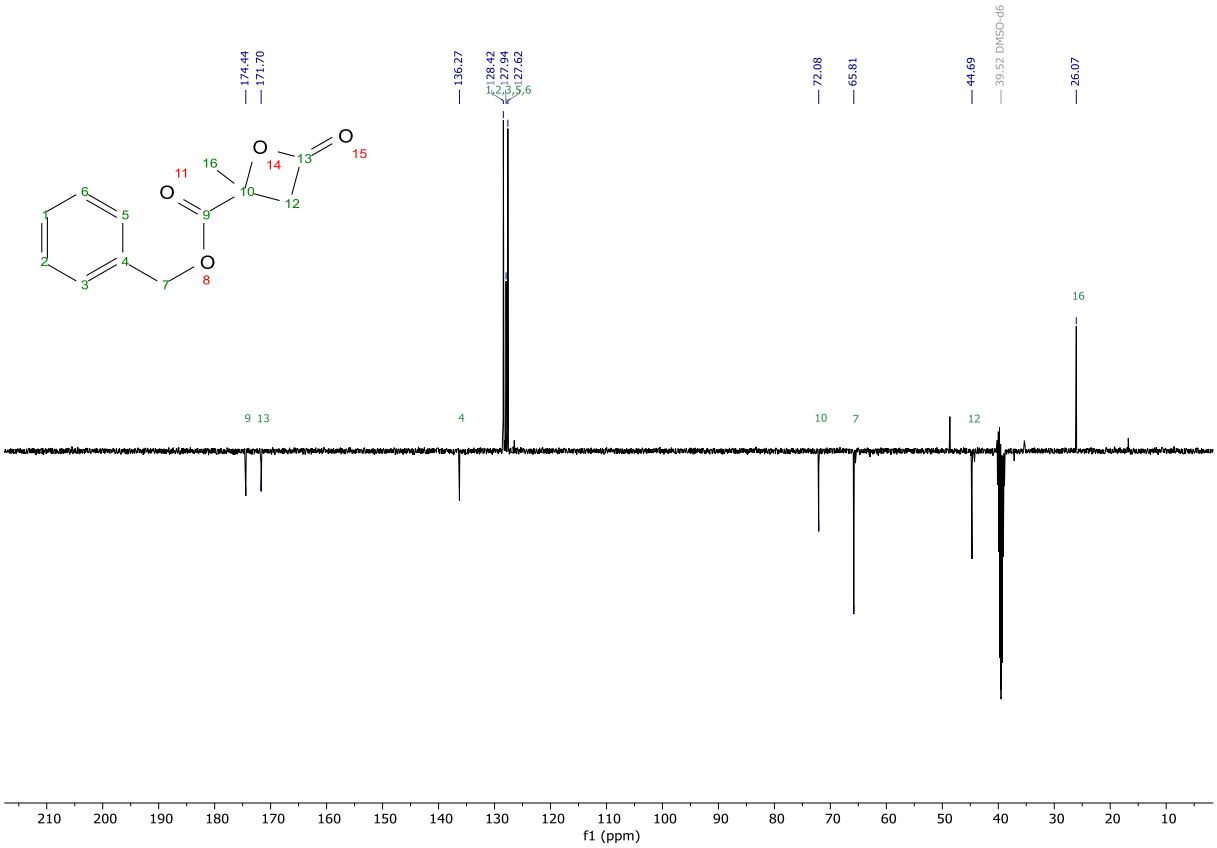

Benzyl 2-methyl-4-oxooxetane-2-carboxylate (17), HSQC spectrum

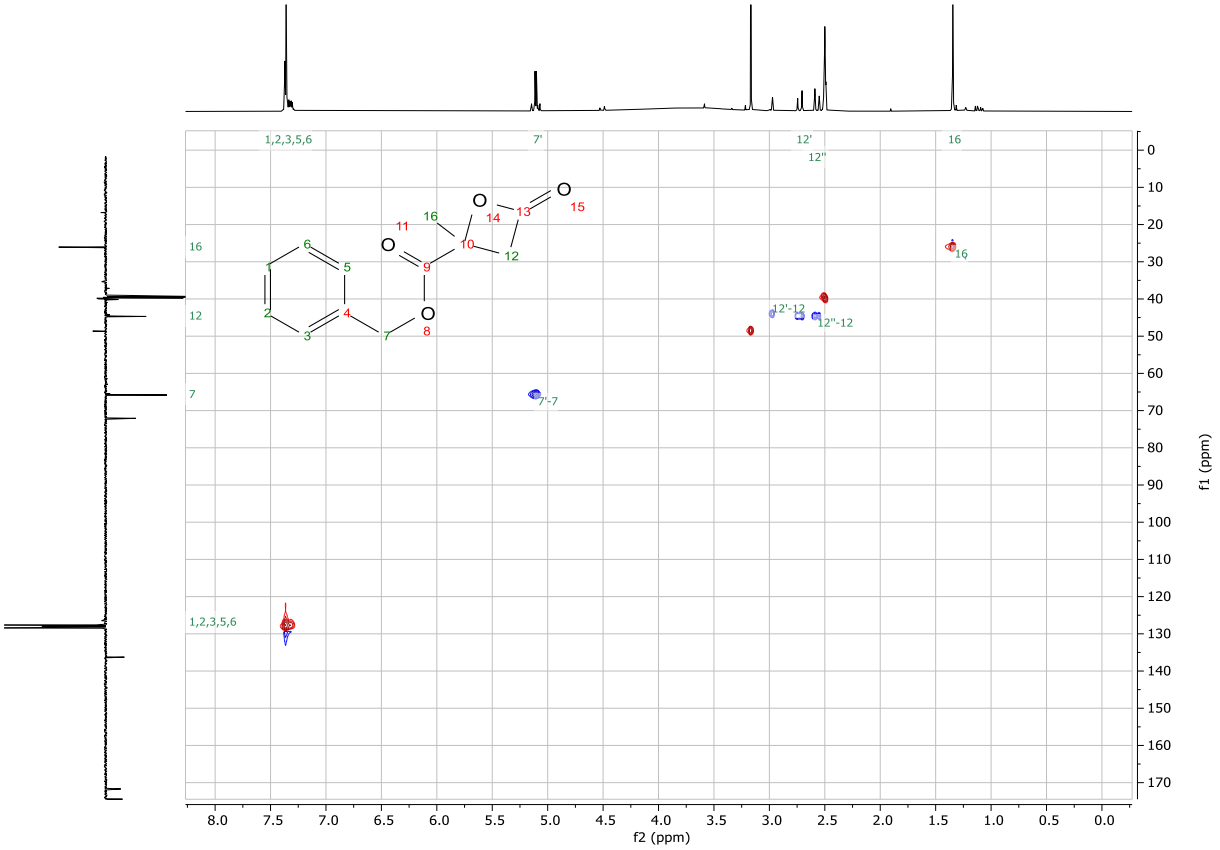

Benzyl 2-methyl-4-oxooxetane-2-carboxylate (17), COSY spectrum

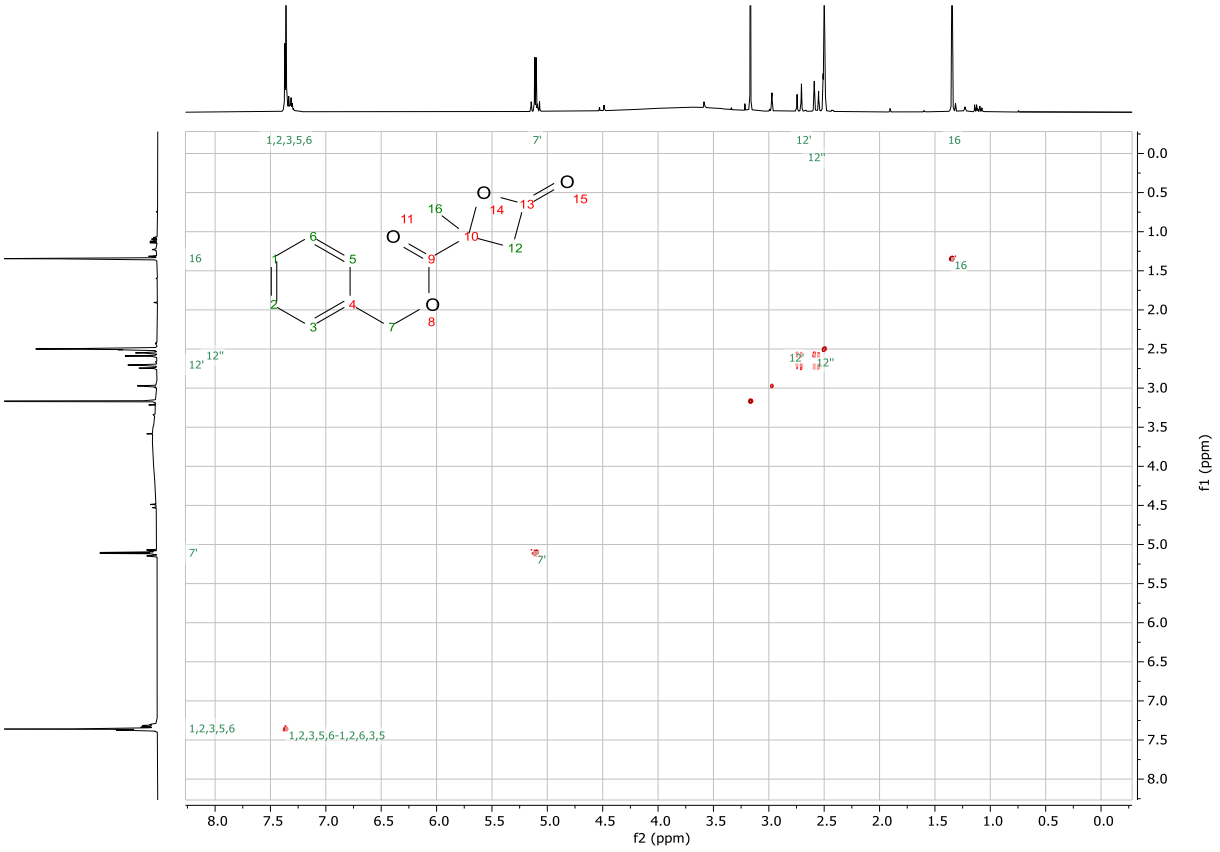

Benzyl 2-methyl-4-oxooxetane-2-carboxylate (17), HMBC spectrum

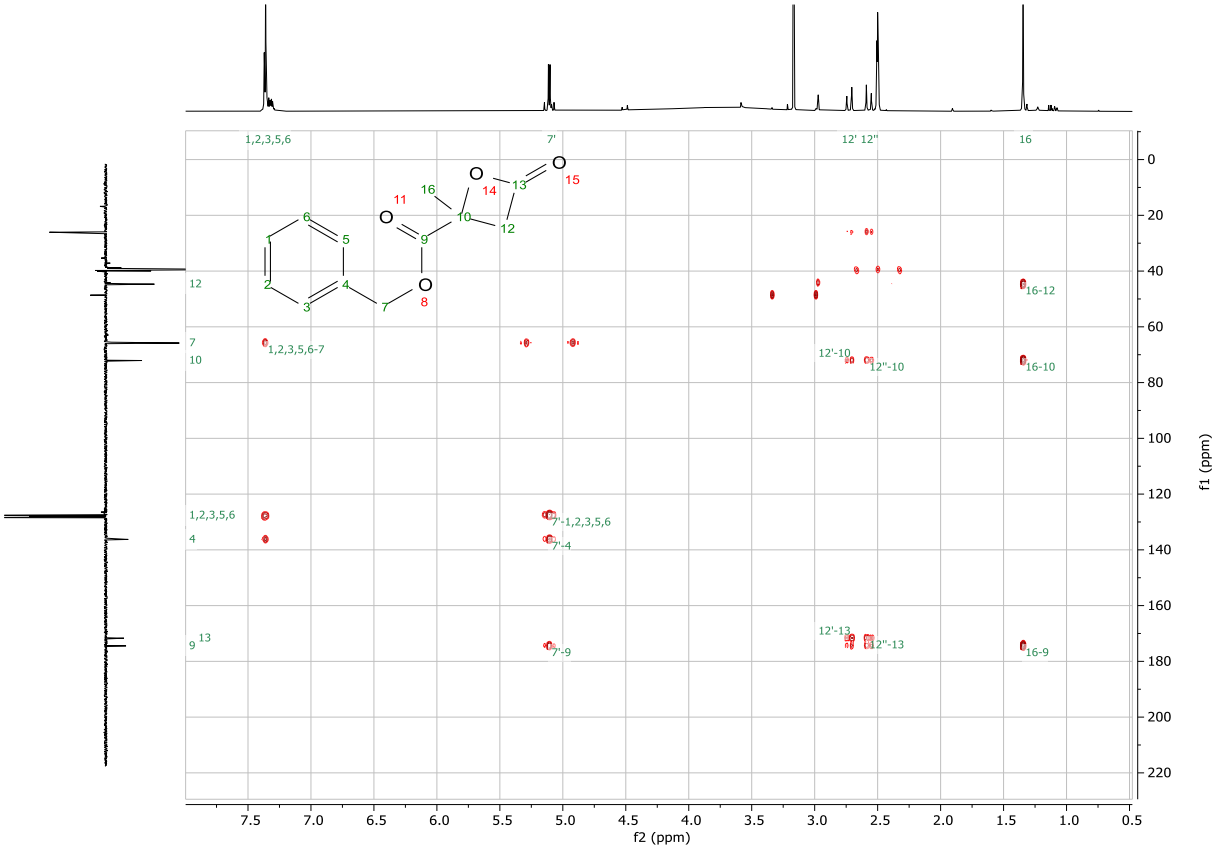

6.2 Other NMR spectra

4-Isopropylphenyl acrylate (7), ^{1}H NMR spectrum (600 MHz, $CDCl_3$)

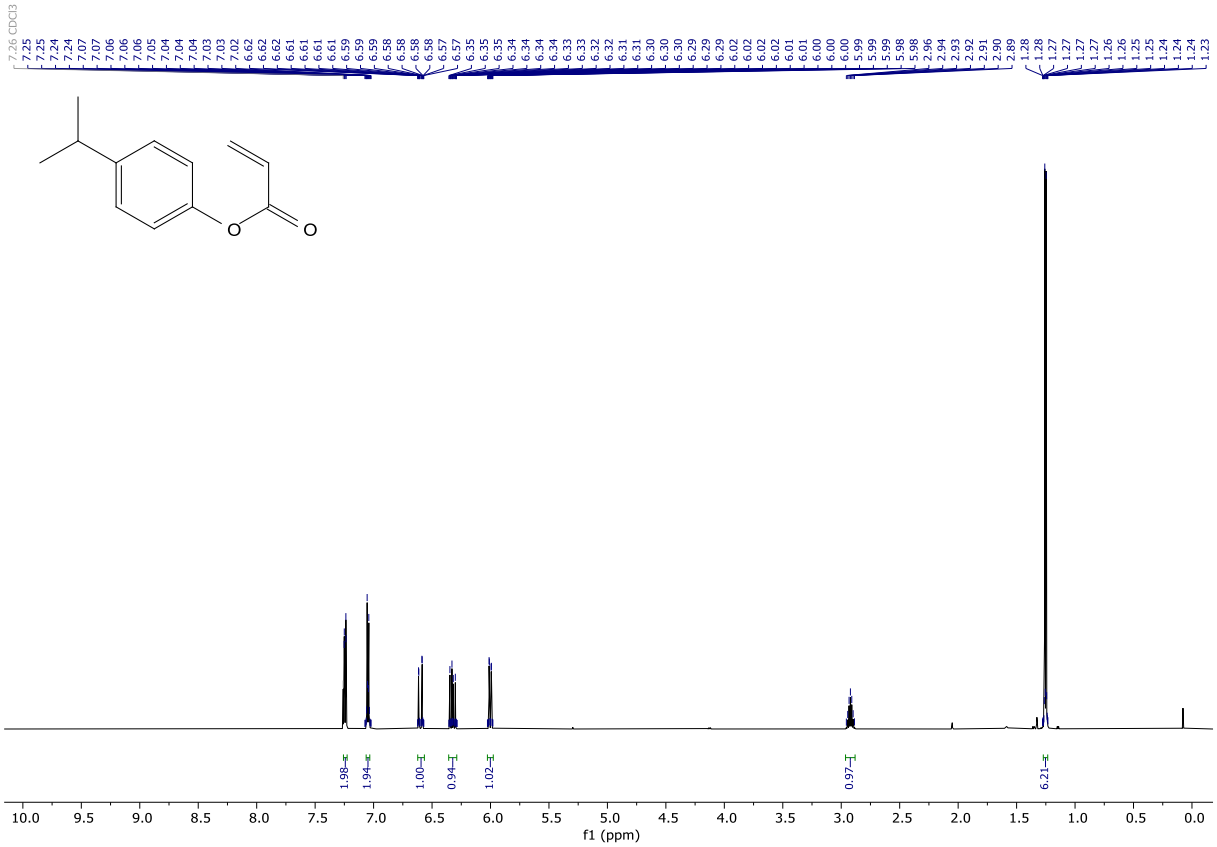

4-Isopropylphenyl acrylate (7), ^{13}C NMR spectrum (151 MHz, $CDCl_3$)

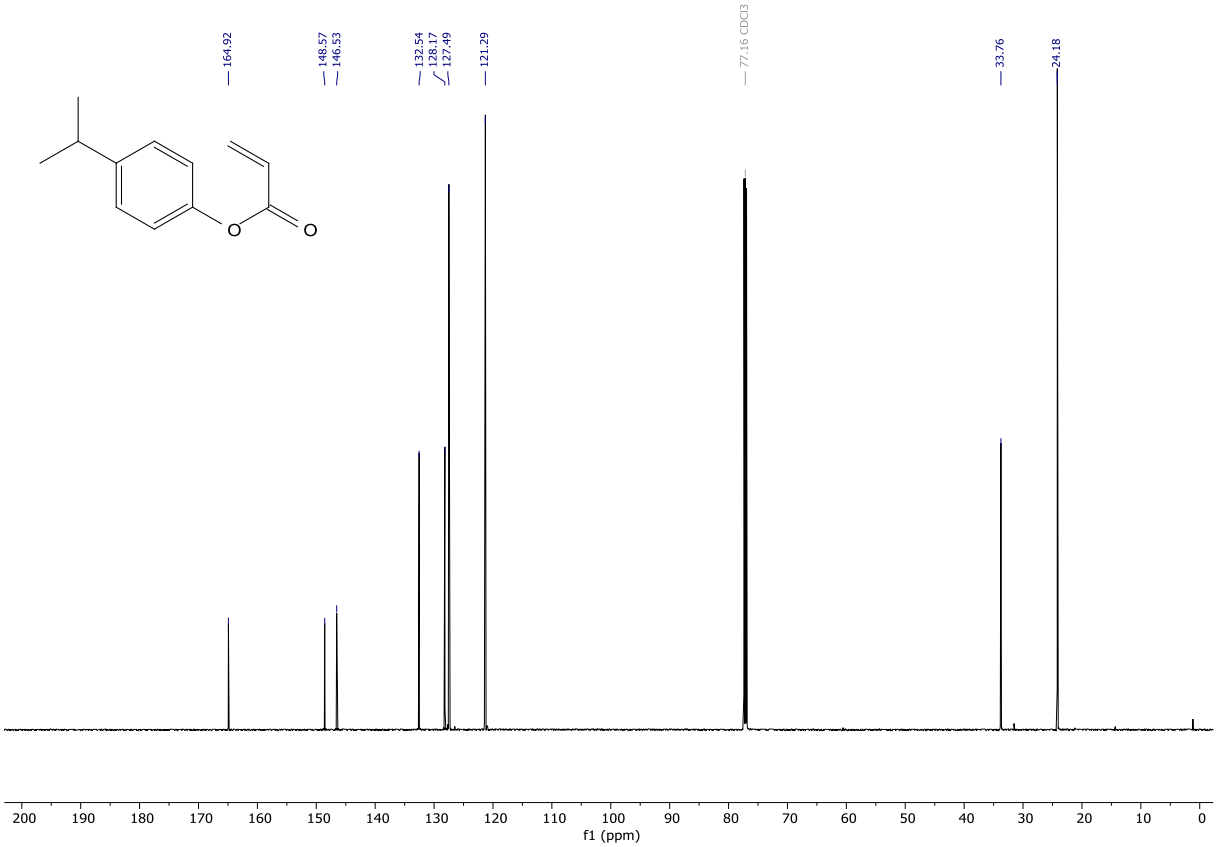

4-Isopropylphenylethenesulfonate (11), ^{1}H NMR spectrum (600 MHz, $CDCl_3$)

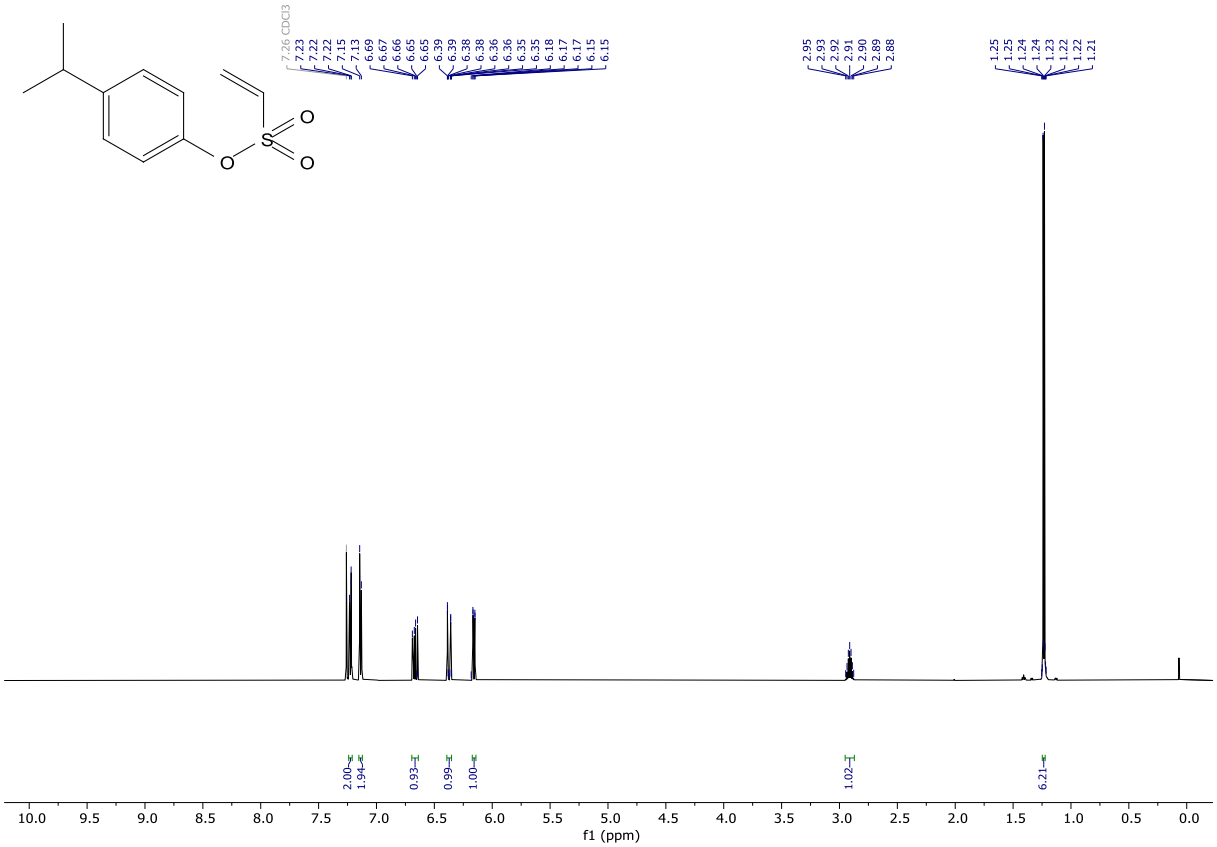

4-Isopropylphenylethenesulfonate (11), ^{13}C NMR spectrum (151 MHz, $CDCl_3$)

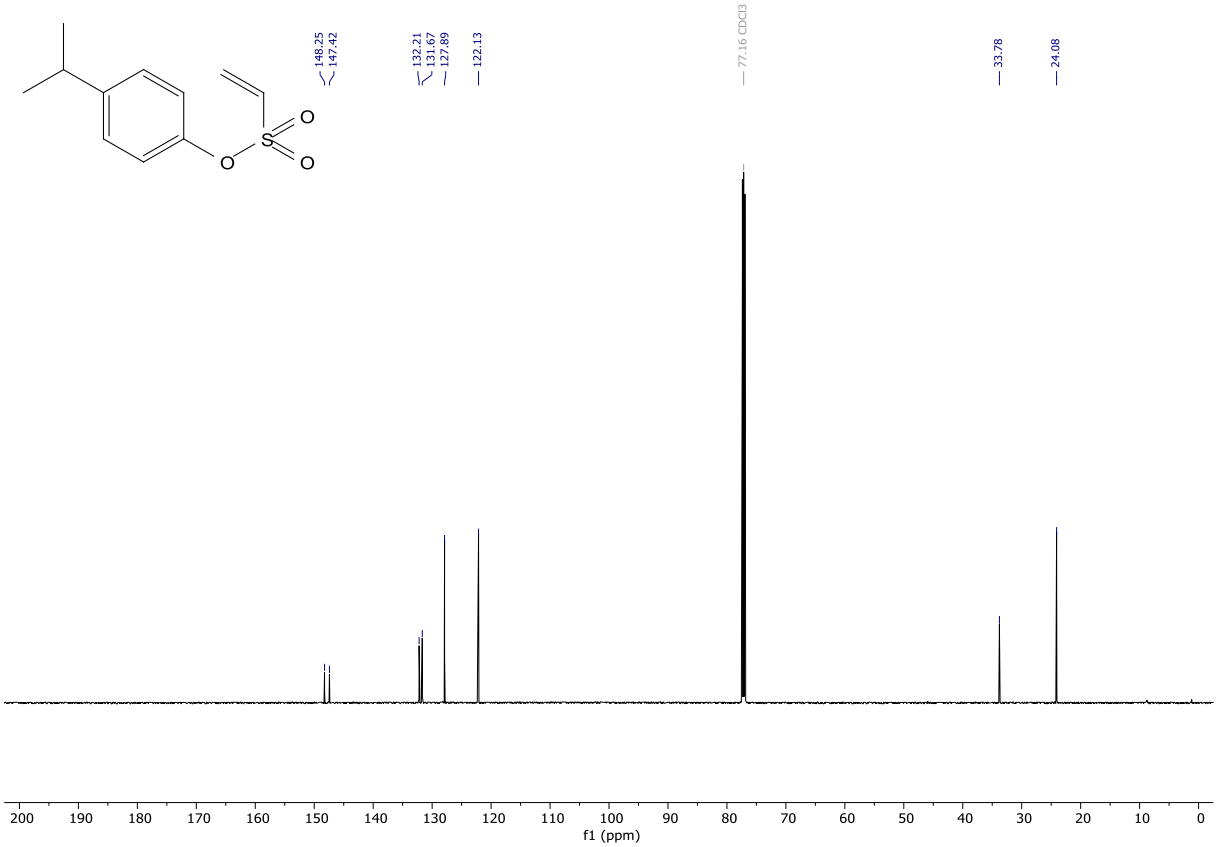

4-(*tert*-butyl)phenyl methacrylate (12), ^{1}H NMR spectrum (600 MHz, $CDCl_3$)

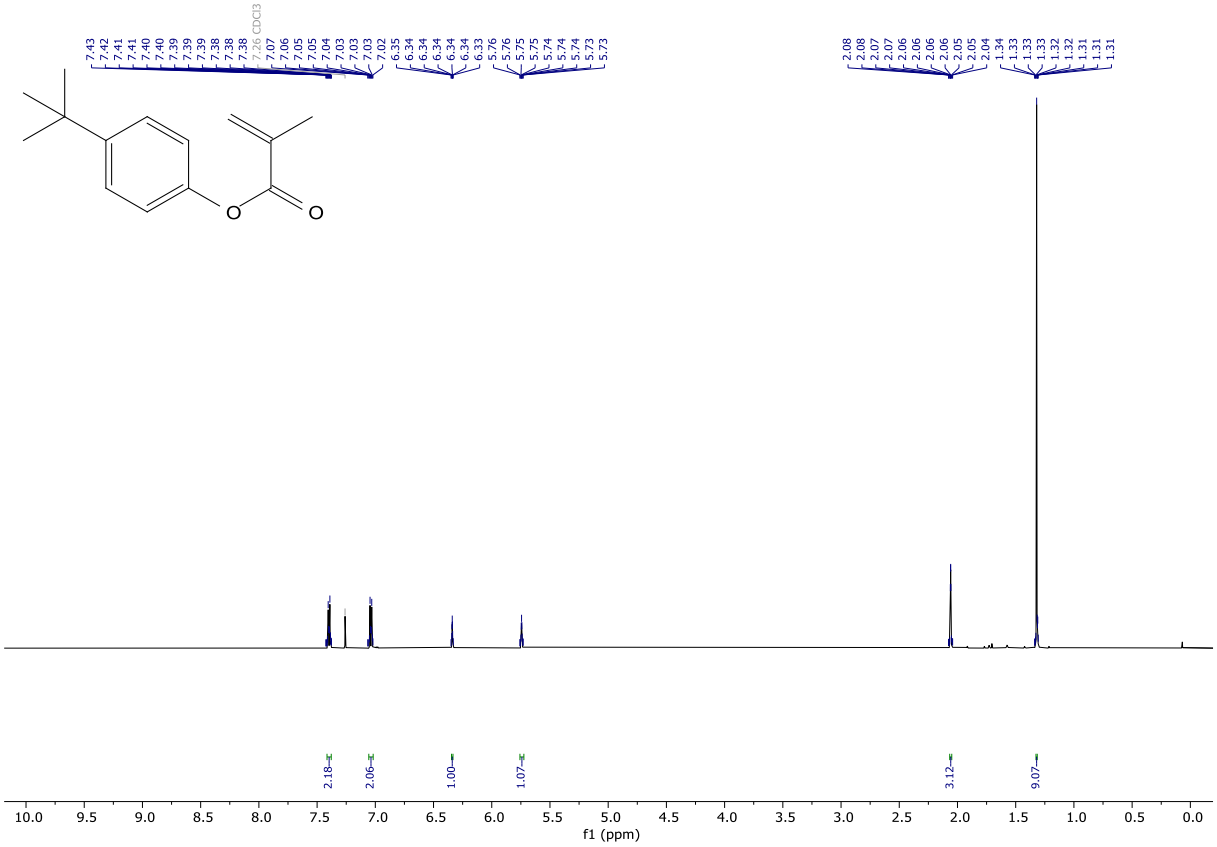

4-(*tert*-butyl)phenyl methacrylate (12), ^{13}C NMR spectrum (151 MHz, $CDCl_3$)

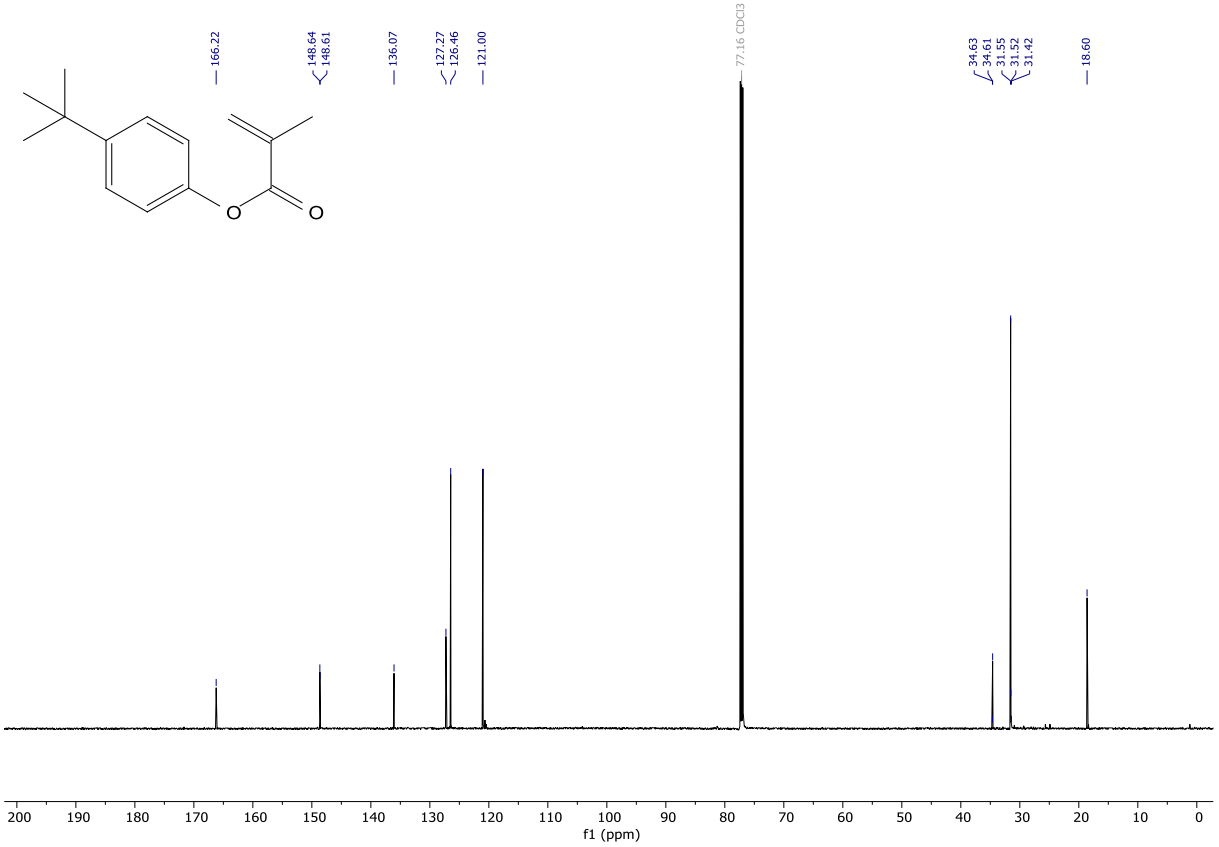

4-(Ethyl(phenyl)amino)-4-oxobutanoic acid (24), ^{1}H NMR spectrum (400 MHz, MeOD)

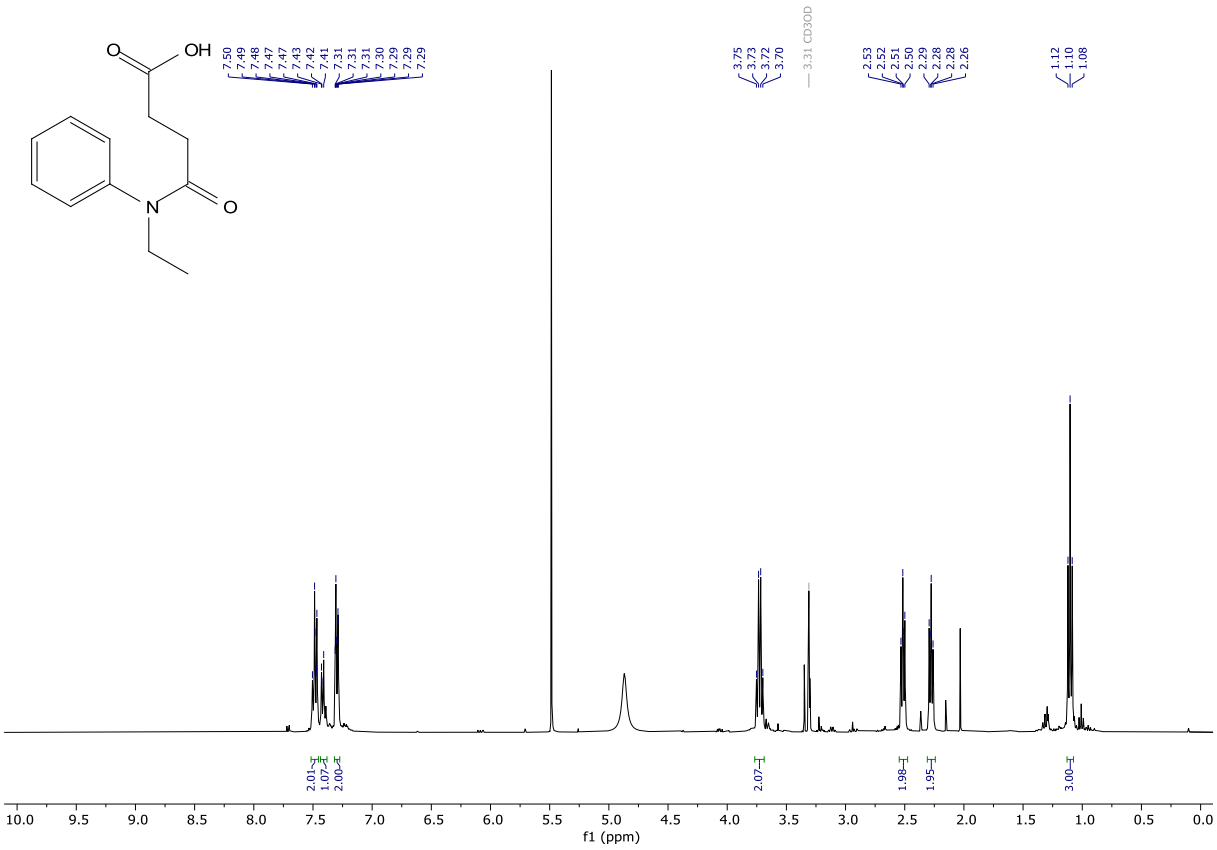

4-(Ethyl(phenyl)amino)-4-oxobutanoic acid (24), ^{13}C NMR spectrum (101 MHz, MeOD)

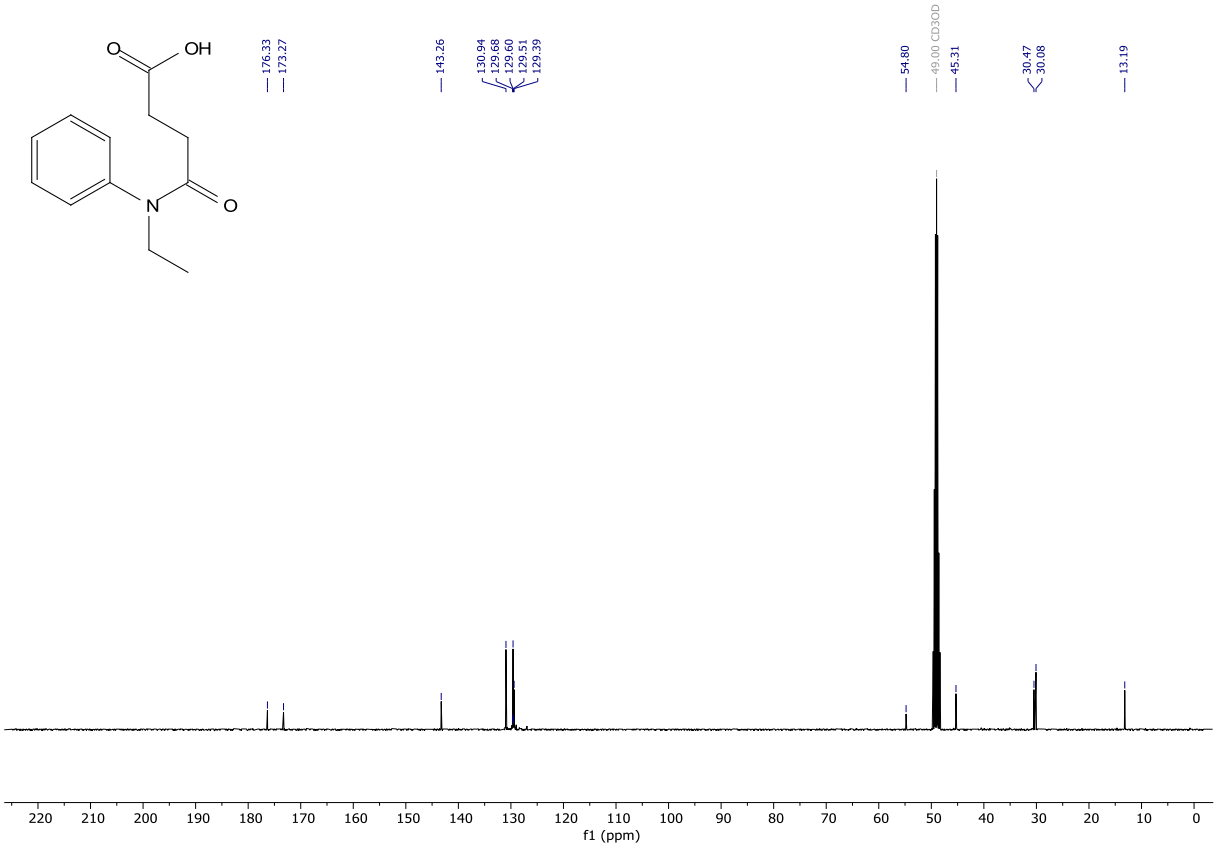

3-(*N*-Ethyl-*N*-phenylsulfamoyl)propanoic acid (27), ^{1}H NMR spectrum (400 MHz, MeOD)

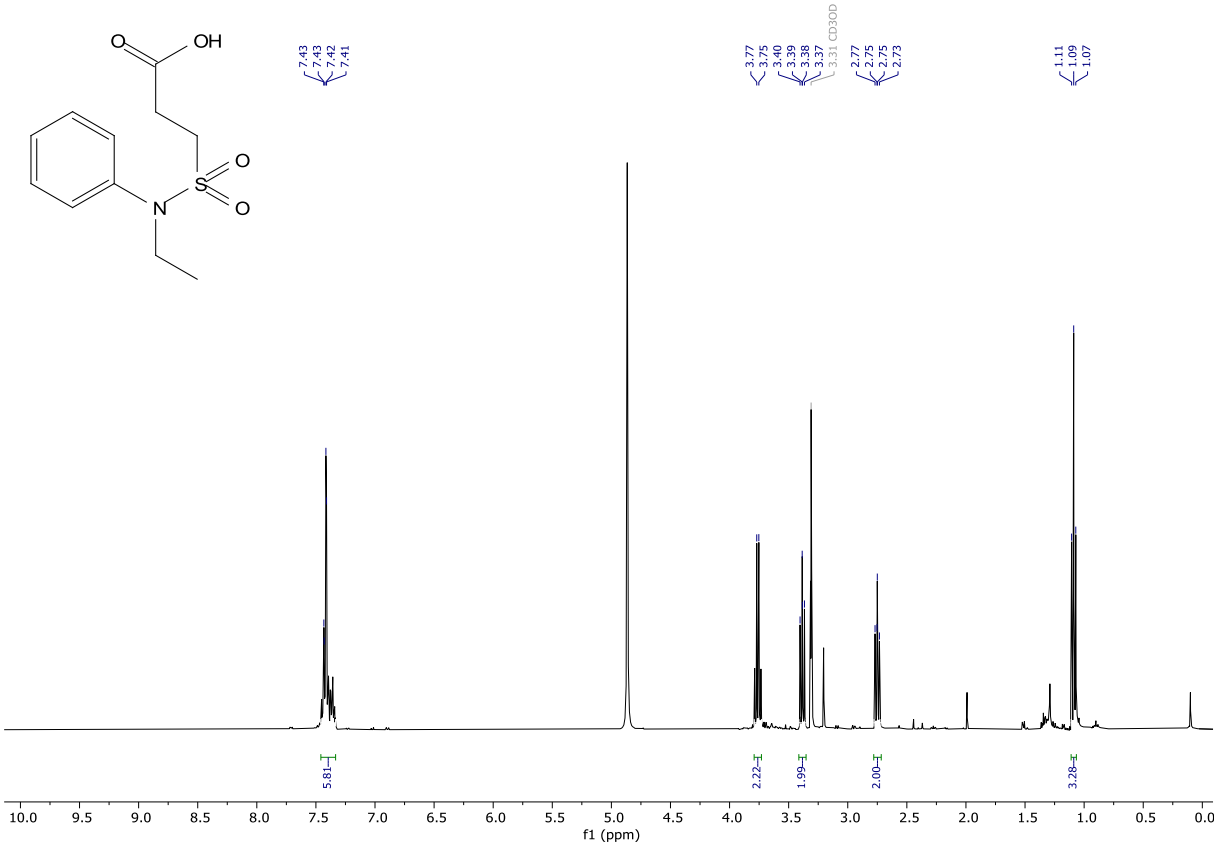

3-(*N*-Ethyl-*N*-phenylsulfamoyl)propanoic acid (27), ^{13}C NMR spectrum (101 MHz, MeOD)

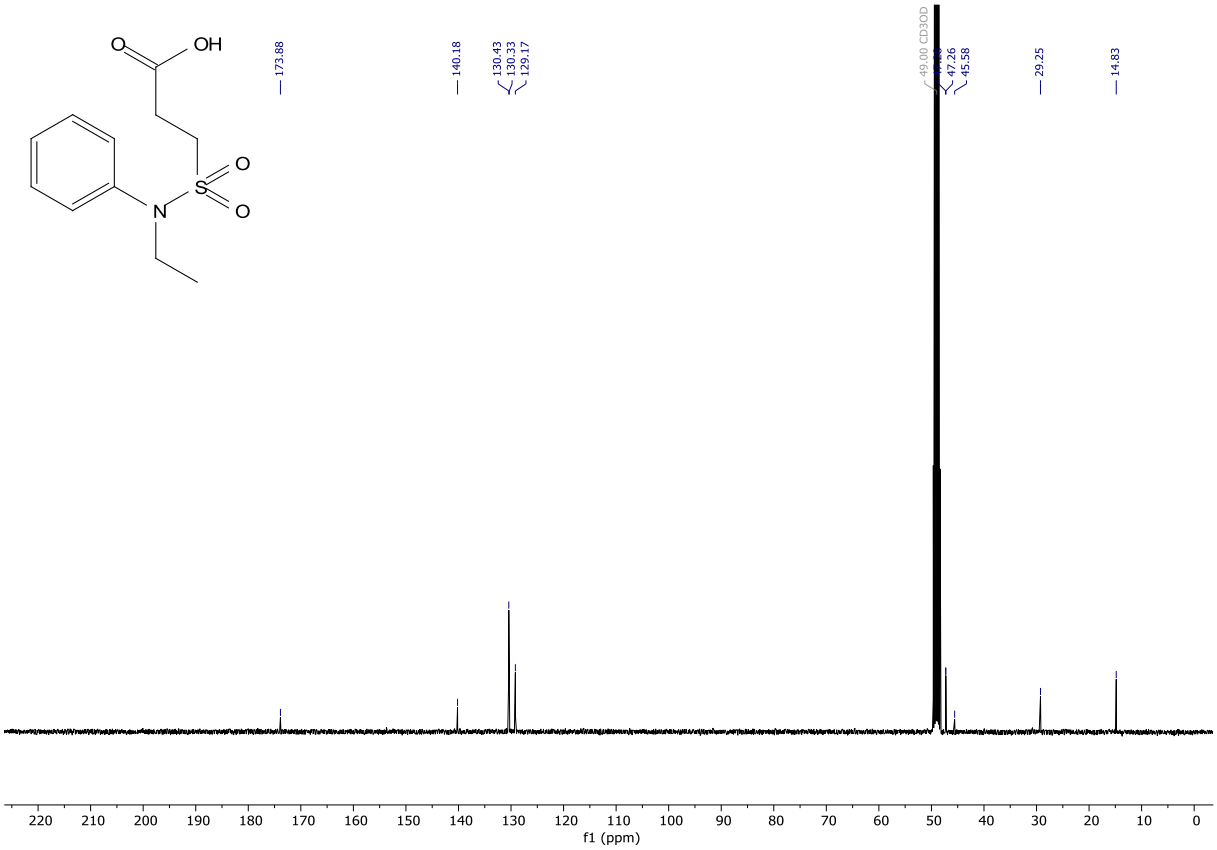

3-(*N*,*N*-Dibutylsulfamoyl)propanoic acid (28), ^{1}H NMR spectrum (400 MHz, MeOD)

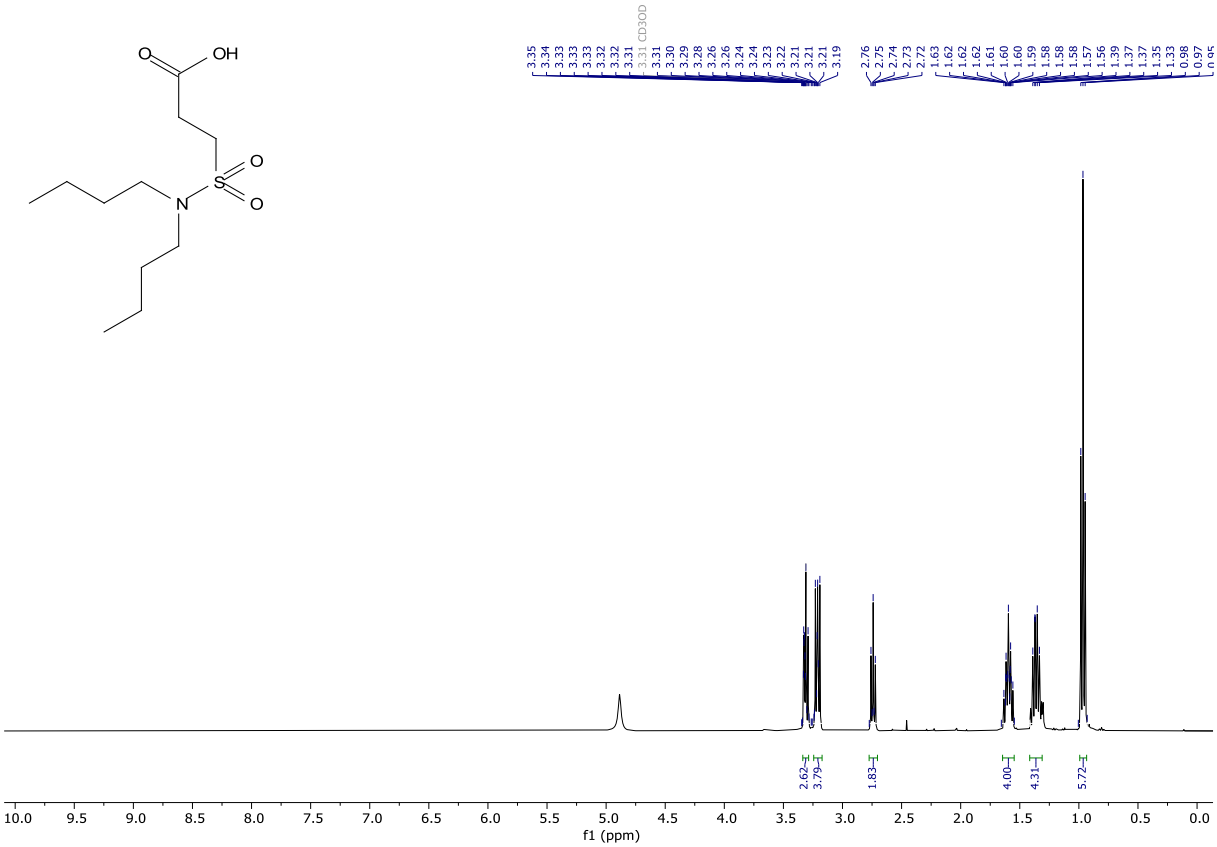

3-(*N*,*N*-Dibutylsulfamoyl)propanoic acid (28), ^{13}C NMR spectrum (101 MHz, MeOD)

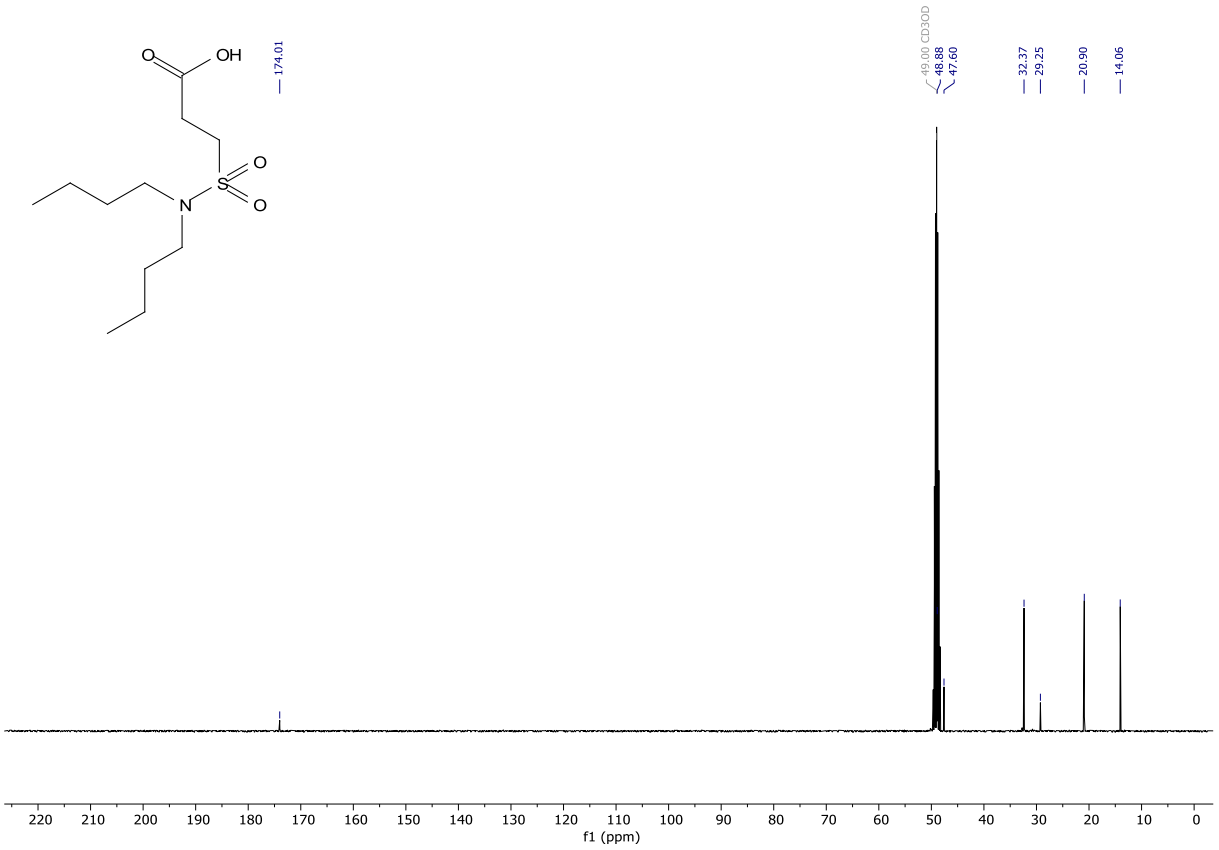

7. References

(1) Badea, G. I.; Radu, G. L. Introductory Chapter: Carboxylic Acids - Key Role in Life Sciences. In *Carboxylic Acid - Key Role in Life Sciences*; InTech, 2018. https://doi.org/10.5772/intechopen.77021.

(2) Valentovic, M. Atorvastatin. In *xPharm: The Comprehensive Pharmacology Reference*; Elsevier, 2007; pp 1–6. https://doi.org/10.1016/B978-008055232-3.61260-7.

(3) Peng, J.-B.; Geng, H.-Q.; Wu, X.-F. The Chemistry of CO: Carbonylation. *Chem* **2019**, *5* (3), 526–552. https://doi.org/10.1016/j.chempr.2018.11.006.

(4) Sang, R.; Hu, Y.; Razzaq, R.; Mollaert, G.; Atia, H.; Bentrup, U.; Sharif, M.; Neumann, H.; Junge, H.; Jackstell, R.; Maes, B. U. W.; Beller, M. A Practical Concept for Catalytic Carbonylations Using Carbon Dioxide. *Nat Commun* **2022**, *13* (1), 4432. https://doi.org/10.1038/s41467-022-32030-8.

(5) Kiss, G. Palladium-Catalyzed Reppe Carbonylation. *Chem Rev* **2001**, *101* (11), 3435–3456. https://doi.org/10.1021/cr010328q.

(6) Bertleff, W.; Roeper, M.; Sava, X. Carbonylation. In *Ullmann's Encyclopedia of Industrial Chemistry*; Wiley-VCH Verlag GmbH & Co. KGaA: Weinheim, Germany, 2007. https://doi.org/10.1002/14356007.a05_217.pub2.

(7) Jin, Y.; Caner, J.; Nishikawa, S.; Toriumi, N.; Iwasawa, N. Catalytic Direct Hydrocarboxylation of Styrenes with CO_2 and H_2. *Nat Commun* **2022**, *13* (1), 7584. https://doi.org/10.1038/s41467-022-35293-3.

(8) Morimoto, T.; Kakiuchi, K. Evolution of Carbonylation Catalysis: No Need for Carbon Monoxide. *Angew Chem Int Ed* **2004**, *43* (42), 5580–5588. https://doi.org/10.1002/anie.200301736.

(9) Simonato, J.-P.; Walter, T.; Métivier, P. Iridium–Formic Acid Based System for Hydroxycarbonylation without CO Gas. *J Mol Catal, A Chem* **2001**, *171* (1–2), 91–94. https://doi.org/10.1016/S1381-1169(01)00114-5.

(10) Wu, L.; Liu, Q.; Jackstell, R.; Beller, M. Carbonylations of Alkenes with CO Surrogates. *Angew Chem Int Ed* **2014**, *53* (25), 6310–6320. https://doi.org/10.1002/anie.201400793.

(11) Simonato, J.-P. New Efficient Catalytic System for Hydroxycarbonylation without CO Gas. *J Mol Catal, A Chem* **2003**, *197* (1–2), 61–64. https://doi.org/10.1016/S1381-1169(02)00676-3.

(12) Wang, Y.; Ren, W.; Shi, Y. An Atom-Economic Approach to Carboxylic Acids *via* Pd-Catalyzed Direct Addition of Formic Acid to Olefins with Acetic Anhydride as a Co-Catalyst. *Org Biomol Chem* **2015**, *13* (31), 8416–8419. https://doi.org/10.1039/C5OB01180A.

(13) Sang, R.; Kucmierczyk, P.; Dong, K.; Franke, R.; Neumann, H.; Jackstell, R.; Beller, M. Palladium-Catalyzed Selective Generation of CO from Formic Acid for Carbonylation of Alkenes. *J Am Chem Soc* **2018**, *140* (15), 5217–5223. https://doi.org/10.1021/jacs.8b01123.

(14) Roth, H. D. The Beginnings of Organic Photochemistry. *Angew Chem Int Ed* **1989**, *28* (9), 1193–1207. https://doi.org/10.1002/anie.198911931.

(15) Liu, W.; Li, C.-J. Recent Synthetic Applications of Catalyst-Free Photochemistry. *Synlett* **2017**, *28* (20), 2714–2754. https://doi.org/10.1055/s-0036-1590900.

(16) Ciamician, G. The Photochemistry of the Future. *Science* **1912**, *36* (926), 385–394. https://doi.org/10.1126/science.36.926.385.

(17) Oelgemöller, M. Solar Photochemical Synthesis: From the Beginnings of Organic Photochemistry to the Solar Manufacturing of Commodity Chemicals. *Chem Rev* **2016**, *116* (17), 9664–9682. https://doi.org/10.1021/acs.chemrev.5b00720.

(18) Hoffmann, N. Photochemical Reactions as Key Steps in Organic Synthesis. *Chem Rev* **2008**, *108* (3), 1052–1103. https://doi.org/10.1021/cr0680336.

(19) Bandara, H. M. D.; Burdette, S. C. Photoisomerization in Different Classes of Azobenzene. *Chem. Soc. Rev.* **2012**, *41* (5), 1809–1825. https://doi.org/10.1039/C1CS15179G.

(20) Romero, N. A.; Nicewicz, D. A. Organic Photoredox Catalysis. *Chem Rev* **2016**, *116* (17), 10075–10166. https://doi.org/10.1021/acs.chemrev.6b00057.

(21) Dantas, J. A.; Correia, J. T. M.; Paixão, M. W.; Corrêa, A. G. Photochemistry of Carbonyl Compounds: Application in Metal-Free Reactions. *ChemPhotoChem* **2019**, *3* (7), 506–520. https://doi.org/10.1002/cptc.201900044.

(22) Sumida, Y.; Ohmiya, H. Direct Excitation Strategy for Radical Generation in Organic Synthesis. *Chem Soc Rev* **2021**, *50* (11), 6320–6332. https://doi.org/10.1039/D1CS00262G.

(23) Abe, M. Recent Progress Regarding Regio-, Site-, and Stereoselective Formation of Oxetanes in Paternò-Büchi Reactions. *J Chin Chem Soc* **2008**, *55* (3), 479–486. https://doi.org/10.1002/jccs.200800072.

(24) Sicignano, M.; Rodríguez, R. I.; Alemán, J. Recent Visible Light and Metal Free Strategies in [2+2] and [4+2] Photocycloadditions. *European J Org Chem* **2021**, *2021* (22), 3303–3321. https://doi.org/10.1002/ejoc.202100518.

(25) Majhi, S. Applications of Norrish Type I and II Reactions in the Total Synthesis of Natural Products: A Review. *Photochem Photobiol Sci* **2021**, *20* (10), 1357–1378. https://doi.org/10.1007/s43630-021-00100-3.

(26) Buzzetti, L.; Prieto, A.; Roy, S. R.; Melchiorre, P. Radical-Based C−C Bond-Forming Processes Enabled by the Photoexcitation of 4-Alkyl-1,4-Dihydropyridines. *Angew Chem Int Ed* **2017**, *56* (47), 15039–15043. https://doi.org/10.1002/anie.201709571.

(27) Pálvölgyi, Á. M.; Ehrschwendtner, F.; Schnürch, M.; Bica-Schröder, K. Photocatalyst-Free Hydroacylations of Electron-Poor Alkenes and Enones under Visible-Light Irradiation. *Org Biomol Chem* **2022**, *20* (36), 7245–7249. https://doi.org/10.1039/D2OB01364A.

(28) Bera, S. K.; Bhanja, R.; Mal, P. Catalyst-Free Photoinduced C–C Bond Formations. *Synthesis* **2023**, *55* (10), 1467–1486. https://doi.org/10.1055/a-2043-3973.

(29) Silvi, M.; Arceo, E.; Jurberg, I. D.; Cassani, C.; Melchiorre, P. Enantioselective Organocatalytic Alkylation of Aldehydes and Enals Driven by the Direct Photoexcitation of Enamines. *J Am Chem Soc* **2015**, *137* (19), 6120–6123. https://doi.org/10.1021/jacs.5b01662.

(30) Crisenza, G. E. M.; Mazzarella, D.; Melchiorre, P. Synthetic Methods Driven by the Photoactivity of Electron Donor–Acceptor Complexes. *J Am Chem Soc* **2020**, *142* (12), 5461–5476. https://doi.org/10.1021/jacs.0c01416.

(31) Mulliken, R. S.; Person, W. B. Donor-Acceptor Complexes. *Annu Rev Phys Chem* **1962**, *13* (1), 107–126. https://doi.org/10.1146/annurev.pc.13.100162.000543.

(32) Arceo, E.; Jurberg, I. D.; Álvarez-Fernández, A.; Melchiorre, P. Photochemical Activity of a Key Donor–Acceptor Complex Can Drive Stereoselective Catalytic α-Alkylation of Aldehydes. *Nat Chem* **2013**, *5* (9), 750–756. https://doi.org/10.1038/nchem.1727.

(33) Shaw, M. H.; Twilton, J.; MacMillan, D. W. C. Photoredox Catalysis in Organic Chemistry. *J Org Chem* **2016**, *81* (16), 6898–6926. https://doi.org/10.1021/acs.joc.6b01449.

(34) Cano-Yelo, H.; Deronzier, A. Photo-Oxidation of Some Carbinols by the Ru(II) Polypyridyl Complex-Aryl Diazonium Salt System. *Tetrahedron Lett* **1984**, *25* (48), 5517–5520. https://doi.org/10.1016/S0040-4039(01)81614-2.

(35) Okada, K.; Okamoto, K.; Morita, N.; Okubo, K.; Oda, M. Photosensitized Decarboxylative Michael Addition through N-(Acyloxy)Phthalimides via an Electron-Transfer Mechanism. *J Am Chem Soc* **1991**, *113* (24), 9401–9402. https://doi.org/10.1021/ja00024a074.

(36) Capaldo, L.; Ravelli, D.; Fagnoni, M. Direct Photocatalyzed Hydrogen Atom Transfer (HAT) for Aliphatic C–H Bonds Elaboration. *Chem Rev* **2022**, *122* (2), 1875–1924. https://doi.org/10.1021/acs.chemrev.1c00263.

(37) Nicewicz, D. A.; MacMillan, D. W. C. Merging Photoredox Catalysis with Organocatalysis: The Direct Asymmetric Alkylation of Aldehydes. *Science* **2008**, *322* (5898), 77–80. https://doi.org/10.1126/science.1161976.

(38) Mao, B.; Wei, J.-S.; Shi, M. Recent Advancements in Visible-Light-Driven Carboxylation with Carbon Dioxide. *Chem Comm* **2022**, *58* (67), 9312–9327. https://doi.org/10.1039/D2CC03380A.

(39) Niu, Y.-N.; Jin, X.-H.; Liao, L.-L.; Huang, H.; Yu, B.; Yu, Y.-M.; Yu, D.-G. Visible-Light-Driven External-Photocatalyst-Free Alkylative Carboxylation of Alkenes with CO_2. *Sci China Chem* **2021**, *64* (7), 1164–1169. https://doi.org/10.1007/s11426-021-1004-y.

(40) Murata, K.; Numasawa, N.; Shimomaki, K.; Takaya, J.; Iwasawa, N. Construction of a Visible Light-Driven Hydrocarboxylation Cycle of Alkenes by the Combined Use of Rh(I) and Photoredox Catalysts. *Chem Comm* **2017**, *53* (21), 3098–3101. https://doi.org/10.1039/C7CC00678K.

(41) Seo, H.; Liu, A.; Jamison, T. F. Direct β-Selective Hydrocarboxylation of Styrenes with CO_2 Enabled by Continuous Flow Photoredox Catalysis. *J Am Chem Soc* **2017**, *139* (40), 13969–13972. https://doi.org/10.1021/jacs.7b05942.

(42) Ye, J.-H.; Miao, M.; Huang, H.; Yan, S.-S.; Yin, Z.-B.; Zhou, W.-J.; Yu, D.-G. Visible-Light-Driven Iron-Promoted Thiocarboxylation of Styrenes and Acrylates with CO_2. *Angew Chem Int Ed* **2017**, *56* (48), 15416–15420. https://doi.org/10.1002/anie.201707862.

(43) Hou, J.; Ee, A.; Cao, H.; Ong, H.; Xu, J.; Wu, J. Visible-Light-Mediated Metal-Free Difunctionalization of Alkenes with CO_2 and Silanes or $C(sp^3)$−H Alkanes. *Angew Chem Int Ed* **2018**, *57* (52), 17220–17224. https://doi.org/10.1002/anie.201811266.

(44) Fu, Q.; Bo, Z.-Y.; Ye, J.-H.; Ju, T.; Huang, H.; Liao, L.-L.; Yu, D.-G. Transition Metal-Free Phosphonocarboxylation of Alkenes with Carbon Dioxide via Visible-Light Photoredox Catalysis. *Nat Commun* **2019**, *10* (1), 3592. https://doi.org/10.1038/s41467-019-11528-8.

(45) Yatham, V. R.; Shen, Y.; Martin, R. Catalytic Intermolecular Dicarbofunctionalization of Styrenes with CO_2 and Radical Precursors. *Angew Chem Int Ed* **2017**, *56* (36), 10915–10919. https://doi.org/10.1002/anie.201706263.

(46) Tan, F.; Yin, G. Homogeneous Light-Driven Catalytic Direct Carboxylation with CO_2. *Chin J Chem* **2018**, *36* (6), 545–554. https://doi.org/10.1002/cjoc.201800011.

(47) Huang, H.; Ye, J.-H.; Zhu, L.; Ran, C.-K.; Miao, M.; Wang, W.; Chen, H.; Zhou, W.-J.; Lan, Y.; Yu, B.; Yu, D.-G. Visible-Light-Driven Anti-Markovnikov Hydrocarboxylation of Acrylates and Styrenes with CO_2. *CCS Chem* **2021**, *3* (6), 1746–1756. https://doi.org/10.31635/ccschem.020.202000374.

(48) Song, L.; Wang, W.; Yue, J.-P.; Jiang, Y.-X.; Wei, M.-K.; Zhang, H.-P.; Yan, S.-S.; Liao, L.-L.; Yu, D.-G. Visible-Light Photocatalytic Di- and Hydro-Carboxylation of Unactivated Alkenes with CO_2. *Nat Catal* **2022**, *5* (9), 832–838. https://doi.org/10.1038/s41929-022-00841-z.

(49) Alektiar, S. N.; Wickens, Z. K. Photoinduced Hydrocarboxylation via Thiol-Catalyzed Delivery of Formate Across Activated Alkenes. *J Am Chem Soc* **2021**, *143* (33), 13022–13028. https://doi.org/10.1021/jacs.1c07562.

(50) Huang, Y.; Hou, J.; Zhan, L.-W.; Zhang, Q.; Tang, W.-Y.; Li, B.-D. Photoredox Activation of Formate Salts: Hydrocarboxylation of Alkenes via Carboxyl Group Transfer. *ACS Catal* **2021**, *11* (24), 15004–15012. https://doi.org/10.1021/acscatal.1c04684.

(51) Mangaonkar, S. R.; Hayashi, H.; Takano, H.; Kanna, W.; Maeda, S.; Mita, T. Photoredox/HAT-Catalyzed Dearomative Nucleophilic Addition of the CO_2 Radical Anion to (Hetero)Aromatics. *ACS Catal* **2023**, *13* (4), 2482–2488. https://doi.org/10.1021/acscatal.2c06192.

(52) Alektiar, S. N.; Han, J.; Dang, Y.; Rubel, C. Z.; Wickens, Z. K. Radical Hydrocarboxylation of Unactivated Alkenes via Photocatalytic Formate Activation. *J Am Chem Soc* **2023**, *145* (20), 10991–10997. https://doi.org/10.1021/jacs.3c03671.

(53) Xiao, W.; Wang, X.; Liu, R.; Wu, J. Quinuclidine and its Derivatives as Hydrogen-Atom-Transfer Catalysts in Photoinduced Reactions. *Chin Chem Lett* **2021**, *32* (6), 1847–1856. https://doi.org/10.1016/j.cclet.2021.02.009.

(54) Nakajima, K.; Miyake, Y.; Nishibayashi, Y. Synthetic Utilization of α-Aminoalkyl Radicals and Related Species in Visible Light Photoredox Catalysis. *Acc Chem Res* **2016**, *49* (9), 1946–1956. https://doi.org/10.1021/acs.accounts.6b00251.

(55) Hendy, C. M.; Smith, G. C.; Xu, Z.; Lian, T.; Jui, N. T. Radical Chain Reduction via Carbon Dioxide Radical Anion ($CO_2^{\bullet-}$). *J Am Chem Soc* **2021**, *143* (24), 8987–8992. https://doi.org/10.1021/jacs.1c04427.

(56) Bolsman, T. A. B. M.; Blok, A. P.; Frijns, J. H. G. Mechanism of the Catalytic Inhibition of Hydrocarbon Autoxidation by Secondary Amines and Nitroxides. *Recl Trav Chim Pays-Bas* **2010**, *97* (12), 313–319. https://doi.org/10.1002/recl.19780971205.

(57) Li, Q.; Li, F. Recent Advances in Molecular Oxygen Activation via Photocatalysis and Its Application in Oxidation Reactions. *J Chem Eng* **2021**, *421*, 129915. https://doi.org/10.1016/j.cej.2021.129915.

(58) Cavedon, C.; Seeberger, P. H.; Pieber, B. Photochemical Strategies for Carbon–Heteroatom Bond Formation. *Eur J Org Chem* **2020**, *2020* (10), 1379–1392. https://doi.org/10.1002/ejoc.201901173.

(59) Buzzetti, L.; Crisenza, G. E. M.; Melchiorre, P. Mechanistic Studies in Photocatalysis. *Angew Chem Int Ed* **2019**, *58* (12), 3730–3747. https://doi.org/10.1002/anie.201809984.

(60) Cismesia, M. A.; Yoon, T. P. Characterizing Chain Processes in Visible Light Photoredox Catalysis. *Chem Sci* **2015**, *6* (10), 5426–5434. https://doi.org/10.1039/C5SC02185E.

(61) Galpin, I. J.; Hardy, P. M.; Kenner, G. W.; McDermott, J. R.; Ramage, R.; Seely, J. H.; Tyson, R. G. Peptides—XXXII. *Tetrahedron* **1979**, *35* (21), 2577–2582. https://doi.org/10.1016/0040-4020(79)88023-0.

(62) Inokuma, T.; Suzuki, Y.; Sakaeda, T.; Takemoto, Y. Synthesis of Optically Active N-Aryl Amino Acid Derivatives through the Asymmetric Petasis Reaction Catalyzed by a Novel Hydroxy-Thiourea Catalyst. *Chem Asian J* **2011**, *6* (11), 2902–2906. https://doi.org/10.1002/asia.201100453.

(63) Liu, D.; Yang, K.; Fang, D.; Li, S.; Lan, Y.; Chen, Y. Formyl Radical Generation from A-Chloro *N* -Methoxyphthalimides Enables Selective Aldehyde Synthesis. *Angew Chem Int Ed* **2023**, *62* (1). https://doi.org/10.1002/anie.202213686.

(64) Cai, L.; Fu, L.; Zhou, C.; Gao, Y.; Li, S.; Li, G. Rh(I)-Catalyzed Regioselective Arylcarboxylation of Acrylamides with Arylboronic Acids and CO_2. *Green Chem* **2020**, *22* (21), 7328–7332. https://doi.org/10.1039/D0GC02667K.

(65) Chanthamath, S.; Takaki, S.; Shibatomi, K.; Iwasa, S. Highly Stereoselective Cyclopropanation of α,β-Unsaturated Carbonyl Compounds with Methyl (Diazoacetoxy)Acetate Catalyzed by a Chiral Ruthenium(II) Complex. *Angew Chem Int Ed* **2013**, *52* (22), 5818–5821. https://doi.org/10.1002/anie.201300468.

(66) Odanaka, Y.; Kanemitsu, T.; Iwasaki, K.; Mochizuki, Y.; Miyazaki, M.; Nagata, K.; Kato, M.; Itoh, T. Asymmetric Michael Addition of Malonic Diesters to Acrylates by Phase-Transfer Catalysis toward the Construction of Quaternary Stereogenic α-Carbons. *Tetrahedron* **2019**, *75* (2), 209–219. https://doi.org/10.1016/j.tet.2018.11.037.

(67) Kim, J. H.; Park, E.-S.; Shim, J. H.; Kim, M.-N.; Moon, W.-S.; Chung, K.-H.; Yoon, J.-S. Antimicrobial Activity of *p* -Hydroxyphenyl Acrylate Derivatives. *J Agric Food Chem* **2004**, *52* (25), 7480–7483. https://doi.org/10.1021/jf0499018.

(68) Pham, T. S.; Gönczi, K.; Kardos, G.; Süle, K.; Hegedűs, L.; Kállay, M.; Kubinyi, M.; Szabó, P.; Petneházy, I.; Tőke, L.; Jászay, Z. Cinchona Based Squaramide Catalysed Enantioselective Michael Addition of α-Nitrophosphonates to Aryl Acrylates:

Enantioselective Synthesis of Quaternary α-Aminophosphonates. *Tetrahedron Asymmetry* **2013**, *24* (24), 1605–1614. https://doi.org/10.1016/j.tetasy.2013.10.008.

(69) Melngaile, R.; Sperga, A.; Baldridge, K. K.; Veliks, J. Diastereoselective Monofluorocyclopropanation Using Fluoromethylsulfonium Salts. *Org Lett* **2019**, *21* (17), 7174–7178. https://doi.org/10.1021/acs.orglett.9b02867.

(70) Vytla, D.; Kaliyaperumal, K.; Velayuthaperumal, R.; Shaw, P.; Gautam, R.; Mathur, A.; Roy, A. Visible-Light-Promoted Radical Cyclization of N-Arylvinylsulfonamides: Synthesis of CF_3/CHF_2/CH_2CF_3-Containing 1,3-Dihydrobenzo[c]Isothiazole 2,2-Dioxide Derivatives. *Synthesis* **2022**, *54* (03), 667–682. https://doi.org/10.1055/s-0040-1720921.

(71) Cruz, C. M.; Ortega-Muñoz, M.; López-Jaramillo, F. J.; Hernández-Mateo, F.; Blanco, V.; Santoyo-González, F. Vinyl Sulfonates: A Click Function for Coupling-and-Decoupling Chemistry and their Applications. *Adv Synth Catal* **2016**, *358* (21), 3394–3413. https://doi.org/10.1002/adsc.201600628.

(72) Fabry, D. C.; Stodulski, M.; Hoerner, S.; Gulder, T. Metal-Free Synthesis of 3,3-Disubstituted Oxoindoles by Iodine(III)-Catalyzed Bromocarbocyclizations. *Chem Eur J* **2012**, *18* (35), 10834–10838. https://doi.org/10.1002/chem.201201232.

(73) Song, Y.; Zheng, B.; Yang, S.; Li, Y.; Liu, Q.; Pan, L. Trifluoromethylations of (Hetero)Arenes and Polarized Alkenes Using Trifluoroacetic Anhydride under Photoredox Catalysis. *Org Lett* **2023**, *25* (13), 2372–2376. https://doi.org/10.1021/acs.orglett.3c00890.

(74) Kaboudin, B.; Pourbafarani, R.; Alavi, S.; Kazemi, F.; Aoyama, H. Metal-Free Selective Acylation Reaction of Aliphatic Alcohols in Neutral Condition. *J Iran Chem Soc* **2023**, *20* (3), 629–635. https://doi.org/10.1007/s13738-022-02694-6.

(75) Tehfe, M.-A.; Schweizer, S.; Chany, A.-C.; Ysacco, C.; Clément, J.-L.; Gigmes, D.; Morlet-Savary, F.; Fouassier, J.-P.; Neuburger, M.; Tschamber, T.; Blanchard, N.; Lalevée, J. On the Synthesis, Characterization and Reactivity of N-Heteroaryl-Boryl Radicals, a New Radical Class Based on Five-Membered Ring Ligands. *Chem Eur J* **2014**, *20* (17), 5054–5063. https://doi.org/10.1002/chem.201400197.

(76) Tanasova, M.; Anyika, M.; Borhan, B. Sensing Remote Chirality: Stereochemical Determination of β-, γ-, and δ-Chiral Carboxylic Acids. *Angew Chem Int Ed* **2015**, *54* (14), 4274–4278. https://doi.org/10.1002/anie.201410371.

(77) Du, B.-W.; Zhang, X.-J.; Shi, N.; Peng, T.; Gao, J.-B.; Azimova, B.; Zhang, R.; Pu, D.-B.; Wang, C.; Abduvaliev, A.; Rakhmanov, A.; Zhang, G.-L.; Xiao, W.-L.; Wang, F. Luteolin-7-Methylether from *Leonurus Japonicus* Inhibits Estrogen Biosynthesis in Human Ovarian Granulosa Cells by Suppression of Aromatase (CYP19). *Eur J Pharmacol* **2020**, *879*, 173154. https://doi.org/10.1016/j.ejphar.2020.173154.

(78) Hizal, S.; Hejl, M.; Jakupec, M. A.; Galanski, M. S.; Keppler, B. K. Synthesis, Characterization, Lipophilicity and Cytotoxic Properties of Novel Bis(Carboxylato)Oxalatobis(1-Propylamine)Platinum(IV) Complexes. *Inorganica Chim Acta* **2019**, *491*, 76–83. https://doi.org/10.1016/j.ica.2019.03.036.

(79) Padwa, A.; Price, A. T.; Zhi, L. A Novel Cycloaddition Reaction of α-Diazo-γ-Amido Ketones Catalyzed by Rhodium(II) Acetate. Scope and Mechanistic Details of the Process. *J Org Chem* **1996**, *61* (7), 2283–2292. https://doi.org/10.1021/jo952078h.

(80) Alvarez-Pérez, M.; Goldup, S. M.; Leigh, D. A.; Slawin, A. M. Z. A Chemically-Driven Molecular Information Ratchet. *J Am Chem Soc* **2008**, *130* (6), 1836–1838. https://doi.org/10.1021/ja7102394.

(81) Graafland, T.; Wagenaar, A.; Kirby, A. J.; Engberts, J. B. F. N. Structure and Reactivity in Intramolecular Catalysis. Catalysis of Sulfonamide Hydrolysis by the Neighboring Carboxyl Group. *J Am Chem Soc* **1979**, *101* (23), 6981–6991. https://doi.org/10.1021/ja00517a034.